Title: A novel *cis*-element enabled bacterial uptake by plant cells

Authors:

Chloé Cathebras[1]†, Xiaoyun Gong[1]†, Rosa Elena Andrade[1], Ksenia Vondenhoff[1], Jean Keller[2], Pierre-Marc Delaux[2], Makoto Hayashi[3], Maximilian Griesmann[1], Martin Parniske[1]*

Affiliations:

[1]Faculty of Biology, Genetics, LMU Munich, Großhaderner Strasse 2-4, 82152 Martinsried, Germany

[2]Laboratoire de Recherche en Sciences Végétales, Université de Toulouse, CNRS, UPS, 24 chemin de Borde Rouge, Auzeville, BP42617, 31326 Castanet Tolosan, France

[3]Center for Sustainable Resource Science, RIKEN, 1-7-22 Suehiro-cho, Tsurumi-ku, Yokohama City, Kanagawa, 230-0045, Japan

† these authors contribute equally to this work

*Correspondence to: Martin Parniske; parniske@lmu.de

Abstract:

The root nodule symbiosis (RNS) of plants with nitrogen-fixing bacteria is phylogenetically restricted to a single clade of flowering plants, which calls for yet unidentified trait acquisitions and genetic changes in the last common ancestor. Here we discovered – within the promoter of the transcription factor gene *Nodule Inception* (*NIN*) – a *cis*-regulatory element (*PACE*), exclusively present in members of this clade. *PACE* was essential for restoring infection threads (ITs) in *nin* mutants of the legume *Lotus japonicus*. *PACE* sequence variants from RNS-competent species appeared functionally equivalent. Evolutionary loss or mutation of *PACE* is associated with loss of this symbiosis. During early stages of nodule development, *PACE* dictates gene expression in a spatially restricted domain containing cortical cells carrying ITs. Consistent with its expression domain, *PACE*-driven *NIN* expression restored the formation of cortical ITs, also when engineered into the *NIN* promoter of tomato. Our data pinpoint *PACE* as a key evolutionary invention that connected *NIN* to a pre-existing symbiosis signal transduction cascade that governs the intracellular accommodation of arbuscular mycorrhiza fungi and is conserved throughout land plants. This connection enabled bacterial uptake into plant cells via intracellular support structures like ITs, a unique and unifying feature of this symbiosis.

Introduction

Nitrogen is essential for plant growth and development (LeBauer & Treseder, 2008). A wide phylogenetic variety of land plants ranging from mosses, gymnosperms to angiosperms have evolved symbioses with nitrogen-fixing bacteria that convert atmospheric nitrogen into ammonium (Masson-Boivin & Sachs, 2018). For example, the fern *Azolla* maintains colonies of nitrogen-fixing cyanobacteria in specialised apoplastic cavities, outside the plant cell wall enclosure (Peters & Meeks, 1989). A major biological breakthrough was the evolution of the nitrogen-fixing root nodule symbiosis (RNS) characterised by the intracellular accommodation of bacteria in lateral organs ("nodules") formed on roots (Kistner & Parniske, 2002; Parniske, 2000, 2018). The occurrence of the RNS is restricted to a monophyletic clade, encompassing four angiosperm orders: the Fabales, Fagales, Rosales and Cucurbitales (FaFaCuRo) (Soltis et al., 1995). Because of this phylogenetic restriction and scattered occurrence of RNS within the FaFaCuRo, Soltis and colleagues (Soltis et al., 1995) postulated that the last common ancestor of the FaFaCuRo clade acquired a genetic change, a "predisposition", which enabled members of this clade to subsequently evolve RNS multiple times independently (Soltis et al., 1995). Intracellular accommodation of bacteria and root nodule development are two genetically separable and to this extend independent features of RNS (Finan et al., 1985; Murray et al., 2007). It is therefore genetically possible that they did evolve sequentially and not at the same time. The phylogenetic diversity of bacterial symbionts plus the variation of nodule anatomy and development across the RNS-competent FaFaCuRo species (Pawlowski & Demchenko, 2012; Sprent et al., 2017) together with the gap of 30 million years between the last common ancestor and the oldest fossil root nodules in this clade (Doyle, 2011) further fuelled the hypothesis that nodule organogenesis evolved several times independently and was not a feature of the last common ancestor (Doyle, 2016; Sprent, 2007). The recent discovery of multiple losses of RNS within the FaFaCuRo clade (Griesmann et al., 2018; van Velzen et al., 2018) has initiated a discussion about whether this genetic change in the common ancestor was perhaps sufficient for the formation of RNS (van Velzen et al., 2019). Nonetheless, the precise nature of this key event in the evolution of nodulation has remained a mystery for more than two decades (Doyle, 2016).

We asked which evolutionary acquisitions by the last common ancestor, in the form of novel traits and the underlying genetic causes, enabled the evolution of the RNS. From a phylogenetic perspective, such acquisitions should be: 1) exclusively present in the FaFaCuRo clade and absent outside of this clade and 2) conserved throughout the FaFaCuRo clade or at least maintained in RNS-competent (hereafter called "nodulating") species. The uptake of bacteria into living plant cells is, with one exception (*Gunnera*), phylogenetically restricted to the FaFaCuRo clade (Parniske, 2000). Uptake of bacteria requires the localised

lysis of the plant cell wall, which threatens cell integrity because of the turgor pressure imposed by the protoplast (Parniske, 2018). A systematic comparison of features associated with the RNS across the entire FaFaCuRo clade pinpoints a single unique and shared trait – the uptake of bacteria into living plant cells with intracellular physical support structures – that fulfils both abovementioned criteria to be acquired by the common ancestor (Parniske, 2018). These structures come in a diversity of shapes (infection threads and infection pegs) and in at least two different cell types (epidermal and cortical), but are all characterised by the apposition of matrix material which is thought to maintain cell integrity during the localised lysis of the plant cell wall. While this matrix material is a common feature of all analysed successful bacteria uptake events in FaFaCuRo species, only one type, cortical infection threads (ITs), can be found in almost all nodulating species (Parniske, 2018). Cortical IT formation is an evolutionary breakthrough because it allowed clonal selection of bacteria (Gage, 2002), specific control of nutrient exchange and increased nitrogen fixation efficiency (Carvalho et al., 2014). By contrast, in *Gunnera*, cell integrity is maintained by physical closure of a multicellular cavity by extracellular matrix material (Johansson & Bergman, 1992). This difference, together with the phylogenetic distance of *Gunnera* from the FaFaCuRo clade, suggests an independent origin of bacterial uptake in this genus (Parniske, 2018). To search for gene gains specific for the FaFaCuRo clade, a genome-wide comparative phylogenomic analysis was performed, however, not a single gene following the aforementioned evolutionary pattern was identified (Griesmann et al., 2018).

Here, we tested the hypothesis that the “predisposition” event involved gain of novel *cis*-regulatory elements. It has been shown that changes in gene regulation are important drivers of functional and morphological evolution. Emergence or loss of even a single *cis*-regulatory element can lead to dramatic phenotypic consequences, e.g. novel organ formation (Kvon et al., 2016; Wittkopp & Kalay, 2011). Phylogeny has dated the common ancestor of the FaFaCuRo clade to approximately 90 Mya (Bell et al., 2010; Li et al., 2015; Wang et al., 2009). A long standing hypothesis states that the evolution of RNS involved co-opting genes from the arbuscular mycorrhiza (AM) symbiosis (Kistner & Parniske, 2002; Parniske, 2000), which can be traced back to the earliest land plant fossils 450 Mya (Redecker et al., 2000; Remy et al., 1994). This hypothesis is underpinned by similarities in intracellular accommodation structures (Parniske, 2018) and the common requirement of both symbioses for a set of so-called “common symbiosis genes” (Kistner & Parniske, 2002) that are conserved across land plant species able to form AM, and encode symbiotic signal transduction and intracellular restructuring machineries (Banba et al., 2008; Chen et al., 2007; Gutjahr et al., 2008; Markmann et al., 2008; Yano et al., 2008).

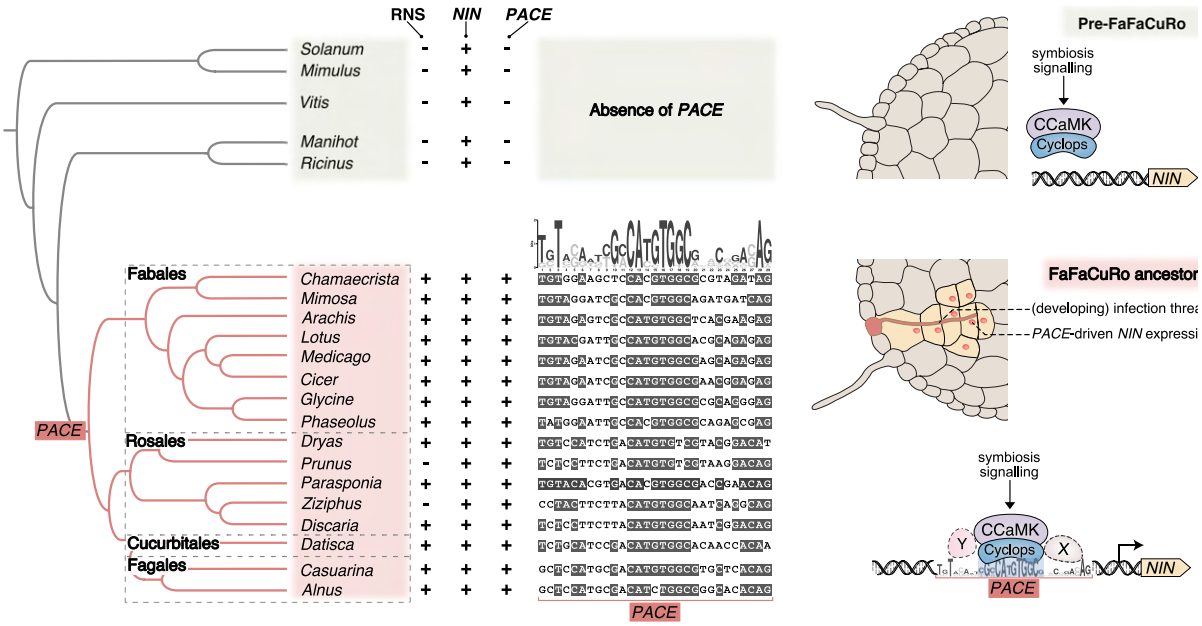

Figure 1. Acquisition of *PACE* was a key step in the evolution of RNS.
Left: Schematic illustration of phylogenetic relationships between species inside (light red shade) and outside (light grey shade) the FaFaCuRo clade and presence (+) and absence (-) pattern of RNS, *NIN* and *PACE* (See **Figure 1 – figure supplement 1 and 2** for additional data support). **Middle:** *PACE* sequence alignment of the displayed species in which grey shadings indicate more than 50% sequence identity. On top of the alignment the *PACE* consensus sequence depicted as Position Weight Matrix calculated from the displayed RNS-competent species. **Right:** Graphical illustration of how *PACE* connected *NIN* to symbiotic transcriptional regulation by CCaMK/Cyclops, enabling IT development in the root cortex. This acquisition coincided with the predisposition event. X and Y: hypothetical proteins binding to *PACE* outside of the Cyclops binding site.

Results and discussion

Discovery of *PACE*

The transcription factor-encoding *Nodule Inception* (*NIN*) gene (Schauser et al., 1999; Soyano et al., 2013) is positioned at the top of a RNS-specific transcriptional regulatory cascade and is indispensable for RNS (Schauser et al., 1999; Singh et al., 2014; Soyano & Hayashi, 2014). The promoter of *NIN* is a potential physical target for such a co-option event, because it defines the molecular interface between common symbiotic signal transduction and the specific transcriptional networks underlying RNS development (Soyano & Hayashi, 2014). We therefore compared the *NIN* promoter sequences of 37 angiosperm species including 27 FaFaCuRo members and identified only one motif fulfilling the aforementioned criteria, which we called *Predisposition-Associated Cis-regulatory Element* (*PACE*) (**Figure 1**; **Figure 1 – figure supplement 1A - D** and **Figure 1 – Source Data 1**). The phylogenetic distribution of *PACE* was further investigated in an expanded search comprising 163 plant species in the promoter of *NIN* and the entire *NIN-like protein* (*NLP*) gene family, including *NLP1* from which *NIN* diverged at the base of the eudicots (Soyano & Hayashi, 2014) (**Figure 1 – figure supplement 1E**; **Figure 1 – figure supplement 2** and **Figure 1 – Source Data 2**). *PACE*

was found in all nodulating FaFaCuRo members and four non-nodulating species that have lost RNS but maintained *NIN* (**Figure 1 – figure supplement 1E** and **Figure 1 – Source Data 3**). Importantly, *PACE* was absent from all the *NLP* promoters analysed (**Figure 1 – figure supplement 2**). Thus, the phylogenetic distribution pattern of *PACE* is FaFaCuRo-clade specific and is consistent with a model in which *PACE* was acquired by the *NIN* promoter of the last common FaFaCuRo ancestor. Intriguingly, the 29 nucleotides-long *PACE* encompassed and extended beyond the previously identified binding site of the transcription factor Cyclops, encoded by a common symbiosis gene required for the development of both AM and RNS (Singh et al., 2014; Yano et al., 2008).

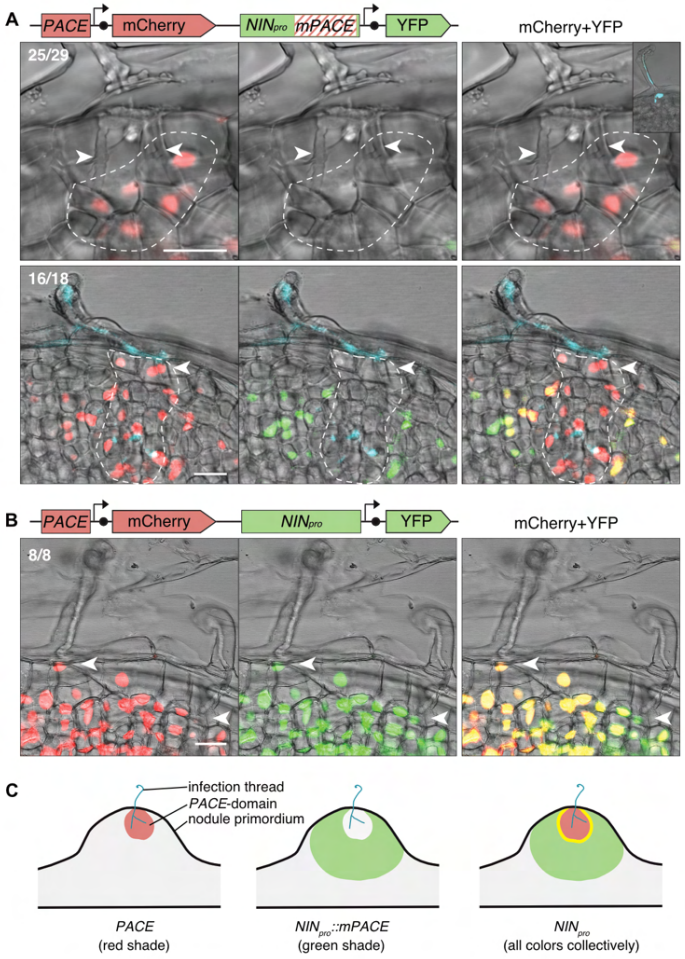

Figure 2. *PACE* drives the expression of *NIN* during IT development in the cortex. Sections of representative *L. japonicus* nodule primordia formed upon inoculation with *M. loti* R7A expressing CFP (blue) imaged by confocal laser-scanning microscopy. Comparison of the expression domains determined by (**A**) *PACE* (*PACE:NINmin$_{pro}$:NLS-mCherry*; red) and a *NIN* promoter carrying a mutated *PACE* (*NIN$_{pro}$::mPACE:NLS-YFP*; green); or (**B**) *PACE* (red) and the intact *NIN* promoter (*NIN$_{pro}$:NLS-YFP*; green). Dashed lines demarcate a group of cortical cells in the *PACE* core territory. Arrowheads indicate ITs. Numbers: nodule primordia showing the presented expression pattern / total number of nodule primordia sectioned and inspected. Bars, 20 µm. (**C**) graphical interpretation of expression patterns presented in (**A and B**). Yellow: overlapping region.

Given this clade-specific distribution of *PACE*, we searched for conserved motifs in the promoter sequences of two genes encoding transcriptional regulators, *ERF Required for Nodulation 1* (*ERN1*) (Cerri et al., 2017) (**Figure 1 – figure supplement 3**) and *Reduced Arbuscular Mycorrhiza 1* (*RAM1*) (Pimprikar et al., 2016) (**Figure 1 – figure supplement 4**) that are also known Cyclops targets. We identified motifs within the promoters of both, *ERN1* and *RAM1*, encompassing the previously identified Cyclops binding sites (Cerri et al., 2017; Pimprikar et al., 2016). In sharp contrast to *PACE*, their presence extended beyond the FaFaCuRo clade (**Figure 1 – figure supplement 3** and **Figure 1 – figure supplement 4**).

We tested the functional relevance of these distinct phylogenetic distribution patterns in transcriptional activation assays in *Nicotiana benthamiana* leaf cells. Transactivation by Cyclops was restricted to *NIN* promoters from FaFaCuRo species, but extended to non-FaFaCuRo species for *RAM1* promoters (**Figure 1 – figure supplement 5**). Importantly, *PACE* was necessary and sufficient for the activation of the *NIN* promoter by Cyclops (**Figure 1 – figure supplement 6**). Together with the exclusive occurrence of *PACE* in the *NIN* promoter of the FaFaCuRo clade, these results are in line with the hypothesis that the mechanistic link between Cyclops and the *NIN* promoter was established in the last common ancestor of this clade (**Figure 1**).

***PACE* drives the expression of *NIN* during IT development in the cortex**

NIN is indispensable for IT development (Schauser et al., 1999; Soyano et al., 2013) and its precise spatiotemporal expression is essential for this process (Liu et al., 2019; Soyano et al., 2013; Vernié et al., 2015; Yoro et al., 2014). Because *cis*-regulatory elements are master determinants of gene expression patterns (Buecker & Wysocka, 2012), we investigated the impact of *PACE* on the expression of *NIN* in physical relation to the bacterial uptake and accommodation stages during nodule development. We used the model legume *Lotus japonicus* in combination with its compatible nitrogen-fixing bacterium *Mesorhizobium loti* as experimental system. The process by which *M. loti* is taken up by *L. japonicus* can be subdivided into successive stages: (1) entrapment of bacteria in a pocket formed by a curled root hair (Perrine-Walker et al., 2014), (2) development of an IT within that root hair (Perrine-Walker et al., 2014), (3) IT progression into and through the outer cortical cell layers (Van Spronsen et al., 2001), (4) IT branching and extension within the nodule primordium (Yoon et al., 2014) (5) release of bacteria from ITs into plant membrane-enclosed organelle-like structures called symbiosomes (Yoon et al., 2014) leading to (6) mature nodules characterised by infected cells densely packed with symbiosomes and the pink colour of leghemoglobin (Ott et al., 2005).

To determine the *PACE*-mediated spatiotemporal expression domain, we introduced a *GUS* reporter gene driven by *PACE* fused to a region comprising the *NIN* minimal promoter and the

5'UTR (Singh et al., 2014) (*PACE:NINmin$_{pro}$:GUS*) into *L. japonicus* wild-type roots. Roots were subsequently inoculated with *M. loti* MAFF 303099 expressing *Ds*Red (*M. loti Ds*Red) facilitating detection of the bacteria through their fluorescence signal in root hairs and nodules. The *NIN* minimal promoter did not mediate reporter gene expression at any stage of bacterial infection (**Figure 2 – figure supplement 1E**). Intriguingly, the earliest detectable GUS activity mediated by *PACE:NINmin$_{pro}$:GUS* was clearly restricted to a zone in the nodule primordia (panel I - II in **Figure 2 – figure supplement 1D**) that roughly correlated with the site of bacterial infection (indicated by a local accumulation of *Ds*Red signal) and later expanded to the entire central tissue of the nodule (panel III in **Figure 2 – figure supplement 1D**). *PACE*-driven reporter expression was neither detected in root hairs harbouring ITs (**Figure 2 – figure supplement 1G**) nor in nodules in which cortical cells were filled with symbiosomes (panel IV in **Figure 2 – figure supplement 1D**). Importantly, *PACE*-mediated expression was distinct from that mediated by the *LjNIN* 3 kb promoter (*NIN$_{pro}$*) or the *NIN$_{pro}$* with *PACE* mutated or deleted (*NIN$_{pro}$::mPACE* and *NIN$_{pro}$::ΔPACE*, respectively) that conferred reporter expression across the central tissue of the nodule (panels II - IV in **Figure 2 – figure supplement 1A - C**). We concluded based on these observations that the *PACE*-mediated expression domain is temporally and spatially restricted and possibly accompanies the development of bacterial accommodation structures in the nodule.

To further resolve this relationship between *PACE* driven gene expression and bacterial accommodation at the cellular level, we compared – simultaneously in the same tissue – the progression of bacterial infection with the expression pattern mediated by *PACE* fused to the *NIN* minimal promoter (*PACE:NINmin*) and by a *NIN* promoter with mutated *PACE* (*NIN$_{pro}$::mPACE*). A red and a yellow fluorescent protein (mCherry and YFP, respectively) targeted to the nucleus by fusion to a nuclear localization signal (NLS) were used as reporters. The resulting promoter:reporter fusions (*PACE:NINmin$_{pro}$:NLS-mCherry* and *NIN$_{pro}$::mPACE:NLS-YFP*) were placed in tandem on the same T-DNA allowing a nucleus-by-nucleus comparison of their relative expression. This T-DNA construct was introduced into *L. japonicus* wild-type roots that were subsequently inoculated with *M. loti* R7A expressing the cyan fluorescent protein (CFP) to facilitate detection (**Figure 2**). In sections of developing nodules, in which infection had progressed to stage 3 or 4, *PACE*-mediated *mCherry* was expressed specifically in a – hereafter called "infection zone" – comprising cortical cells that carried ITs and in some, but not all, directly adjacent cells (25 out of 29 nodules inspected; **Figure 2A**). Intriguingly, the expression domains marked by mCherry and YFP fluorescence were distinct from each other: while the *PACE*-driven mCherry signal was consistently marking the infection zone, the *NIN$_{pro}$::mPACE*-driven YFP signal was observed in cortical cells surrounding this zone (16 out of 18 nodules inspected; **Figure 2A, 2C**). The thin (approx. 1-2

cells thick) border between the two domains was characterised by nuclei emitting both YFP and mCherry signals (**Figure 2A**). In so-marked cells, ITs were typically not detected. The expression pattern mediated by the *NIN* promoter (containing *PACE*) was congruent with the sum of both promoter fragments (8 out of 8 nodules inspected; **Figure 2B, 2C**).

Based on these clearly distinct and complementary reporter expression domains governed by *PACE* versus the remaining promoter, we concluded that 1) *PACE* directs *NIN* expression to a specific infection zone and that 2) the *NIN* promoter comprises *cis*-regulatory elements that drive expression outside the *PACE* territory i.e. in root hairs (together with *PACE*), non-infected cortical cells and cells filled with symbiosomes. These additional *cis*-regulatory elements might be addressed by other transcription factors that have been reported to bind to this promoter (Hirsch et al., 2009; Singh et al., 2014; Xiao et al., 2020; Zhu et al., 2008).

Mutational dissection of *PACE* reveals a quantitative impact of regions flanking the *CYC-box* on IT development

To test the relevance and specific role of *PACE* in nodule and IT development, we performed complementation experiments using plants homozygous for the *nin-2* or *nin-15* mutant alleles (Schauser et al., 1999). The *nin-2* mutant allele harbours a frameshift mutation of the *NIN* gene, leading to a *NIN* loss-of-function phenotype, i.e. absence of both IT formation and nodule organogenesis (Schauser et al., 1999) while the *nin-15* mutant allele carries a *Lotus Retrotransposon 1* insertion within the *NIN* promoter 143 bp 3' of *PACE* (**Figure 3 – figure supplement 1**). We examined the restoration of bacterial infection 21 days after inoculation with *M. loti Ds*Red by quantifying the number of root hairs harbouring ITs and the number of infected nodules (**Figure 3** and **Figure 3 – Source Data 1**).

Nodule development in the legume *Medicago truncatula* is dependent on *NIN* expression mediated by a regulatory region containing several putative cytokinin responsive elements (*CE*) (Liu et al., 2019). In *L. japonicus*, a similar *CE* region is positioned 45 kb upstream of the *NIN* transcriptional start site (Liu et al., 2019). To enable transgenic complementation experiments, we synthetically fused a 1 kb or 5 kb region encompassing this distant *CE* to the 5' end of a 3 kb *NIN* promoter. The *NIN* gene driven by these promoters (CE_{1kb}:NIN_{pro}:*NIN* and CE_{5kb}:NIN_{pro}:*NIN*) restored the formation of root hair ITs on 78% and 95% and infected nodules on 40% and 88% of *nin-2* transgenic root systems, respectively (**Figure 3A**; **Figure 3 – figure supplement 2, 3, 4, 5 and 6**). Importantly, this complementation success relied on the presence of *PACE*; *nin-2* roots transformed with the same fusion design but carrying a mutation of *PACE* (CE_{1kb}:NIN_{pro}::*mPACE:NIN* and CE_{5kb}:NIN_{pro}::*mPACE:NIN*) did not restore root hair ITs but nodule formation was not impaired when using the cytokinin element-containing region of 5 kb (CE_{5kb}:NIN_{pro}::*mPACE:NIN*). We concluded that *PACE* is indispensable for bacterial infection but not for nodule development.

The 29 bp long *PACE* sequence encompasses and extends beyond the previously identified Cyclops binding site (**Figure 1**). To dissect the specific contributions of the Cyclops binding site (*CYC-box* (Singh et al., 2014), "box") and *PACE* sequences flanking the *CYC-box* ("flanking") to *PACE* function, we mutated the box and the flanking region independently (*CE:NIN*$_{pro}$*::mbox:NIN* and *CE:NIN*$_{pro}$*::mflanking:NIN*, respectively). Mutation of the *CYC-box* abolished root hair ITs. Interestingly, mutation of the flanking sequences led to a 50% reduction of the number of transgenic root systems carrying infected nodules, while the formation of root hair ITs was not impaired (**Figure 3 – figure supplement 2, 3, 4, 5 and 6**). This mutational dissection revealed two separable functions of *PACE*: while the *PACE*-Cyclops connection is essential for IT development, the flanking sequences are positively regulating the infection of newly developed nodules and possibly act as binding sites for additional, yet undefined, transcription factors (**Figure 1**). The existence of transcription factors that act synergistically with Cyclops is in line with the original *cyclops* mutant phenotype description which called for the existence of CCaMK phosphorylation targets that can partially compensate for the loss of Cyclops in nodule development but not in infection (Yano et al., 2008). Our data suggest that *PACE* comprises synergistic binding sites for both Cyclops and cooperating transcription factors.

PACE-mediated *NIN* expression defined an infection zone in the nodule cortex (**Figure 2**). To genetically separate the initiation of nodule development from IT formation and thereby enable a focussed analysis of the role of *PACE* in cortical IT formation, we utilised the *nin-15* mutant, which is impaired in IT formation but retains the capacity to form nodules. Most of these nodules were uninfected (92% and 86% plants carrying no root hair ITs and no infected nodules, respectively) and cortical cells filled with symbiosomes were never observed (**Figure 3 – figure supplement 1**). This mutant therefore provided an ideal background to study the role of *PACE* in cortical IT formation, circumventing the negative epistatic effect of the inability of *nin* loss-of-function mutants to initiate cell divisions (Clavijo et al., 2015; Liu et al., 2019; Schauser et al., 1999; Vernié et al., 2015; Yoro et al., 2014) (**Figure 3B - D**; **Figure 3 – figure supplement 7**; **Figure 4**; **Figure 4 – figure supplement 1** and **Figure 3 – Source Data 1**).

Transformation with the *L. japonicus NIN* gene driven by the *NIN* minimal promoter (*NINmin*$_{pro}$*:NIN*) did not alter the symbiotic phenotype of *nin-15* roots (**Figure 3B**). In contrast, the *NIN* gene driven by the *NIN* promoter (*NIN*$_{pro}$*:NIN*) led to restoration of the complete infection process in *nin-15* roots from root hair ITs to symbiosome formation (100% and 92% of transgenic root systems carried root hairs ITs and infected nodules, respectively; **Figure 3B**). Similar to observations in complementation experiments of *nin-2*, mutation or deletion of *PACE* (*NIN*$_{pro}$*::mPACE:NIN* and *NIN*$_{pro}$*::* Δ*PACE:NIN,* respectively) drastically reduced the

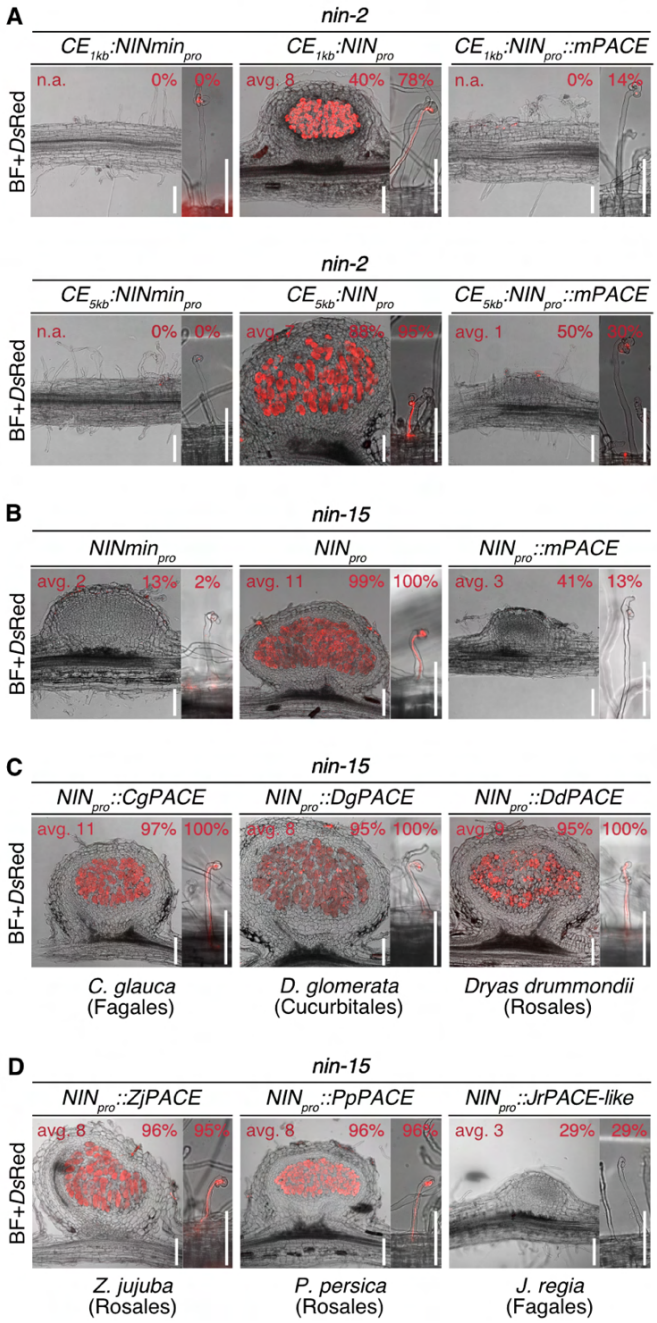

Figure 3. *PACE* is necessary for bacterial infection and functionally conserved across the FaFaCuRo clade. Microscopy images of representative nodule sections or root hairs harbouring an IT or an infection pocket from (**A**) *nin-2* or (**B - D**) *nin-15* roots transformed with the *LjNIN* gene driven by: (**A - B**) indicated promoters, and in (**C - D**) the *L. japonicus NIN* promoter in which *LjPACE* was replaced by *PACE* from (**C**) nodulating and (**D**) non-nodulating FaFaCuRo species or with a *PACE*-like sequence identified in the *JrNLP1b* promoter. %: percentage of transgenic root systems carrying infected nodules or root hair ITs. Avg.: average number of infected nodules on plants carrying infected nodules. n.a.: not applicable. Bars, 100 µm.

restoration of bacterial infection in root hairs and nodules in *nin-15* (**Figure 3B**; **Figure 3 – figure supplement 2, 3, 4, 5, 6 and 7**).

PACEs from different nodulating FaFaCuRo species are functionally equivalent

PACE was detected by MEME searches as a conserved motif within *NIN* promoters of the FaFaCuRo clade. However, the individual *PACE* sequences from different species differed from each other (**Figure 1** and **Figure 1 – figure supplement 1**). We therefore tested whether and to what extend this sequence variation of *PACE* would affect its function. Replacement of *PACE* within the *L. japonicus* (Fabales) 3 kb *NIN* promoter with *PACE* sequence variants (*NIN_{pro}::Species abbreviation PACE:NIN*) originating from *Casuarina glauca* (*Cg*, Fagales), *Datisca glomerata* (*Dg*, Cucurbitales) or *Dryas drummondii* (*Dd*, Rosales) restored the complete infection process in *nin-15* to similar level as *NIN_{pro}:NIN*, demonstrating the functional conservation of *PACE* from nodulating species across the entire FaFaCuRo clade (**Figure 3C** and **Figure 3 – figure supplement 7**). Similarly, the *PACE* versions from two non-nodulating Rosales that maintained the *NIN* gene, *Ziziphus jujuba* and *Prunus persica*, restored the complete infection process in *nin-15* (**Figure 3D** and **Figure 3 – figure supplement 7**). The results of these complementation experiments were consistent with the conserved expression pattern mediated by *PACEs* in *L. japonicus* (**Figure 3 – figure supplement 8**) and the CCaMK/Cyclops-mediated transactivation via these *PACE* variants (Extended Data Fig. 3a) or chimeric promoter:reporter fusions (**Figure 1 – figure supplement 6B**) tested in *N. benthamiana* leaves.

Loss of _PACE_ is associated with a loss of nodulation

Griesmann et al. (Griesmann et al., 2018) and van Velzen et al. (van Velzen et al., 2018) discovered that RNS was lost multiple times independently during evolution, via independent truncations or losses of the *NIN* gene. However, at least 10 out of 28 FaFaCuRo species that lost RNS have maintained a full-length *NIN* open reading frame (**Figure 1 – Source Data 3**). Based on our complementation data, *PACE* is indispensable for the *NIN* promoter function in symbiosis (**Figure 3** and **Figure 3 – figure supplement 2, 3, 4, 5, 6 and 7**). Therefore, the absence of *PACE* from 5 out of these 10 species (**Figure 1 – Source Data 1, 2 and 3**), is potentially sufficient to explain these losses of RNS. Consequently, at least 82% of all losses can now be attributed to either the *NIN* ORF (18/28, 64%) or loss of *PACE* (5/28, 18%) (**Figure 1 – Source Data 3**). The presence of *PACE* in all nodulating species (31/31, 100%; **Figure 1 – Source Data 1 and 2**) together with a correlation between the absence of *PACE* with the absence of RNS adds strong support for the evolutionary relevance of *PACE* both in the gain and potential loss of RNS.

PACE was not detected in the promoters of *NIN-like protein* (*NLP*) genes (**Figure 1 – figure supplement 2** and **Figure 1 – Source Data 1 and 2**) with the possible exception of the curious case of *Juglans regia* (Fagales). While it was also absent from the promoter of the so-annotated *NIN* gene, a *PACE*-like motif was identified in the promoter of the closest gene

family member, *NIN-like protein 1 JrNLP1b* (*JrPACE-like*; **Figure 1 – Source Data 1**). This *PACE*-like element was not able to restore IT formation in *nin-15* (**Figure 3D** and **Figure 3 – figure supplement 7**). Regardless of whether this exceptional presence/absence pattern of *PACE* may be caused by a miss-annotation of *NIN* and *NLP1* in *J. regia*, either a loss-of-function mutation within *PACE* or a loss of the entire *PACE* element in the *JrNIN* promoter could explain the absence of the RNS observed in this species.

PACE* is sufficient to restore cortical IT formation in *nin-15

We tested whether *PACE* on its own, only supported by the minimal *NIN* promoter (*PACE:NINmin*$_{pro}$) is sufficient to restore IT development in cortical cells. For this purpose, we transformed *nin-15* roots with *PACE:NINmin*$_{pro}$ fused to the transcribed region of the *NIN* gene. *PACE*-mediated *NIN* expression led to an increased success in restoration of infection (49% of transgenic root systems carried infected nodules) compared to *NINmin*$_{pro}$*:NIN*-transformed roots (17%; **Figure 4A**; **Figure 4 – figure supplement 1** and **Figure 3 – Source Data 1**). Root hair ITs were rarely observed on *PACE:NINmin*$_{pro}$*:NIN*-transformed *nin-15* roots (**Figure 4A**) and infected nodules harbouring cortical cells filled with symbiosomes were never observed (**Figure 4 – figure supplement 1**), consistent with the restricted expression domain defined by *PACE* (**Figure 2 – figure supplement 1**).

Strikingly, the vast majority of infected nodules transformed with *PACE:NINmin*$_{pro}$*:NIN* (25 out of 28 nodules inspected) carried ITs in the outer cortex, originating from a focused hyperaccumulation of bacteria, locally constricted by root cell wall boundaries (**Figure 4A**). This phenomenon was not observed in most of the rarely occurring infected nodules formed on *NINmin*$_{pro}$*:NIN*-transformed *nin-15* roots (11 out of the 16 nodules inspected did not carry ITs in the outer cortex). Bacterial colonies within cell wall boundaries resembling this phenomenon have been described in a variety of legumes including *Sesbania* and *Mimosa* (D'Haeze et al., 1998; De Faria et al., 1988). Our data imply that *PACE* promotes this type of cortical IT initiation. Altogether, these findings revealed that *PACE* promotes IT development in cortex cells but not within root hairs.

***PACE* insertion into the tomato *NIN* promoter confers RNS capability**

To artificially recapitulate the functional consequence of *PACE* acquisition into a non-FaFaCuRo *NIN* promoter, we chose tomato (*Solanum lycopersicum*) which belongs to the Solanaceae, a family phylogenetically distant from the FaFaCuRo clade. Consistent with the absence of *PACE*, a *GUS* reporter gene driven by the tomato *NIN* promoter (*SlNIN*$_{pro}$) was not transactivated by Cyclops in *N. benthamiana* leaf cells (**Figure 1** and **Figure 1 – figure supplement 5B and 6C**), while the insertion of the *L. japonicus PACE* (*SlNIN*$_{pro}$*::PACE*), but not of a mutated *PACE* (*SlNIN*$_{pro}$*::mPACE*) conferred transactivation by Cyclops (**Figure 1 – figure supplement 6C**).

We tested the ability of the *LjNIN* expressed under the control of these synthetic promoters to restore the bacterial infection process in *nin-15*. Similar to *NINmin*$_{pro}$*:NIN*-transformed *nin-15* roots, *SlNIN*$_{pro}$*:NIN* did not restore bacterial infection (0% and 7% of transgenic root systems carried root hair ITs and infected nodules, respectively; **Figure 4A - C**). In contrast, *nin-15* roots transformed with *SlNIN*$_{pro}$*::PACE:NIN* restored the formation of root hair ITs and infected nodules on 36% and 26% of transgenic root systems, respectively (**Figure 4B** and **Figure 4**

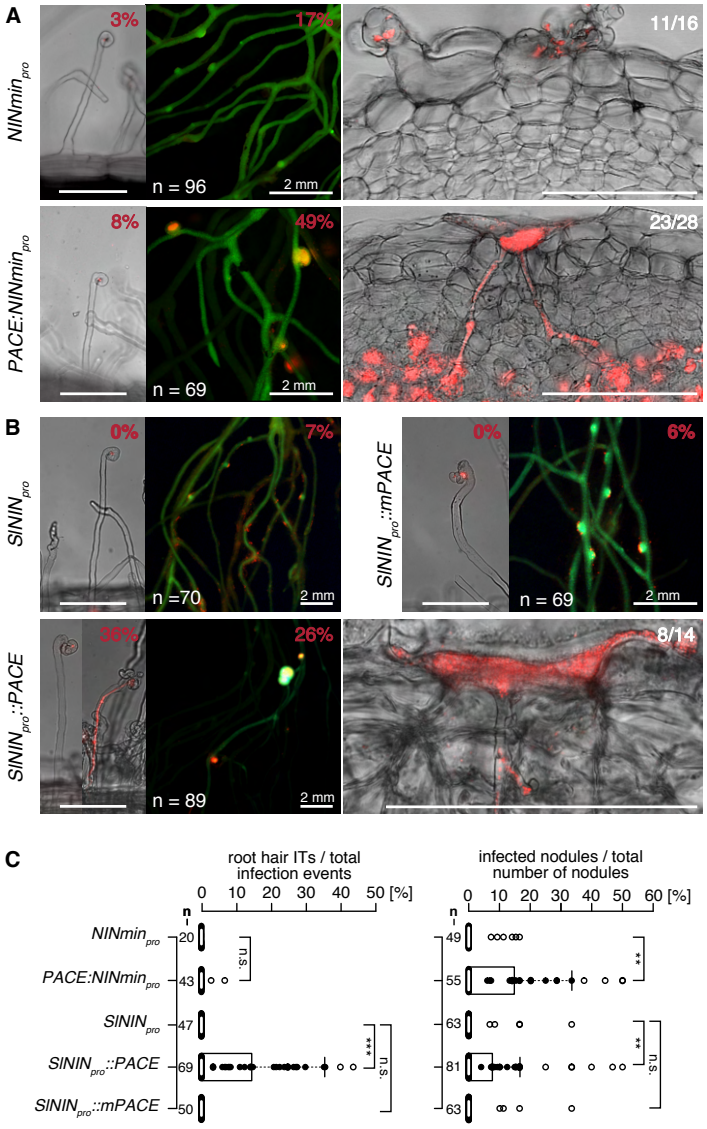

Figure 4. *PACE* enables IT formation in the cortex. Representative pictures of *nin-15* root hairs, root and nodule sections (see Extended Data Fig. 10 for overview pictures), transformed with the *L. japonicus NIN* gene driven by (**A**) *NINmin*$_{pro}$ or *PACE:NINmin*$_{pro}$; (**B**) *S. lycopersicum NIN* promoter (*SlNIN*$_{pro}$) and *SlNIN*$_{pro}$ with *LjPACE* or *mPACE* inserted. %: percentage of transgenic root systems carrying root hair ITs or infected nodules; Ratios: number of nodules showing the presented pattern / total number of nodules sectioned and inspected. (**C**) Boxplots displaying the percentage of root hair ITs and infected nodules per transgenic root system. n, number of transgenic root systems or root pieces analysed. The applied statistical method was Fisher's exact test: $**p<0.01$; $***p<0.001$; n.s., not significant. Unlabelled scale bars, 100 µm.

– **figure supplement 1**). This increase in infection success was not observed on *SlNIN$_{pro}$::mPACE:NIN*-transformed roots. ITs in the outer cortex that originated from a focal accumulation of bacteria were also observed in the *SlNIN$_{pro}$::PACE:NIN*-transformed *nin-15* nodules (8 out of 14 nodules inspected; **Figure 4B**) resembling those in the *PACE:NINmin$_{pro}$:NIN*-transformed *nin-15* nodules (**Figure 4A**). The gained ability of the *SlNIN::PACE* promoter to restore root hair ITs suggested that additional *cis*-regulatory elements within the *SlNIN* promoter function together with *PACE* for root hair IT formation. All together, these findings obtained with the tomato *NIN* promoter carrying an artificially inserted *PACE* agree with the hypothesis that the acquisition of *PACE* by a non-FaFaCuRo *NIN* promoter enabled its regulation via Cyclops and laid the foundation for IT formation in cortical cells.

Conclusion

The mechanistic connection between *PACE* and cortical IT formation together with their congruent phylogenetic distribution strongly support the idea that the acquisition of *PACE* by the latest common ancestor of the FaFaCuRo clade enabled cortical ITs and thus laid the foundation for the evolution of present day RNS. Our findings support an evolutionary model in which an ancestral symbiotic transcription factor complex (comprising CCaMK and Cyclops), that facilitated intracellular symbiosis with AM fungi already in the earliest land plants (Delaux et al., 2014, 2015), gained control over the transcriptional regulation of the *NIN* gene by the acquisition of *PACE* (**Figure 1**). This genetic innovation in the last common ancestor of the FaFaCuRo clade extended the function of the ancestral CCaMK complex to initiate cortical IT development. The *NIN*-like protein family underwent important evolutionary steps preceding the origin of RNS including a gene duplication leading to *NIN* and *NLP1* as closest paralogs (Liu & Bisseling, 2020). It is very likely that the NIN protein itself underwent changes that enabled its role in nodulation (Soyano & Hayashi, 2014). Loss of *NIN* events associated with the loss of nodulation are scattered across all four FaFaCuRo orders (Griesmann et al., 2018; van Velzen et al., 2018), suggesting that *NIN* acquired its relevance for nodulation probably before or latest in the last common ancestor. Because our phylogenomic analysis dates the acquisition of *PACE* to the latest ancestor of the FaFaCuRo clade, we conclude that the critical changes within NIN must have occurred simultaneously or earlier. From a statistical point of view, it is likely that the *PACE* acquisition and the RNS-enabling changes within NIN occurred independently from each other. It will be interesting to determine what these critical changes within NIN are and where they occurred phylogenetically.

A “young” primary cell wall characteristic for recently divided cells is considered an important prerequisite for cortical IT initiation (Geurts et al., 2016; Parniske, 2018) but cell division is not restricted to the formation of novel organs (Murray et al., 2007). It is therefore conceptually

possible that the common ancestor of the FaFaCuRo clade was forming ITs in recently divided cortical cells but in the absence of root nodules. Multiple lines of evidence indicate that the diverse types of lateral organs harbouring nitrogen-fixing bacteria ("nodules") evolved multiple times independently. Indeed, *CE*-mediated *NIN* expression is important for nodule organogenesis in legumes, but upon searching for this regulatory element in a region of 0.1 Mb upstream and downstream of the *NIN* gene, Liu and colleagues (Liu et al., 2019) found its presence to be restricted to legume species, indicating an evolutionary emergence independently of and significantly later than the last common ancestor (Liu et al., 2019; Liu & Bisseling, 2020). ITs in root hairs are only found in Fabales and Fagales and therefore also considered a more recent acquisition (Madsen et al., 2010; Parniske, 2018). *CE* only in combination with *PACE* facilitates root hair ITs (**Figure 3 – figure supplement 2, 3, 4, 5 and 6**) and additional elements in the 3 kb promoter are necessary for nodule and cortical IT development (**Figure 3 – figure supplement 2, 3, 4, 5 and 6**). These observations highlight the enormous complexity of concerted activity of *cis*-elements and transcription factors underlying the spatiotemporal expression control by present day *NIN* promoters in RNS-competent species. Our data pinpoint the acquisition of *PACE* as a key event during the evolution of nodulation. Together with our discovery that multiple independent losses of *PACE* are associated with multiple losses of RNS within the FaFaCuRo clade, our data underpin the essential position of *PACE* in the evolutionary gain and loss of RNS.

Materials and Methods:

Bioinformatic analyses

Based on the phylogenetic classification of the RWP-RK gene family (Clavijo et al., 2015; Griesmann et al., 2018), 144 NIN/NLP genes were selected from 37 plant species and 13 orders ranging from monocotyledons to dicotyledons including the FaFaCuRo clade (**Figure 1 – Source Data 1**). For each selected gene, 3 kb of sequence upstream of the translational start site including promoter and 5'UTR region was defined and extracted from the corresponding species' genomic sequence, if contig length allowed it. If contig length was limiting, the longest possible sequence stretch was extracted. For the identification of a *cis*-regulatory element specific for *NIN* promoters of the FaFaCuRo clade, the tool MEME (http://meme-suite.org/tools/meme) was used in discriminative mode (option: "search given strand only", default parameters) with *NIN* promoter regions of only nodulating plants. The control group consisted of promoter regions of all *NIN* genes outside of the FaFaCuRo clade and all NLP genes listed in **Figure 1 – Source Data 1**. The highest scoring motif (E-value: 1.6e-058) was 27 bp long and contained the much shorter previously described *CYC-box* (Singh et al., 2014) (**Figure 1 – figure supplement 1A**).

To refine the conserved region in this motif, MEME analysis was performed again in normal mode (option: “search given strand only”, default parameters) with *NIN* promoters from only nodulating species. This analysis revealed that the most conserved nucleotides are found within 29 nucleotides (nucleotides 10 to 38 in **Figure 1 – figure supplement 1B**). The previous MEME analysis was repeated, but an exactly 29 nucleotides long motif was searched for (resulting in a motif in **Figure 1 – figure supplement 1C**) and the best scoring *NIN* paralog per searched species, i.e. lowest p-value per species were identified (**Figure 1 – Source Data 1**). In a final step, one best scoring *NIN* promoter region per nodulating species were analysed with MEME (option: “search given strand only”, default parameters) by searching for an exactly 29 nucleotides long motif. The resulting motif was named *PACE* (**Figure 1 – figure supplement 1D**). This final MEME run was done for two reasons: first in order to avoid a sequence bias towards a single species with multiple *NIN* paralog promoter regions (e.g. soybean); second to avoid a potential sequence bias generated by the promoter region of a *NIN* paralog that might be no longer functional and therefore has mutated sites in its promoter region due to positive selection.

As a control, the FIMO tool was used (http://meme-suite.org/tools/fimo, option: “scan given strand only”, default parameters, fdr < 0.1) to search all 144 *NIN* and *NLP* promoter regions (**Figure 1 – Source Data 1**). *PACE* was found within *NIN* promoter regions of all nodulating species analysed and two non-nodulating FaFaCuRo species (*Prunus persica* and *Ziziphus jujuba*) (**Figure 1 – Source Data 1**).

The presence or absence of *PACE* was further investigated in promoters of *NIN* and *NLPs* in an expanded database of 163 species covering all Viridiplantae lineages. Orthologs of the whole *NLP* family were retrieved using tBLASTn v2.11.0+ (Camacho et al., 2009) with reference sequences from *Medicago truncatula* as query and a cut-off e-value of 1e-10. Sequences were then aligned using MAFFT v7.380 (Katoh & Standley, 2013) with default parameters. Alignments were subjected to phylogenetic analysis to identify orthologs using Maximum Likelihood approach and the IQ-TREE v1.6.7 software (Nguyen et al., 2015). Prior to phylogenetic reconstruction, the best-fitting evolution model was determined for each alignment using ModelFinder (Kalyaanamoorthy et al., 2017) as implemented in IQ-TREE. Branch support was tested using 10,000 replicates of UltraFast Bootstraps using UFBoot2 (Hoang et al., 2018). For each identified ortholog, a 5 kb region upstream of the translational start site was extracted. The three different consensuses identified in the previous MEME analyses (**Figure 1 – figure supplement 1A, B, D**) were then searched in all *NLP* upstream regions using FIMO 5.0.2 and a q-value threshold of 0.1. If several motifs were identified in a given upstream region, only the one with the lowest q-value was conserved for further analysis (**Figure 1 – figure supplement 1E and 2** and **Figure 1 – Source Data 2**). *PACE* from

Parasponia andersonii (a nodulating species from Rosales) was identified in this analysis and included to generate the consensus in **Figure 1**.

Promoters of *ERN1* and *RAM1* genes were analysed independently of the previous analysis, using 87 plant genomes covering the main Angiosperms orders (**Supplementary file 1**). Orthologs of each gene were retrieved using tBLASTn v2.7.1+ (Camacho et al., 2009) with reference sequences from *Medicago truncatula* as query and a cut-off e-value of 1e-10. Sequences were then aligned using MAFFT v7.380 (Katoh & Standley, 2013) with default parameters. Alignments were subjected to phylogenetic analysis to identify orthologs using Maximum Likelihood approach and the IQ-TREE v1.6.7 software (Nguyen et al., 2015). Prior to phylogenetic reconstruction, the best-fitting evolution model was determined for each alignment using ModelFinder (Kalyaanamoorthy et al., 2017) as implemented in IQ-TREE. Branch support was tested using 10,000 replicates of UltraFast Bootstraps using UFBoot2 (Hoang et al., 2018). For each identified ortholog, regions upstream of the translational start site of different lengths (1 to 5 kb) were extracted. For each length of region upstream of the translational start site, sequences were analysed using MEME software v5.0.1 (Bailey & Elkan, 1994) with the following parameters: a motif size comprised between 5 - 45 bp and 5 - 25 bp for *ERN1* and *RAM1* respectively and a maximum number of discovered motifs of 20 (**Figure 1 – figure supplement 3 and 4**). In addition, MEME search was set on “zoops” mode, assuming that each sequence can contain zero or one occurrence of the motif.

Biological material

L. japonicus seed bags, bacterial strains and days post inoculation for each experiment are listed in **Supplementary file 2**.

Plant growth conditions and symbiotic inoculations

Lotus japonicus seeds were scarified and surface-sterilized as described (Gossmann et al., 2012) before germination on ½ Gamborg's B5 medium solidified with 0.8 % Bacto™ agar in square plates (12 x 12 x 1.7 cm) (Gamborg et al., 1968). Plates were kept in dark for three days before transferring to light condition in a Panasonic growth cabinet (MLR-352H-PE) at 24 °C under a 16 h/8 h light/dark regime (50 µmol·m-2·s-1). Six-days-old seedlings were (1) subject to hairy root transformation as described (Charpentier et al., 2008) (**Figure 2, 3 and 4**; **Figure 2 – figure supplement 1**; **Figure 3 – figure supplement 1, 3, 4, 5, 6, 7 and 8** and **Figure 4 – figure supplement 1**); or (2) transferred to Weck jars (SKU 745 or 743; J.Weck GmbH u. Co. KG) containing 300 ml of sand:vermiculite mixture (2:1) and 20 ml of a modified ¼ strength Hoagland’s medium with Fe-EDDHA used as iron source (Hoagland & Arnon, 1950) (**Figure 3 – figure supplement 1E**). For *in vivo* promoter expression analysis (**Figure 2**), transgenic roots expressing a kanamycin-resistance gene were kept on square plates supplemented with kanamycin (25 µg/ml) 10 days after *Agrobacterium rhizogenes* inoculation.

Plants with transformed roots were kept on 0.8% Bacto™ agar including a nitrogen-reduced version of FAB medium (500 µM $MgSO_4 \cdot 7H_2O$; 250 µM KH_2PO_4; 250 µM KCl; 250 µM $CaCl_2 \cdot 2H_2O$; 100 µM KNO_3; 25 µM Fe-EDDHA; 50 µM H_3BO_3; 25 µM $MnSO_4 \cdot H_2O$; 10 µM $ZnSO_4 \cdot 7H_2O$; 0.5 µM $Na_2MoO_4 \cdot 2H_2O$; 0.2 µM $CuSO_4 \cdot 5H_2O$; 0.2 µM $CoCl_2 \cdot 6H_2O$; pH 5.7) in square plates for 1 week before transferring to a growth chamber at 24 °C under a 16 h/8 h light/dark regime (275 µmol·m-2·s-1) in Weck jars (SKU 745 or 743) containing 300 ml of sand:vermiculite mixture (2:1) and 30 ml of nitrogen-reduced FAB medium containing *Mesorhizobium loti* MAFF 303099 *Ds*Red (*M. loti Ds*Red; **Figure 3 - 4**; **Figure 3 – figure supplement 1, 3, 4, 5, 6 and 7** and **Figure 4 – figure supplement 1**) or *M. loti* R7A CFP (**Figure 2**) set to a final optical density at 600 nm (OD_{600}) of 0.05. For **Figure 2 – figure supplement 1** and **Figure 3 – figure supplement 8**, plants were grown in Weck jars (SKU 745 or 743) containing 300 ml of sand:vermiculite mixture (2:1) and 60 ml of nitrogen-reduced FAB medium containing *M. loti Ds*Red or MAFF 303099 *lacZ* (*M. loti lacZ*) (OD_{600} = 0.01).

Cloning and DNA constructs

For the construction of promoter:*NIN* fusions for complementation experiments (**Figure 3**; **Figure 3 – figure supplement 2, 3, 4, 5, 6 and 7** and **Figure 4 – figure supplement 1**), the *NIN* genomic sequence without the 5' and 3'UTRs served as a cloning module. A 3 kb region of the *L. japonicus NIN* promoter plus the 244 bp *NIN* 5'UTR was cloned from *L. japonicus* Gifu and used for complementation experiments (**Figure 3**; **Figure 3 – figure supplement 2, 3, 4, 5, 6 and 7**), dual luciferase assays (**Figure 1 – figure supplement 5**), fluorimetric GUS assay (**Figure 1 – figure supplement 6**) and promoter activity analysis (**Figure 2**; **Figure 2 – figure supplement 1**). For all the other versions of the *L. japonicus NIN* promoter tested (**Figure 2, 3 and 4**; **Figure 1 – figure supplement 6**; **Figure 2 – figure supplement 1**; **Figure 3 – figure supplement 1, 2, 3, 4, 5, 6, 7 and 8** and **Figure 4 – figure supplement 1**), the *LjNIN* minimal promoter (98 bp (Singh et al., 2014)) plus the *LjNIN* 5'UTR was fused to 3' end of the promoter. A 472 bp region containing multiple cytokinin response elements and highly conserved in eight legume species was identified 5' of the *NIN* transcriptional start site by Liu et al. (Liu et al., 2019). We used this conserved region of 472 bp from *L. japonicus* and added flanking regions (192 bp upstream and 366 bp downstream; 2399 bp upstream and 2231 bp downstream, respectively) to obtain cytokinin element-containing regions of 1 kb and 5 kb (CE_{1kb} and CE_{5kb}, respectively). The *Solanum lycopersicum* gene ID Solyc01g112190.2.1 was identified as the closest homologue of *LjNIN* gene based on phylogenetic analysis (Griesmann et al., 2018), and is referred to as *SlNIN*. A 3 kb region of the *SlNIN* promoter plus the 238 bp *SlNIN* 5'UTR was cloned from *S. lycopersicum* cv. "Moneymaker" and *PACE* or *mPACE* (**Figure 1 – figure supplement 6A**) was inserted 184 bp upstream of the *SlNIN* 5'UTR and used for complementation experiments (**Figure 4** and **Figure 4 – figure supplement 1**), dual

luciferase assays (**Figure 1 – figure supplement 5**) and fluorimetric GUS assay (**Figure 1 – figure supplement 6**). A detailed description of constructs and a list of oligonucleotides can be found in **Supplementary file 3** and **Supplementary file 4**, respectively. Constructs were generated with the Golden Gate cloning system (Binder et al., 2014).

Imaging

Microscope and scanner settings as well as parameters for image acquisition are listed in **Supplementary file 5**.

Phenotypic analysis and quantification of infection events

Infected and non-infected nodules were discriminated by the presence and absence of a *Ds*Red signal (representing *M. loti Ds*Red) detected or not detected inside of the nodules, respectively. Presence or absence of bacteria was later confirmed by examination of sections of representative nodules. Infection threads (ITs) and *M. loti* entrapments in root hairs were detected by their *Ds*Red fluorescence (for microscope settings see **Supplementary file 5**).

For phenotypic analysis of *nin-15* (**Figure 3 – figure supplement 1C, F**), quantification was performed 21 days after inoculation (dpi) with *M. loti Ds*Red as follows: (1) the total number of nodules (including infected and non-infected) was determined under white light illumination (WLI); (2) the number of infected nodules and root hair ITs were counted as described above. Shoot dry weight was measured after drying the shoot at 60 °C for 1 h (**Figure 3 – figure supplement 1E**).

For complementation experiments of *nin-2* and *nin-15* (**Figure 3 and 4**; **Figure 3 – figure supplement 2, 3, 4, 5, 6 and 7** and **Figure 4 – figure supplement 1**), quantifications and sectioning were performed 21 or 35 dpi with *M. loti Ds*Red with the microscope settings listed in **Supplementary file 5** in the following order: (1) transgenic roots were identified by GFP fluorescence-emanating nuclei with a GFP filter; (2) infected nodules were counted as described above; (3) the total number of nodules (including infected and non-infected ones) was then determined under WLI; (4) the number of non-infected nodules was calculated by subtracting the number of infected nodules from the total number of nodules. To quantify infection events in root hairs, the number of bacterial entrapment and ITs in root hairs were counted on a 0.5 cm root piece for each transgenic root system, excised from a region where bacterial accumulation was detected by *Ds*Red fluorescence. Sectioning was performed on non-infected and infected nodules and the presence/absence of ITs and symbiosomes in cortical cells was examined. Nodule primordia and nodules were embedded in 6% low-melting agarose and sliced into 40 - 50 µm thick sections using a vibrating-blade microtome (Leica VT1000 S).

Transient expression in *Nicotiana benthamiana* leaves

Agrobacterium tumefaciens strain AGL1 carrying promoter:reporter fusions on T-DNA were infiltrated as described in (Cerri et al., 2012) with the acetosyringone concentration in the infiltration buffer modified to 150 µM. *A. tumefaciens* strains AGL1 and GV3101 containing plasmids *$35S_{pro}$:3xHA-Cyclops* (Singh et al., 2014) and *$35S_{pro}$:CCaMK$^{1-314}$-mOrange* (Takeda et al., 2015), respectively, were co-infiltrated with the reporter constructs as indicated. An AGL1 strain carrying a K9 plasmid constitutively expressing red fluorescent protein was used as needed to equalize the density of the *A. tumefaciens* suspension infiltrated per leaf, together with an *A. tumefaciens* strain carrying a plasmid for the expression of the viral P19 silencing suppressor to reduce post-transcriptional gene silencing (Voinnet et al., 2003) (**Figure 1 – figure supplement 5 and 6**). *N. benthamiana* leaf discs with a diameter of 0.5 cm were harvested 60 hours post infiltration and used for quantitative fluorometric GUS assay and dual luciferase assay.

Dual luciferase assay

The dual luciferase assay (**Figure 1 – figure supplement 5**) was based on the Dual-Luciferase® reporter assay system (Promega). *N. benthamiana* leaf discs were ground to a fine powder in liquid nitrogen in 2 ml Eppendorf Safe-Lock tube (1 leaf disc in each tube) and subsequently incubated 5 min at room temperature (RT) with 200 µl of the Passive lysis buffer (Promega catalog number E1910). The resulting crude leaf extract was centrifuged at 20,000 g for 2 min at RT. An aliquot of the supernatant was subjected to the dual luciferase assay according to manufacturer's instruction for Promega Dual Luciferase Kit (catalog number E1910) and chemiluminescence was quantified with a fluorescence plate reader (TECAN Infinite® 200 PRO; TECAN Group Ltd.) in white 96 well plates (Greiner Bio-One International GmbH). For each reporter construct, the promoter of interest was fused to the *Firefly* luciferase gene and constitutively expressed *Renilla* luciferase from the same vector was used for normalization (**Supplementary file 3**). The ratio of the two signals (*Firefly* luciferase signal to the *Renilla* luciferase) was calculated and normalized to the vector control. A total number of at least 4 biological and 2 technical replicates per indicated vector were analysed in at least 2 independent experiments.

Quantitative fluorometric GUS assay and analysis

Quantitative fluorometric GUS assays (**Figure 1 – figure supplement 6**) were performed as described (Jefferson, 1987) adapted to 96 well format. A total number of 4 to 8 leaf discs per indicated vector combination were analysed in at least 2 independent experiments performed in different weeks.

Promoter activity analysis

For promoter activity analyses with the *GUS* reporter gene (**Figure 2 – figure supplement 1A - F** and **Figure 3 – figure supplement 8**), transgenic nodule primordia and nodules were excised 10 - 14 dpi with *M. loti Ds*Red and stained for GUS activity using 5-bromo-4-chloro-3-indolyl-beta-D-glucuronic acid (X-Gluc; x-gluc.com) as catalytic substrate (Cerri et al., 2012) for 3 h at 37 °C. To visualise the root hair ITs together with the promoter activity with the *GUS* reporter gene (**Figure 2 – figure supplement 1G**), plants with transgenic root systems were inoculated with *M. loti lacZ*. Transgenic roots were first stained for GUS activity with X-Gluc for 3 h at 37 °C and then for *lacZ* expression with Magenta-Gal for 18 h at 28 °C (as described in (Cerri et al., 2012), which were visualized in blue and purple colour after staining, respectively). For promoter activity analyses with fluorescent reporters (**Figure 2**), transgenic root systems were harvested 10 - 14 dpi. Nodule primordia with bacterial infection at stage 3 or 4 (for stage description see main text) were selected by locating the CFP signal (*M. loti* R7A CFP) via rapid (around 10 seconds) Z-stack analysis with the confocal light scanning microscope (**Supplementary file 5**). Nodule primordia were sectioned and imaged as described in **Supplementary file 5**.

Data visualization and statistical analysis

Statistical analyses and data visualization were performed with RStudio 1.1. 383 (RStudio Inc.). Boxplots were used to display data in **Figure 4**; **Figure 1 – figure supplement 5 and 6**; **Figure 3 – figure supplement 1, 2, 3, 4 and 7** and **Figure 4 – figure supplement 1** (thick black or white lines: median; box: interquartile range; whiskers: lowest and highest data point within 1.5 interquartile range (IQR); black filled circles, data points inside 1.5 IQR; white filled circles, data points outside 1.5 IQR of the upper/lower quartile). The R package “beeswarm” with the method “center” was used to plot the individual data points for the boxplots (http://CRAN.R-project.org/package=beeswarm). The R package “agricolae” was used to perform ANOVA statistical analysis with post hoc Tukey and statistical results were displayed in small letters where different letters indicated statistical significance (https://cran.rproject.org/web/packages/agricolae/index.html). Tests applied are stated in the figure legend.

Data availability:

Correspondence and requests for materials should be addressed to Martin Parniske.

Acknowledgments:

The authors thank David Chiasson for providing the MAFF 303099 *lacZ* and R7A CFP *M. loti* strains, Niels Sandal and Jens Stougaard for providing the *nin-15* mutant. This project has received funding from the European Research Council (ERC) under the European Union’s

635 Seventh Framework Programme (FP7/2007-2013) under grant agreement n° 340904
636 (EvolvingNodules) which supported the work of MG and XG. MP acknowledges funding from
637 the German Research Foundation (DFG) in the context of the SFB924 'Molecular mechanisms
638 regulating yield and yield stability in plants' which supported the work of REA and CC and the
639 ANR-DFG project 'COME-IN' which supported the work of CC. This project has received
640 funding from the European Union's Horizon 2020 research and innovation programme under
641 the Marie Sklodowska-Curie grant agreement No H2020-MSCA-IF-2015-703186 to KV and
642 postdoctoral fellowship from Alexander von Humboldt Foundation to KV. PMD and JK belong
643 to the LRSV laboratory, which is part of the TULIP Laboratoire d'Excellence (LABEX) (ANR-
644 10-LABX-41). MH received funding from the JSPS KAKENHI Grant Number 17H06472.

645 **Author contributions:**

646 MG performed bioinformatic analysis of *NIN* promoters and discovered *PACE* presented in
647 **Figure 1** and **Figure 1 – figure supplement 1A - D**. CC performed *in vivo* expression analysis
648 presented in **Figure 2** and prepared all confocal and light microscopy images of root hairs and
649 nodule sections (**Figure 3 and 4**; **Figure 3 – figure supplement 5 and 6**; **Figure 4 – figure**
650 **supplement 1**). Complementation experiments of *nin-15* were performed by REA (**Figure 3B**
651 **- D**, **Figure 4A, 4C**; **Figure 3 – figure supplement 7**; **Figure 4 – figure supplement 1A, 1B**),
652 CC (**Figure 3 and 4**; **Figure 3 – figure supplement 7C**; **Figure 4 – figure supplement 1**)
653 and XG (**Figure 3D and 4B - C**; **Figure 3 – figure supplement 7**; **Figure 4 – figure**
654 **supplement 1C, 1D**). Complementation experiments of *nin-2* were performed by CC and XG
655 (**Figure 3A**; **Figure 3 – figure supplement 2, 3, 4, 5 and 6**). REA, CC and XG performed *nin-*
656 *15* mutant phenotyping (**Figure 3 – figure supplement 1**). XG performed transient expression
657 assays presented in **Figure 1 – figure supplement 6** and promoter expression analysis in
658 **Figure 2 – figure supplement 1** and **Figure 3 – figure supplement 8**. KV performed
659 transient expression assays presented in **Figure 1 – figure supplement 5** and drafted **Figure**
660 **1**. JK and PMD performed motif search in *ERN1*, *NIN* and *RAM1* promoters presented in
661 **Figure 1 – figure supplement 1E, 2, 3 and 4**. CC, XG, REA, KV, PMD, MH, MG and MP
662 formulated research hypothesis. CC, XG, REA, KV, MG and MP designed experiments. MP
663 conceived and supervised the project. XG and MP coordinated research activities. MP, CC
664 and XG wrote the manuscript and XG finalized all figures with inputs and comments from co-
665 authors.

666 **Competing interests:**

667 Authors declare no competing interests.

668 **References:**

669 Bailey, T. L., & Elkan, C. (1994). Fitting a mixture model by expectation maximization to

discover motifs in biopolymers. *Proc. 2nd Int. Conf. on Intelligent Systems for Molecular Biology*, *2*, 28–36. https://doi.org/citeulike-article-id:878292

Banba, M., Gutjahr, C., Miyao, A., Hirochika, H., Paszkowski, U., Kouchi, H., & Imaizumi-Anraku, H. (2008). Divergence of evolutionary ways among common sym genes: CASTOR and CCaMK show functional conservation between two symbiosis systems and constitute the root of a common signaling pathway. *Plant and Cell Physiology*, *49*(11), 1659–1671. https://doi.org/10.1093/pcp/pcn153

Bell, C. D., Soltis, D. E., & Soltis, P. S. (2010). The age and diversification of the angiosperms re-revisited. *American Journal of Botany*, *97*(8), 1296–1303. https://doi.org/10.3732/ajb.0900346

Binder, A., Lambert, J., Morbitzer, R., Popp, C., Ott, T., Lahaye, T., & Parniske, M. (2014). A modular plasmid assembly kit for multigene expression, gene silencing and silencing rescue in plants. *PLoS ONE*, *9*(2). https://doi.org/10.1371/journal.pone.0088218

Buecker, C., & Wysocka, J. (2012). Enhancers as information integration hubs in development: Lessons from genomics. *Trends in Genetics*, *28*(6), 276–284. https://doi.org/10.1016/j.tig.2012.02.008

Camacho, C., Coulouris, G., Avagyan, V., Ma, N., Papadopoulos, J., Bealer, K., & Madden, T. L. (2009). BLAST+: Architecture and applications. *BMC Bioinformatics*, *10*, 1–9. https://doi.org/10.1186/1471-2105-10-421

Carvalho, T. L. G., Balsemão-Pires, E., Saraiva, R. M., Ferreira, P. C. G., & Hemerly, A. S. (2014). Nitrogen signalling in plant interactions with associative and endophytic diazotrophic bacteria. *Journal of Experimental Botany*, *65*(19), 5631–5642. https://doi.org/10.1093/jxb/eru319

Cerri, M. R., Frances, L., Laloum, T., Auriac, M.-C., Niebel, A., Oldroyd, G. E. D., Barker, D. G., Fournier, J., & de Carvalho-Niebel, F. (2012). *Medicago truncatula* ERN transcription factors: regulatory interplay with NSP1/NSP2 GRAS factors and expression dynamics throughout rhizobial Infection. *Plant Physiology*, *160*(4), 2155–2172. https://doi.org/10.1104/pp.112.203190

Cerri, M. R., Wang, Q., Stolz, P., Folgmann, J., Frances, L., Katzer, K., Li, X., Heckmann, A. B., Wang, T. L., Downie, J. A., Klingl, A., de Carvalho-Niebel, F., Xie, F., & Parniske, M. (2017). The *ERN1* transcription factor gene is a target of the CCaMK/CYCLOPS complex and controls rhizobial infection in *Lotus japonicus*. *New Phytologist*, *215*(1), 323–337. https://doi.org/10.1111/nph.14547

Charpentier, M., Bredemeier, R., Wanner, G., Takeda, N., Schleiff, E., & Parniske, M.

(2008). *Lotus japonicus* Castor and Pollux are ion channels essential for perinuclear calcium spiking in legume root endosymbiosis. *Plant Cell*, *20*(12), 3467–3479. https://doi.org/10.1105/tpc.108.063255

Chen, C., Gao, M., Liu, J., & Zhu, H. (2007). Fungal symbiosis in rice requires an ortholog of a legume common symbiosis gene encoding a Ca^{2+}/calmodulin-dependent protein kinase. *Plant Physiology*, *145*(4), 1619–1628. https://doi.org/10.1104/pp.107.109876

Clavijo, F., Diedhiou, I., Vaissayre, V., Brottier, L., Acolatse, J., Moukouanga, D., Crabos, A., Auguy, F., Franche, C., Gherbi, H., Champion, A., Hocher, V., Barker, D., Bogusz, D., Tisa, L. S., & Svistoonoff, S. (2015). The *Casuarina NIN* gene is transcriptionally activated throughout *Frankia* root infection as well as in response to bacterial diffusible signals. *New Phytologist*, *208*(3), 887–903. https://doi.org/10.1111/nph.13506

D'Haeze, W., Gao, M., De Rycke, R., Van Montagu, M., Engler, G., & Holsters, M. (1998). Roles for azorhizobial nod factors and surface polysaccharides in intercellular invasion and nodule penetration, respectively. *Molecular Plant-Microbe, 11*(10), 999–1008. https://doi.org/10.1094/MPMI.1998.11.10.999

De Faria, S. M., Hay, G. T., & Sprent, J. I. (1988). Entry of rhizobia into roots of *Mimosa scabrella* bentham occurs between epidermal cells. *Microbiology*, *134*(8), 2291–2296. https://doi.org/10.1099/00221287-134-8-2291

Delaux, P. M., Radhakrishnan, G. V., Jayaraman, D., Cheema, J., Malbreil, M., Volkening, J. D., Sekimoto, H., Nishiyama, T., Melkonian, M., Pokorny, L., Rothfels, C. J., Sederoff, H. W., Stevenson, D. W., Surek, B., Zhang, Y., Sussman, M. R., Dunand, C., Morris, R. J., Roux, C., … Ane, J. M. (2015). Algal ancestor of land plants was preadapted for symbiosis. *Proceedings of the National Academy of Sciences of the United States of America*, *112*(43), 13390–13395. https://doi.org/10.1073/pnas.1515426112

Delaux, P. M., Varala, K., Edger, P. P., Coruzzi, G. M., Pires, J. C., & Ané, J. M. (2014). Comparative phylogenomics uncovers the impact of symbiotic associations on host genome evolution. *PLoS Genetics*, *10*(7). https://doi.org/10.1371/journal.pgen.1004487

Doyle, J. J. (2011). Phylogenetic perspectives on the origins of nodulation. *Molecular Plant-Microbe Interactions*, *24*(11), 1289–1295. https://doi.org/10.1094/MPMI-05-11-0114

Doyle, J. J. (2016). Chasing unicorns: nodulation origins and the paradox of novelty. *American Journal of Botany*, *103*(11), 1865–1868. https://doi.org/10.3732/ajb.1600260

Finan, T. M., Hirsch, A. M., Leigh, J. A., Johansen, E., Kuldau, G. A., Deegan, S., Walker, G. C., & Signer, E. R. (1985). Symbiotic mutants of *Rhizobium meliloti* that uncouple plant from bacterial differentiation. *Cell*, *40*(4), 869–877. https://doi.org/10.1016/0092-

8674(85)90346-0

Gage, D. J. (2002). Analysis of infection thread development using GFP- and *Ds*Red-expressing *Sinorhizobium meliloti*. *Journal of Bacteriology*, *184*(24), 7042–7046. https://doi.org/10.1128/JB.184.24.7042-7046.2002

Gamborg, O. L., Miller, R. A., & Ojima, K. (1968). Nutrient requirements of suspension cultures of soybean root cells. *Experimental Cell Research*, *50*(1), 151–158. https://doi.org/10.1016/0014-4827(68)90403-5

Geurts, R., Xiao, T. T., & Reinhold-Hurek, B. (2016). What does it take to evolve a nitrogen-fixing endosymbiosis? *Trends in Plant Science*, *21*(3), 199–208. https://doi.org/10.1016/j.tplants.2016.01.012

Gossmann, J. A., Markmann, K., Brachmann, A., Rose, L. E., & Parniske, M. (2012). Polymorphic infection and organogenesis patterns induced by a *Rhizobium leguminosarum* isolate from *Lotus* root nodules are determined by the host genotype. *New Phytologist*, *196*(2), 561–573. https://doi.org/10.1111/j.1469-8137.2012.04281.x

Griesmann, M., Chang, Y., Liu, X., Song, Y., Haberer, G., Crook, M., Billault-Penneteau, B., Lauressergues, D., Keller, J., Imanishi, L., Roswanjaya, Y., Kohlen, W., Pujic, P., Battenberg, K., Alloisio, N., Liang, Y., Hilhorst, H., Salgado, M., Hocher, V., … Cheng, S. (2018). Phylogenomics reveals multiple losses of the nitrogen-fixing root nodule symbiosis. *Science*, *13*(361). https://doi.org/10.1126/science.aat1743

Gutjahr, C., Banba, M., Croset, V., An, K., Miyao, A., An, G., Hirochika, H., Imaizumi-Anraku, H., & Paszkowski, U. (2008). Arbuscular mycorrhiza-specific signaling in rice transcends the common symbiosis signaling pathway. *The Plant Cell*, *20*(11), 2989–3005. https://doi.org/10.1105/tpc.108.062414

Hirsch, S., Kim, J., Muñoz, A., Heckmann, A. B., Downie, J. A., & Oldroyd, G. E. D. (2009). GRAS proteins form a DNA binding complex to induce gene expression during nodulation signaling in *Medicago truncatula*. *Plant Cell*, *21*(2), 545–557. https://doi.org/10.1105/tpc.108.064501

Hoagland, D. R., & Arnon, D. I. (1950). The water-culture method for growing plants without soil. Circular California Agricultural Experiment Station 347, ed. 2, Berkeley: University of California.

Hoang, D. T., Chernomor, O., von Haeseler, A., Minh, B. Q., & Le, S. V. (2018). UFBoot2: Improving the Ultrafast Bootstrap Approximation. *Molecular Biology and Evolution*, *35*(2), 518–522. https://doi.org/10.5281/zenodo.854445

771 Jefferson, R. A. (1987). Assaying chimeric genes in plants: The *GUS* gene fusion system.
772 *Plant Molecular Biology Reporter*, *5*(4), 387–405. https://doi.org/10.1007/BF02667740

773 Johansson, C., & Bergman, B. (1992). Early events during the establishment of the *Gunnera*
774 / *Nostoc* symbiosis. *Planta*, *188*(3), 403–413.

775 Kalyaanamoorthy, S., Minh, B. Q., Wong, T. K. F., Von Haeseler, A., & Jermiin, L. S. (2017).
776 ModelFinder: Fast model selection for accurate phylogenetic estimates. *Nature*
777 *Methods*, *14*(6), 587–589. https://doi.org/10.1038/nmeth.4285

778 Katoh, K., & Standley, D. M. (2013). MAFFT multiple sequence alignment software version
779 7: Improvements in performance and usability. *Molecular Biology and Evolution*, *30*(4),
780 772–780. https://doi.org/10.1093/molbev/mst010

781 Kistner, C., & Parniske, M. (2002). Evolution of signal transduction in intracellular symbiosis.
782 *Trends in Plant Science*, *7*(11), 511–518. https://doi.org/10.1016/S1360-
783 1385(02)02356-7

784 Kvon, E. Z., Kamneva, O. K., Melo, U. S., Barozzi, I., Osterwalder, M., Mannion, B. J.,
785 Tissières, V., Pickle, C. S., Plajzer-Frick, I., Lee, E. A., Kato, M., Garvin, T. H.,
786 Akiyama, J. A., Afzal, V., Lopez-Rios, J., Rubin, E. M., Dickel, D. E., Pennacchio, L. A.,
787 & Visel, A. (2016). Progressive loss of function in a limb enhancer during snake
788 evolution. *Cell*, *167*(3), 633–642. https://doi.org/10.1016/j.cell.2016.09.028

789 LeBauer, D., & Treseder, K. (2008). Nitrogen limitation of net primary productivity in
790 terrestrial ecosystems is globally distributed. *Ecology*, *89*(7), 371–379.
791 https://doi.org/10.1007/BF00153104

792 Li, H. L., Wang, W., Mortimer, P. E., Li, R. Q., Li, D. Z., Hyde, K. D., Xu, J. C., Soltis, D. E., &
793 Chen, Z. D. (2015). Large-scale phylogenetic analyses reveal multiple gains of
794 actinorhizal nitrogen-fixing symbioses in angiosperms associated with climate change.
795 *Scientific Reports*, *5*(January), 1–8. https://doi.org/10.1038/srep14023

796 Liu, J., & Bisseling, T. (2020). Evolution of *NIN* and *NIN-like* genes in relation to nodule
797 symbiosis. *Genes*, *11*(7), 1–15. https://doi.org/10.3390/genes11070777

798 Liu, J., Rutten, L., Limpens, E., Van Der Molen, T., Van Velzen, R., Chen, R., Chen, Y.,
799 Geurts, R., Kohlen, W., Kulikova, O., & Bisseling, T. (2019). A remote *cis*-regulatory
800 region is required for nin expression in the pericycle to initiate nodule primordium
801 formation in *Medicago truncatula*. *Plant Cell*, *31*(1), 68–83.
802 https://doi.org/10.1105/tpc.18.00478

803 Madsen, L. H., Tirichine, L., Jurkiewicz, A., Sullivan, J. T., Heckmann, A. B., Bek, A. S.,

804 Ronson, C. W., James, E. K., & Stougaard, J. (2010). The molecular network governing
805 nodule organogenesis and infection in the model legume *Lotus japonicus*. *Nature*
806 *Communications*, *1*(1). https://doi.org/10.1038/ncomms1009

807 Markmann, K., Giczey, G., & Parniske, M. (2008). Functional adaptation of a plant receptor-
808 kinase paved the way for the evolution of intracellular root symbioses with bacteria.
809 *PLoS Biology*, *6*(3), 0497–0506. https://doi.org/10.1371/journal.pbio.0060068

810 Masson-Boivin, C., & Sachs, J. L. (2018). Symbiotic nitrogen fixation by rhizobia — the roots
811 of a success story. *Current Opinion in Plant Biology*, *44*, 7–15.
812 https://doi.org/10.1016/j.pbi.2017.12.001

813 Murray, J. D., Karas, B. J., Sato, S., Tabata, S., Amyot, L., & Szczyglowski, K. (2007). A
814 cytokinin perception mutant colonized by *Rhizobium* in the absence of nodule
815 organogenesis. *Science*, *305*(5808), 101–104.

816 Nguyen, L. T., Schmidt, H. A., Von Haeseler, A., & Minh, B. Q. (2015). IQ-TREE: A fast and
817 effective stochastic algorithm for estimating maximum-likelihood phylogenies. *Molecular*
818 *Biology and Evolution*, *32*(1), 268–274. https://doi.org/10.1093/molbev/msu300

819 Ott, T., Van Dongen, J. T., Günther, C., Krusell, L., Desbrosses, G., Vigeolas, H., Bock, V.,
820 Czechowski, T., Geigenberger, P., & Udvardi, M. K. (2005). Symbiotic leghemoglobins
821 are crucial for nitrogen fixation in legume root nodules but not for general plant growth
822 and development. *Current Biology*, *15*(6), 531–535.
823 https://doi.org/10.1016/j.cub.2005.01.042

824 Parniske, M. (2000). Intracellular accommodation of microbes by plants: a common
825 developmental program for symbiosis and disease? *Curr Opin Plant Biol*, *3*, 320–328.

826 Parniske, M. (2018). Uptake of bacteria into living plant cells, the unifying and distinct feature
827 of the nitrogen-fixing root nodule symbiosis. *Current Opinion in Plant Biology*, *44*, 164–
828 174. https://doi.org/10.1016/j.pbi.2018.05.016

829 Pawlowski, K., & Demchenko, K. N. (2012). The diversity of actinorhizal symbiosis.
830 *Protoplasma*, *249*(4), 967–979. https://doi.org/10.1007/s00709-012-0388-4

831 Perrine-Walker, F. M., Lartaud, M., Kouchi, H., & Ridge, R. W. (2014). Microtubule array
832 formation during root hair infection thread initiation and elongation in the
833 *Mesorhizobium-Lotus* symbiosis. *Protoplasma*, *251*(5), 1099–1111.
834 https://doi.org/10.1007/s00709-014-0618-z

835 Peters, G., & Meeks, J. (1989). The *Azolla-Anabaena* symbiosis : basic biology. *Annu. Rev.*
836 *Plant Physiol. Plant Mol. Biol.*, *40*, 193–210.

837 Pimprikar, P., Carbonnel, S., Paries, M., Katzer, K., Klingl, V., Bohmer, M. J., Karl, L., Floss,
838 D. S., Harrison, M. J., Parniske, M., & Gutjahr, C. (2016). A CCaMK-CYCLOPS-DELLA
839 complex activates transcription of *RAM1* to regulate arbuscule branching. *Current*
840 *Biology*, *26*(8), 987–998. https://doi.org/10.1016/j.cub.2016.01.069

841 Redecker, D., Kodner, R., & Graham, L. E. (2000). Glomalean fungi from the Ordovician.
842 *Science*, *289*(5486), 1920–1921. https://doi.org/8819 [pii]

843 Remy, W., Taylort, T. N., Hass, H., & Kerp, H. (1994). Four hundred-million-year-old
844 vesicular arbuscular mycorrhizae. *Proceedings of National Academy of Sciences, USA*,
845 *91*(December), 11841–11843. https://doi.org/10.1073/pnas.91.25.11841

846 Schauser, L., Roussis, A., Stiller, J., & Stougaard, J. (1999). A plant regulator controlling
847 development of symbiotic root nodules. *Nature*, *402*(6758), 191–195.
848 https://doi.org/10.1038/46058

849 Singh, S., Katzer, K., Lambert, J., Cerri, M., & Parniske, M. (2014). CYCLOPS, A DNA-
850 binding transcriptional activator, orchestrates symbiotic root nodule development. *Cell*
851 *Host and Microbe*, *15*(2), 139–152. https://doi.org/10.1016/j.chom.2014.01.011

852 Soltis, D. E., Soltis, P. S., Morgant, D. R., Swensent, S. M., Mullin, B. C., Dowdi, J. M., &
853 Peter, G. M. (1995). Chloroplast gene sequence data suggest a single origin of the
854 predisposition for symbiotic nitrogen fixation in angiosperms. *Proceedings of National*
855 *Academy of Sciences, USA*, *92*(March), 2647–2651.
856 https://doi.org/10.1073/pnas.92.7.2647

857 Soyano, T., & Hayashi, M. (2014). Transcriptional networks leading to symbiotic nodule
858 organogenesis. *Current Opinion in Plant Biology*, *20*, 146–154.
859 https://doi.org/10.1016/j.pbi.2014.07.010

860 Soyano, T., Kouchi, H., Hirota, A., & Hayashi, M. (2013). NODULE INCEPTION directly
861 targets *NF-Y* bubunit genes to regulate essential processes of root nodule development
862 in *Lotus japonicus*. *PLoS Genetics*, *9*(3). https://doi.org/10.1371/journal.pgen.1003352

863 Sprent, J. I. (2007). Evolving ideas of legume evolution and diversity: A taxonomic
864 perspective on the occurrence of nodulation: Tansley review. *New Phytologist*, *174*(1),
865 11–25. https://doi.org/10.1111/j.1469-8137.2007.02015.x

866 Sprent, J. I., Ardley, J., & James, E. K. (2017). Biogeography of nodulated legumes and their
867 nitrogen-fixing symbionts. *New Phytologist*, *215*(1), 40–56.
868 https://doi.org/10.1111/nph.14474

869 Takeda, N., Handa, Y., Tsuzuki, S., Kojima, M., Sakakibara, H., & Kawaguchi, M. (2015).

Gibberellins interfere with symbiosis signaling and gene expression and alter colonization by arbuscular mycorrhizal fungi in *Lotus japonicus*. *Plant Physiology*, *167*(2), 545–557. https://doi.org/10.1104/pp.114.247700

Van Spronsen, P. C., Grønlund, M., Bras, C. P., Spaink, H. P., & Kijne, J. W. (2001). Cell biological changes of outer cortical root cells in early determinate nodulation. *Molecular Plant-Microbe Interactions*, *14*(7), 839–847. https://doi.org/10.1094/MPMI.2001.14.7.839

van Velzen, R., Doyle, J. J., & Geurts, R. (2019). A resurrected scenario: single gain and massive loss of nitrogen-fixing nodulation. *Trends in Plant Science*, *24*(1), 49–57. https://doi.org/10.1016/j.tplants.2018.10.005

van Velzen, R., Holmer, R., Bu, F., Rutten, L., van Zeijl, A., Liu, W., Santuari, L., Cao, Q., Sharma, T., Shen, D., Roswanjaya, Y., Wardhani, T. A. K., Kalhor, M. S., Jansen, J., van den Hoogen, J., Güngör, B., Hartog, M., Hontelez, J., Verver, J., … Geurts, R. (2018). Comparative genomics of the nonlegume *Parasponia* reveals insights into evolution of nitrogen-fixing rhizobium symbioses. *Proceedings of the National Academy of Sciences*, *115*(20), E4700–E4709. https://doi.org/10.1073/pnas.1721395115

Vernié, T., Kim, J., Frances, L., Ding, Y., Sun, J., Guan, D., Niebel, A., Gifford, M. L., de Carvalho-Niebel, F., & Oldroyd, G. E. D. (2015). The NIN transcription factor coordinates diverse nodulation programs in different tissues of the *Medicago truncatula* root. *The Plant Cell*, *27*(12), 3410–3424. https://doi.org/10.1105/tpc.15.00461

Voinnet, O., Rivas, S., Mestre, P., & Baulcombe, D. (2003). An enhanced transient expression system in plants based on suppression of gene silencing by the p19 protein of tomato bushy stunt virus. *The Plant Journal*, *33*, 949–956.

Wang, H., Moore, M. J., Soltis, P. S., Bell, C. D., Brockington, S. F., Alexandre, R., Davis, C. C., Latvis, M., Manchester, S. R., & Soltis, D. E. (2009). Rosid radiation and the rapid rise of angiosperm-dominated forests. *Proceedings of the National Academy of Sciences*, *106*(10), 3853–3858. https://doi.org/10.1073/pnas.0813376106

Wittkopp, P., & Kalay, G. (2011). *Cis*-regulatory elements: molecular mechanisms and evolutionary processes underlying divergence. *Nat Rev Genet*, *13*(1), 59–69. https://doi.org/10.1038/nrg3095

Xiao, A., Yu, H., Fan, Y., Kang, H., Ren, Y., Huang, X., Gao, X., Wang, C., Zhang, Z., Zhu, H., & Cao, Y. (2020). Transcriptional regulation of *NIN* expression by IPN2 is required for root nodule symbiosis in *Lotus japonicus*. *New Phytologist*, *227*(2), 513–528. https://doi.org/10.1111/nph.16553

Yano, K., Yoshida, S., Muller, J., Singh, S., Banba, M., Vickers, K., Markmann, K., White, C., Schuller, B., Sato, S., Asamizu, E., Tabata, S., Murooka, Y., Perry, J., Wang, T. L., Kawaguchi, M., Imaizumi-Anraku, H., Hayashi, M., & Parniske, M. (2008). CYCLOPS, a mediator of symbiotic intracellular accommodation. *Proceedings of the National Academy of Sciences*, *105*(51), 20540–20545. https://doi.org/10.1073/pnas.0806858105

Yoon, H. J., Hossain, M. S., Held, M., Hou, H., Kehl, M., Tromas, A., Sato, S., Tabata, S., Andersen, S. U., Stougaard, J., Ross, L., & Szczyglowski, K. (2014). *Lotus japonicus SUNERGOS1* encodes a predicted subunit A of a DNA topoisomerase VI that is required for nodule differentiation and accommodation of rhizobial infection. *Plant Journal*, *78*(5), 811–821. https://doi.org/10.1111/tpj.12520

Yoro, E., Suzaki, T., Toyokura, K., Miyazawa, H., Fukaki, H., & Kawaguchi, M. (2014). A positive regulator of nodule organogenesis, NODULE INCEPTION, acts as a negative regulator of rhizobial infection in *Lotus japonicus*. *Plant Physiology*, *165*(2), 747–758. https://doi.org/10.1104/pp.113.233379

Zhu, H., Chen, T., Zhu, M., Fang, Q., Kang, H., Hong, Z., & Zhang, Z. (2008). A novel ARID DNA-binding protein interacts with SymRK and is expressed during early nodule development in *Lotus japonicus*. *Plant Physiology*, *148*(1), 337–347. https://doi.org/10.1104/pp.108.119164

Additional references:

Handberg, K. & Stougaard, J. (1992). *Lotus japonicus*, an autogamous, diploid legume species for classical and molecular genetics. *Plant J*ournal, *2*(4), 487–496. https://doi.org/10.1111/j.1365-313X.1992.00487.x

Leong, J. M., Nunes-Duby, S., Lesser, C. F., Youderian, P., Susskind, M. M., Landy, A. (1985). The Φ80 and P22 attachment sites. Primary structure and interaction with *Escherichia coli* integration host factor. *Journal of Biological Chemistry 260*(7), 4468–4477.

Maekawa, T., Maekawa-Yoshikawa, M., Takeda, N., Imaizumi-Anraku, H., Murooka, Y., Hayashi, M. (2009). Gibberellin controls the nodulation signaling pathway in *Lotus japonicus*. *Plant Journal, 58*(2), 183–194. https://doi.org/10.1111/j.1365-313X.2008.03774.x

Małolepszy, A., Mun, T., Niels, S., Gupta, V., Dubin, M., Urbański, D., Shah, N., Bachmann, A., Fukai, E., Hirakawa, H., Tabata, S., Nadzieja, M., Markmann, K., Su, J., Umehara,

938 Y., Soyano, T., Miyahara, A., Sato, S., Hayashi, M., Stougaard, J., Andersen, S. U.
939 (2016). The *LORE1* insertion mutant resource. *Plant Journal, 88*(2), 306–317.
940 https://doi.org/10.1111/tpj.13243

941 Stevens, P. F. (2001 onwards). Angiosperm phylogeny website. Version 14, July 2017
942 http://www.mobot.org/MOBOT/research/APweb/.

Supplementary Figures:

Figure 1 – figure supplement 1 | Discovery of *PACE* by MEME analyses. (**A - D**) Consensus sequence of the Position Weight Matrix identified by MEME analyses using the regions upstream of the translational start site (ATG) thus representing the promoters and 5'UTRs of *NIN* and *NLP* genes from 37 angiosperm species (see Methods): (**A**) in a discriminative search for a motif that is present in 3 kb upstream regions of the *NIN* genes from nodulating FaFaCuRo species, but absent in 3 kb upstream regions of the *NIN* genes from species outside of the FaFaCuRo clade and absent in the 3 kb upstream regions of *NLP* genes; (**B**) in an independent, non-discriminative search in the 3 kb upstream regions of the *NIN* genes from nodulating species revealing that the most conserved nucleotides span a larger region than (**A**); (**C**) the resulted most conserved 29 nucleotides derived from upstream regions of *NIN* genes of nodulating FaFaCuRo species; (**D**) the resulted most conserved 29 nucleotides (*PACE*) derived from the upstream region of one representative *NIN* gene per species of nodulating FaFaCuRo species. (**E**) Motif analyses by FIMO using the upstream regions of the *NIN* and *NLP* genes from an expanded list of 163 species (see Methods). Left: pruned tree from the whole *NLP* tree (demarcated in the black rectangle in **Figure 1 – figure supplement 2**) corresponding to the *NIN* orthologs. Right: three versions of consensus sequence (left to right, (**A, B and D**), respectively) were used to retrieve motifs from the 5 kb upstream region of *NIN* genes *via* FIMO search, the output of which is displayed underneath the consensus sequences. Sequence names of nodulating species are coloured in blue. Blank lines represent the absence of significant motifs.

Figure 1 – figure supplement 2 | *PACE* is present exclusively in the FaFaCuRo clade. Motif analyses by FIMO using the using the regions upstream of the translational start site (ATG) thus representing the promoters and 5'UTRs of the *NIN* and *NLP* genes from an expanded list of 163 species (see Methods). Left: Maximum likelihood tree of *NLP* family (model: GTR+F+R10) of 163 species (**Figure 1 – Source Data 2**). Tree was rooted on the Charophytes algae *Klebsormidium nitens*. Black box demarcates the area that is displayed in **Figure 1 – figure supplement 1E**. Blank lines represent the absence of significant motifs. Sequence names of nodulating species are coloured in blue. The different NLP clades are indicated by branch colours and named according to the *Arabidopsis thaliana* nomenclature. Right: three versions of consensus sequence (left to right, **Figure 1 – figure supplement 1A, 1B and 1D**, respectively) were used to retrieve motifs from the 5 kb upstream region of *NIN* genes via FIMO search, the output of which is displayed underneath the consensuses sequences.

Figure 1 – figure supplement 3 | The presence of a motif encompassing the previously identified Cyclops binding site within the regions upstream of the translational start

site (ATG) thus representing the promoters and 5'UTRs of *ERN1* genes extends beyond the FaFaCuRo clade. (**A**) Maximum likelihood of *ERN1/ERN2* (model: JTT+F+R5) from 87 species (**Supplementary file 1**) based on protein sequences. Tree was rooted using sequences from the *ERN1/ERN2* paralog *ERN3* (outgroup clade collapse and indicated by grey triangle marked "Outgroup"). Species belonging to the monophyletic FaFaCuRo clade (Stevens, 2017) are indicated by thicker black branches. *ERN1* and *ERN2* subclades are indicated. Sequence names of nodulating species are coloured in blue. These conserved motifs identified by MEME analyses in the 3 kb upstream regions were aligned and displayed next to species names. While the presence of a conserved Cyclops binding site containing motif in species outside of the FaFaCuRo clade is consistent with the role of *RAM1* in arbuscular mycorrhizal symbiosis, a function of *ERN1* in arbuscular mycorrhizal symbiosis has not been described and suggests a yet unidentified function of *ERN1* outside of the FaFaCuRo clade. (**B**) Consensus sequence of the Position Weight Matrix identified by MEME analyses of all the species. (**C**) Consensus sequence of the Position Weight Matrix identified by MEME analyses when analysing only the nodulating species.

Figure 1 – figure supplement 4 | The presence of a motif encompassing the previously identified Cyclops binding site within the regions upstream of the translational start site (ATG) thus representing the promoters and 5'UTRs of *RAM1* genes extends beyond the FaFaCuRo clade. (**A**) Maximum likelihood of *RAM1* (model: JTT+F+R4) from 87 species (**Supplementary file 1**) engaging in arbuscular mycorrhizal symbiosis. Tree was rooted on the early-diverging angiosperm *Amborella trichopoda*. Species belonging to the monophyletic FaFaCuRo clade (Stevens, 2017) are indicated by thicker black branches. Sequence names of nodulating species are coloured in blue. These conserved motifs identified by MEME analyses in the 3 kb upstream regions are aligned and displayed next to species names. Blank lines represent the absence of identified motif due to genome contiguity issues. (**B**) Consensus sequence of the Position Weight Matrix identified by MEME analyses when analysing all the mycorrhizal species. (**C**) Consensus sequence of the Position Weight Matrix identified by MEME analyses when analysing only the nodulating species.

Figure 1 – figure supplement 5 | Transcriptional activation of *NIN promoter:Firefly luciferase* reporter gene by CCaMK$^{1-314}$/Cyclops is restricted to *NIN* promoters from species of the FaFaCuRo clade. *Nicotiana benthamiana* leaf cells were transformed with T-DNAs carrying a *Firefly luciferase* reporter gene driven by either of the indicated promoters in tandem with the *AtACT2*$_{pro}$:*Renilla luciferase* reporter fusion that provides a quantitative internal standard. (**A**) List of species within the FaFaCuRo clade (light red shade) and outside (light grey shade) and abbreviations. (**B**) Reporter gene activation by *L. japonicus* CCaMK$^{1-314}$/Cyclops via *NIN* promoters (*NIN*$_{pro}$) originating from listed species. (**C**) Comparison of the

transactivation potential of Cyclops versions from *L. japonicus* and *S. lycopersicum*. Note that the expression of the *Firefly luciferase* reporter gene driven by $LjNIN_{pro}$, the *RAM1* promoters from *L. japonicus* and *S. lycopersicum* ($LjRAM1_{pro}$ and $SlRAM1_{pro}$, respectively) was induced in the presence of $CCaMK^{1-314}$/Cyclops regardless of the origin of Cyclops. In contrast, the transactivation failed with the *SlNIN* promoter (panel (**A**)). The applied statistical method was ANOVA with *post hoc* Tukey: (**B**), $F_{14,214} = 71.07$, $p < 2x10^{-16}$; (**C**), plots from left to right: $F_{5,18} = 20.58$, $p = 7.14x10^{-7}$; $F_{5,18} = 25.38$, $p = 1.45x10^{-7}$ and $F_{5,18} = 40.49$, $p = 3.55x10^{-9}$, respectively. Different small letters indicate significant differences.

Figure 1 – figure supplement 6 | *PACE* sequence variants from species across the FaFaCuRo clade were able to functionally replace *L. japonicus PACE* in a $LjNIN_{pro}$*:GUS* reporter fusion. *N. benthamiana* leaf cells were transformed with T-DNAs carrying a *GUS* reporter gene driven by either of the indicated promoters: (**A**) the *L. japonicus NIN* promoter (NIN_{pro}), the *LjNIN* promoter with *PACE* mutated or deleted (NIN_{pro}*::mPACE* and NIN_{pro}*::ΔPACE*, respectively), or *PACE* sequence variants from the nodulating FaFaCuRo species fused to the *LjNIN* minimal promoter ($NINmin_{pro}$); (**B**) chimeric promoters where *LjPACE* in the *LjNIN* promoter was replaced with either one of the *PACE* variants from species tested in (**A**) or from non-nodulating FaFaCuRo species including the *Juglans regia PACE-like* motif (*JrPACE-like*); (**C**) the *S. lycopersicum NIN* promoter ($SlNIN_{pro}$), the *SlNIN* promoter with *LjPACE* ($SlNIN_{pro}$*::PACE*) or *mPACE* ($SlNIN_{pro}$*::mPACE*) inserted. For species abbreviations see **Figure 1 – figure supplement 5A**. Note in (**A**) that the deletion or mutation of *PACE* in *LjNIN* promoter resulted in a drastic reduction in reporter gene expression and in (**C**) insertion of *LjPACE* but not *mPACE* into the *S. lycopersicum* promoter confers transactivation by $CCaMK^{1-314}$/Cyclops. The applied statistical method was ANOVA with *post hoc* Tukey: (**A**) $F_{20,144} = 51.38$, $p < 2x10^{-16}$; (**B**), $F_{18,166} = 149.1$, $p < 2x10^{-16}$; (**C**) $F_{7,62} = 30.5$, $p = 7.02x10^{-7}$. Different small letters indicate significant difference. n.d., not determined.

Figure 2 – figure supplement 1 | Spatio-temporal *GUS* expression driven by *PACE* and the *NIN* promoter in *L. japonicus* roots during the bacterial infection process. *L. japonicus* wild-type hairy roots were transformed with T-DNAs carrying a $Ubq10_{pro}$*:NLS-GFP* transformation marker together with a *GUS* reporter gene driven by either of the indicated promoters: (**A**) the 3 kb *LjNIN* promoter (NIN_{pro}); the *LjNIN* promoter with *PACE* (**B**) mutated ($LjNIN_{pro}$*::mPACE*) or (**C**) deleted (NIN_{pro}*::ΔPACE*); (**D**) *PACE* fused to the *LjNIN* minimal promoter (*PACE:*$NINmin_{pro}$) or (**E**) the *LjNIN* minimal promoter ($NINmin_{pro}$). The progression of bacterial infection was determined by the *Ds*Red signal 10 - 14 days post inoculation (dpi) with *M. loti Ds*Red. Nodules undergoing different stages of infection (panels I to IV) were stained with X-Gluc to reveal the *GUS* expression pattern. Note the overlapping bacterial invasion zone and *PACE:*$NINmin_{pro}$*:GUS* expression in early infection stages (red and blue

arrowheads in (**D**)) as well as the differences between *PACE:NINmin$_{pro}$:GUS* and the much broader *NIN$_{pro}$:GUS* expression at that stage (red and blue arrows in (**A**)). Red arrow and arrowheads: *M. loti Ds*Red. Blue arrow and arrowheads: GUS activity in root hairs bearing ITs and nodule primordia, respectively. The *NINmin$_{pro}$:GUS* fusion gave only rarely detectable signal, and if so in the vasculature (yellow arrowhead in (**E**)). Only pictures taken under white light illumination (WLI) are displayed for nodules in panel VI to reveal the pink colour of leghemoglobin, characteristic for mature and fully infected nodules. Note that *PACE:NINmin$_{pro}$:GUS* expression was absent at this stage, whereas the *NIN$_{pro}$:GUS* resulted in strong blue staining in the nodule regardless of the presence of *PACE* (compare panel IV in (**D**) and (**A - C**)). (**F**) Quantification of transgenic root systems exhibiting *GUS* expression in different cell types and tissues exemplarily displayed in (**A - E**). (**G**) *PACE* drove *GUS* reporter gene expression in the central tissue of primordia and nodules, but was not sufficient for expression in root hairs. Transgenic roots carrying promoter:GUS fusions same as in (**A, D and E**) were inoculated with *M. loti lacZ* and dual-stained with X-Gluc and Magenta-Gal. Purple: *M. loti lacZ*. Blue: GUS activity. Note the co-existence of blue and purple staining in root hairs on roots transformed by *NIN$_{pro}$:GUS*, but not that transformed by *PACE:NINmin$_{pro}$:GUS*. Bars, 250 µm.

Figure 3 – figure supplement 1 | *L. japonicus nin-15* mutant phenotype. (**A**) A representative picture of *L. japonicus* wild-type (WT, left) and *nin-15* (right) plants 21 dpi with *M. loti Ds*Red. (**B**) Position of the *Lotus Retrotransposon 1* (*LORE1*) insertion within the *NIN* promoter in the *nin-15* mutant. (**C**) Representative pictures of *nin-15* root hairs and nodule sections 21 dpi with *M. loti Ds*Red. Forty-nine plants with a total number of 436 nodules were analysed: only four plants bore one or two IT(s) within root hairs and seven plants bore one or two infected nodule(s). Deformed or curled root hairs in the presence of *M. loti Ds*Red were abundant but infection threads were rarely found. Arrowheads: uninfected nodules. Unlabelled bars, 100 µm. (**D - E**) Phenotype of *nin-15* in the presence of a symbiosis-independent nitrogen source (15 mM KNO_3) for 28 days. (**D**) Pictures documenting the healthy status of *L. japonicus* WT and *nin-15* plants (compare (**D**) and (**A**)) and (**E**) quantitative assessment of parameters displayed in boxplots. Thirty plants per genotype were analysed. Each dot represents one plant. Lateral root density: number of lateral roots/primary root length (cm). The applied statistical method was pairwise *t*-test: $*p < 0.05$; $**p < 0.01$; n.s.: not significant. (**F**) Segregation analysis of *nin-15.* The applied statistical method was ANOVA with *post hoc* Tukey: $F_{3,120} = 84.1$, $p = 2x10^{-16}$. Different small letters indicate significant difference. (**G**) Representative pictures of *nin-15* plants with hairy roots transformed with the *NIN* gene driven by the *L. japonicus NIN* minimal promoter (*NINmin$_{pro}$*) or the 3 kb *NIN* promoter (*NIN$_{pro}$*) 24 dpi with *M. loti Ds*Red. WLI: white light illumination.

Figure 3 – figure supplement 2 | The *CYC-box* and flanking sequences of *PACE* are required for the complete restoration of the bacterial infection process in the *L. japonicus nin-2* mutant. *nin-2* roots were transformed with T-DNAs carrying a $Ubq10_{pro}$*:NLS-GFP* transformation marker in tandem with the *LjNIN* gene driven by either of the following promoter versions: the cytokinin element-containing region of 1 kb (CE_{1kb}) fused to the 3 kb or 9 kb *LjNIN* promoter (CE_{1kb}*:*NIN_{pro} or CE_{1kb}*:*NIN_{9kbpro}, respectively); CE_{1kb}*:*NIN_{pro} or CE_{1kb}*:*NIN_{9kbpro} with *PACE* mutated (CE_{1kb}*:*NIN_{pro}*::mPACE* or CE_{1kb}*:*NIN_{9kbpro}*::mPACE*, respectively); CE_{1kb}*:*NIN_{pro} carrying a mutated Cyclops binding site (*CYC-box*) (CE_{1kb}*:*NIN_{pro}*::mbox*); CE_{1kb}*:*NIN_{pro} carrying mutated sequences flanking the *CYC-box* in *PACE* (CE_{1kb}*:*NIN_{pro}*::mflanking*); CE_{1kb} fused to the *LjNIN* minimal promoter (CE_{1kb}*:*$NINmin_{pro}$); CE_{1kb} fused to *PACE* and to $NINmin_{pro}$ (CE_{1kb}*:PACE:*$NINmin_{pro}$); NIN_{pro}, *PACE:*$NINmin_{pro}$ or $NINmin_{pro}$. (**A**) Representative overview pictures of transgenic root systems. Roots were analysed 21 dpi with *M. loti Ds*Red. White asterisks and arrowheads: infected and non-infected nodules, respectively. Bars, 2 mm. (**B - C**) Boxplots displaying the number of root hair ITs or infected nodules and the percentage of root hair ITs among total infection events (sum of bacterial entrapments and ITs). Each dot represents one transgenic *nin-2* root system or root piece. *L. japonicus* WT roots transformed with NIN_{pro}*:NIN* or CE_{1kb}*:*NIN_{pro}*:NIN* were included as controls. Note the loss of restoration of nodules and IT formation associated with the mutation of *PACE* or only the *CYC-box* in *PACE*; and the reduction of same when sequences flanking the *CYC-box* in *PACE* were mutated. n: number of transgenic root systems or root pieces analysed. Numbers above the boxplots: the value of individual data points outside of the plotting area. n.d.: not determined. WLI: white light illumination.

Figure 3 – figure supplement 3 | The *CYC-box* and flanking sequences of *PACE* are required for the complete restoration of the bacterial infection process in the *L. japonicus nin-2* mutant. Roots were from a subset of plants from the same experiment depicted in **Figure 3 – figure supplement 2** but analysed 35 dpi with *M. loti Ds*Red. (**A - B**) Boxplots displaying the number of root hair ITs or infected nodules and the percentage of root hair ITs among total infection events (sum of bacterial entrapments and ITs). Each dot represents one transgenic *nin-2* root system or root piece. *L. japonicus* WT roots transformed with NIN_{pro}*:NIN* or CE_{1kb}*:*NIN_{pro}*:NIN* were included as controls. Note that the results follow the same trend as those obtained 21 dpi with *M. loti Ds*Red (**Figure 3 – figure supplement 2**). n: number of transgenic root systems or root pieces analysed. Numbers above the boxplots: the value of individual data points outside of the plotting area.

Figure 3 – figure supplement 4 | The *CYC-box* and flanking sequences of *PACE* are required for the complete restoration of the bacterial infection process but are dispensable for the nodule organogenesis process in the *L. japonicus nin-2* mutant.

nin-2 roots were transformed with T-DNAs carrying a *Ubq10$_{pro}$:NLS-GFP* transformation marker in tandem with the *LjNIN* gene driven by either of the following promoter versions: the cytokinin element-containing region of 5 kb (*CE$_{5kb}$*) fused to the 3 kb *LjNIN* promoter (*CE$_{5kb}$:NIN$_{pro}$*); *CE$_{5kb}$:NIN$_{pro}$* with *PACE* mutated (*CE$_{5kb}$:NIN$_{pro}$::mPACE*); *CE$_{5kb}$:NIN$_{pro}$* carrying a mutated Cyclops binding site (*CYC-box*) (*CE$_{5kb}$:NIN$_{pro}$::mbox*); *CE$_{5kb}$:NIN$_{pro}$* carrying mutated sequences flanking the *CYC-box* in *PACE* (*CE$_{5kb}$:NIN$_{pro}$::mflanking*); *CE$_{5kb}$* fused to the *LjNIN* minimal promoter (*CE$_{5kb}$:NINmin$_{pro}$*); *CE$_{5kb}$* fused to *PACE* and to *NINmin$_{pro}$* (*CE$_{5kb}$:PACE:NINmin$_{pro}$*) or *NIN$_{pro}$*. (**A**) Representative overview pictures of transgenic root systems. Roots were analysed 21 dpi with *M. loti Ds*Red. White asterisks and arrowheads: infected and non-infected nodules, respectively. Bars, 2 mm. (**B**) Boxplots displaying the number of infected nodules, the percentage of infected nodules among total organogenesis events (sum of infected and non-infected nodules) and the number of organogenesis events. (**C**) Boxplots displaying the number of root hair ITs and the percentage of root hair ITs among total infection events (sum of bacterial entrapments and ITs). Each dot represents one transgenic *nin-2* root system or root piece. *L. japonicus* WT roots transformed with *NIN$_{pro}$:NIN* or *CE$_{5kb}$:NIN$_{pro}$:NIN* were included as controls. Note that the mutation of *PACE* or only the *CYC-box* in *PACE* led to an almost complete loss of IT formation and infected nodules per root system while nodule organogenesis was not significantly reduced; and that mutation of sequences flanking the *CYC-box* in *PACE* led to a reduction of the number of infected nodules per root systems. n: number of transgenic root systems or root pieces analysed. Numbers above the boxplots: the value of individual data points outside of the plotting area. n.a.: not applicable. WLI: white light illumination.

Figure 3 – figure supplement 5 | The *CYC-box* and flanking sequences of *PACE* are required for the complete restoration of the bacterial infection process but are dispensable for the nodule organogenesis process in the *L. japonicus nin-2* mutant. Pictures of nodule sections or roots from *L. japonicus nin-2* roots 21 dpi with *M. loti Ds*Red from the same experiments depicted in **Figure 3 – figure supplement 2** (**A**) and **Figure 3 – figure supplement 4** (**B**). Nodule sections from *L. japonicus* WT roots transformed with *NIN$_{pro}$:NIN* and *CE$_{5kb}$NIN$_{pro}$:NIN* were included for comparison. Note that when the cytokinin element-containing region of 1 kb was fused to *NIN$_{pro}$* nodule organogenesis was abolished by mutation of *PACE* or only the *CYC-box* in *PACE* and that these mutations did not abolish organogenesis when the cytokinin element-containing region of 5 kb was fused to *NIN$_{pro}$*. Bars, 100 µm.

Figure 3 – figure supplement 6 | The *CYC-box* and flanking sequences of *PACE* are required for the complete restoration of the bacterial infection process in the *L. japonicus nin-2* mutant. Pictures of nodule sections or roots from *L. japonicus nin-2* roots 35

dpi with *M. loti Ds*Red from the same experiments depicted in **Figure 3 – figure supplement 3**. Upper left corner: a nodule section from a *L. japonicus* WT root transformed with NIN_{pro}*:NIN* was included for comparison. Bars, 100 µm.

Figure 3 – figure supplement 7 | *PACEs* from FaFaCuRo species are functionally equivalent in restoring bacterial infection in the *L. japonicus nin-15* mutant. *L. japonicus nin-15* roots were transformed with T-DNAs carrying a $Ubq10_{pro}$*:NLS-GFP* transformation marker in tandem with the *LjNIN* gene driven by either of the following promoters: (**A**) the 3 kb *LjNIN* promoter (NIN_{pro}), the *LjNIN* minimal promoter ($NINmin_{pro}$), the 3 kb *LjNIN* promoter with *PACE* deleted (NIN_{pro}*::ΔPACE*) or mutated (NIN_{pro}*::mPACE*); (**B**) the 3 kb *LjNIN* promoter with *LjPACE* replaced with either of the *PACE* sequence variants from nodulating or non-nodulating FaFaCuRo species and analysed 21 dpi with *M. loti Ds*Red. (**A - B**) Representative overview pictures of *nin-15* transgenic roots systems. Sections of representative nodules are displayed in **Figure 3**. Note the drastic reduction of restoration of infection in nodules and root hairs associated with the mutation or deletion of *PACE* as well as the replacement of *PACE* with *JrPACE-like* in the context of the *LjNIN* promoter. White asterisks and arrowheads: infected and non-infected nodules, respectively. (**C - E**) Boxplots displaying **c,** the percentage of root hair ITs among total infection events (sum of bacterial entrapments and ITs) and (**D - E**) the number of infected nodules from two independent experiments. Each dot in (**D - E**) represents one *nin-15* transgenic root system. (**C**) displays merged data from all experiments as the percentage represents a normalised value calculated for each root piece (see **Figure 3 – Source Data 1**). n: number of transgenic root systems or root pieces analysed. For species abbreviations see **Figure 1 – figure supplement 5A**. The applied statistical method was ANOVA with *post hoc* Tukey: (**C**) $F_{9,313} = 106.7$, $p < 2x10^{-16}$; (**D**) $F_{6,346} = 82.89$, $p < 2x10^{-16}$; (**E**) $F_{4,135} = 20.18$, $p = 4.76x10^{-13}$. Different small letters indicate significant differences. Bars, 2 mm. WLI: white light illumination.

Figure 3 – figure supplement 8 | Spatio-temporal *GUS* expression driven by *PACE* variants in *L. japonicus* roots during the bacterial infection process. *L. japonicus* WT roots were transformed with T-DNAs carrying a $Ubq10_{pro}$*:NLS-GFP* transformation marker together with a *GUS* reporter gene driven by either of the *PACE* variants from nodulating FaFaCuRo species fused to the *LjNIN* minimal promoter ($NINmin_{pro}$). For species abbreviations and experimental details see **Figure 1 – figure supplement 5A and Figure 2 – figure supplement 1**, respectively. Note the overlapping bacterial invasion zone and *PACE:*$NINmin_{pro}$*:GUS* expression in early infection stages (red and blue arrowheads in (**A - C**)). Red arrowheads: *M. loti Ds*Red. Blue arrowheads: GUS activity in nodule primordia. Only pictures taken under white light illumination (WLI) are displayed for nodules in panel VI to reveal the pink colour of leghemoglobin, characteristic for mature and fully infected nodules.

Note that like *LjPACE*, the *PACE* variants-driven *GUS* expressions were absent at this stage (panel IV in (**A - C**) and panel IV in **Figure 2 – figure supplement 1D**). (**D**) Quantification of transgenic root systems exhibiting *GUS* expression in different cell types and tissues exemplarily displayed in (**A - C**). n.d.: not determined. Bars, 250 µm.

Figure 4 – figure supplement 1 | *PACE* alone or in the context of the *S. lycopersicum NIN* promoter (a species outside of the FaFaCuRo clade) enables IT formation in the cortex. (**A - D**) Representative pictures of sections of nodules formed on *L. japonicus nin-15* roots transformed with T-DNAs carrying a $Ubq10_{pro}$*:NLS-GFP* transformation marker together with the *LjNIN* gene driven by either of the following promoters: (**A - B**) the *L. japonicus NIN* minimal promoter ($NINmin_{pro}$) or *PACE* fused to $NINmin_{pro}$ ($PACE:NINmin_{pro}$); (**C - D**) the 3 kb *S. lycopersicum NIN* promoter ($SlNIN_{pro}$), the 3 kb *SlNIN* promoter with mutated *PACE* ($SlNIN_{pro}$*::mPACE*) or with *L. japonicus PACE* inserted ($SlNIN_{pro}$*::PACE*), 21 dpi with *M. loti Ds*Red (from the same experiments depicted in **Figure 4**). Black rectangles in (**A**) demarcate the enlarged area displayed in **Figure 4A and 4B** to focus on the initial infection structures. Note the absence of cells filled with symbiosomes in nodules transformed with the *LjNIN* gene driven by $PACE:NINmin_{pro}$ or $NINmin_{pro}$. By contrast, infected cells were often filled with symbiosomes in the $SlNIN_{pro}$*::PACE:NIN*-transformed nodules, like those resulted by NIN_{pro}*:NIN* (see (**C**) and compare the two sections in (**D**)). (**E - F**) Boxplots displaying the percentage of root hair ITs among total infection events (sum of bacterial entrapments and ITs) or the percentage of infected nodules among total number of nodules (**E**) 21 dpi and (**F**) 35 dpi with *M. loti Ds*Red, respectively. Each dot represents one *nin-15* transgenic root system or root piece. (**E**) displays results from an independent repetition from the experiment depicted in **Figure 4**. n: number of transgenic root systems or root pieces analysed. Numbers above the boxplots: the value of individual data points outside of the plotting area. The applied statistical method was Fisher's exact test: $*p < 0.05$; $***p < 0.001$; n.s.: not significant. Bars, (**A and C**) 100 µm; (**B and D**) 50 µm.

Source Data:

Figure 1 – Source Data 1 | Summary of the bioinformatic analysis resulting in the discovery of *PACE* using 37 species.

Figure 1 – Source Data 2 | Results of the FIMO analysis of *PACE* in 163 species.

Figure 1 – Source Data 3 | Status of *PACE* and *NIN* in non-nodulating FaFaCuRo species.

Figure 3 – Source Data 1 | Complementation results of the *L. japonicus* Gifu *nin-2* and *nin-15* mutant lines.

Additional Files:

Supplementary file 1 | List of plant genomes used for the search of conserved motifs within *ERN1* and *RAM1* promoters.

Supplementary file 2 | List of seed bags, bacterial strains and incubation times.

Supplementary file 3 | List of plasmids used.

Supplementary file 4 | Sequences and IDs of oligonucleotides (DNA) used.

Supplementary file 5 | Microscope/scanner settings and image analysis.

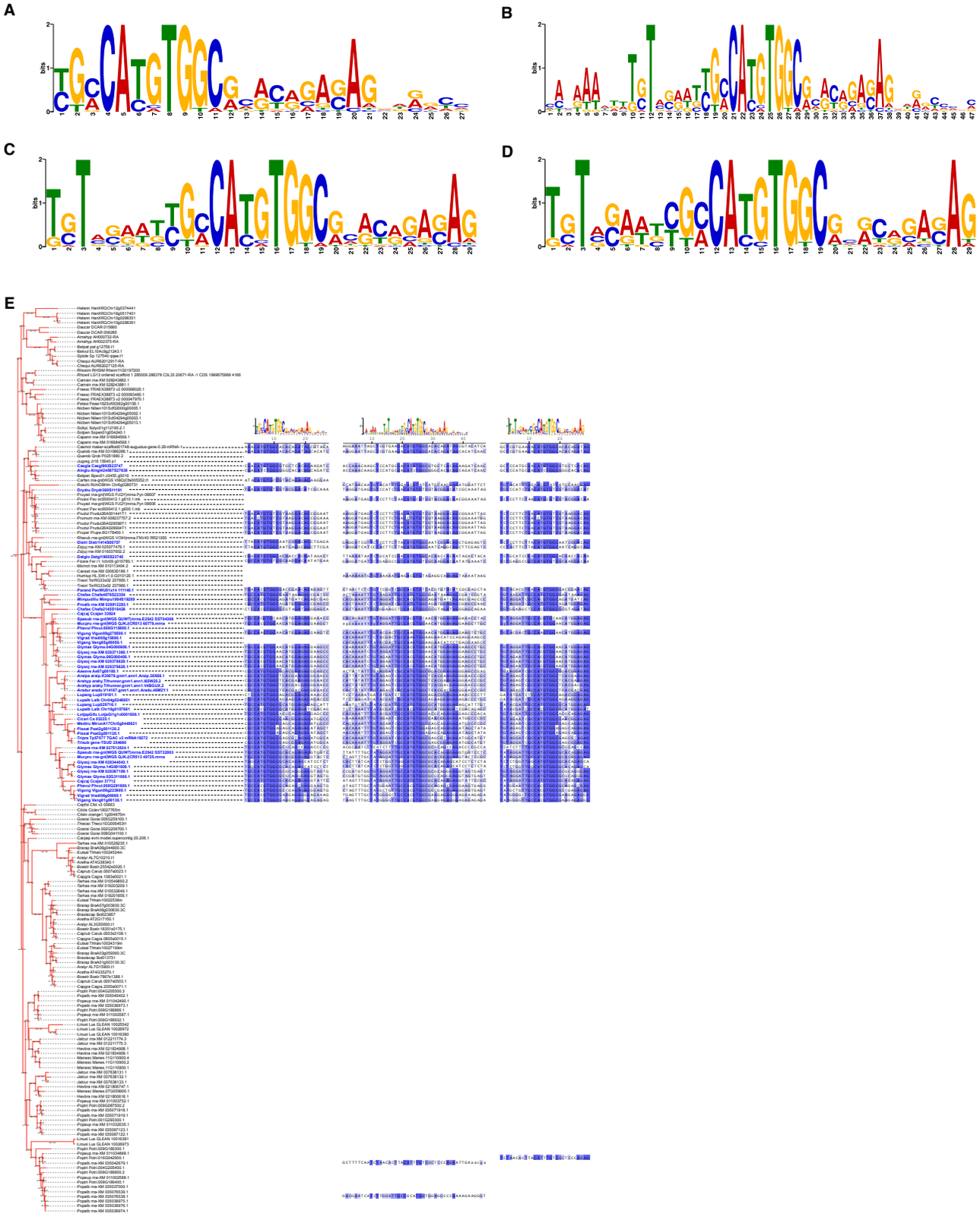

Figure 1 – figure supplement 1 | Discovery of *PACE* by MEME analyses. (**A - D**) Consensus sequence of the Position Weight Matrix identified by MEME analyses using the regions upstream of the translational start site (ATG) thus representing the promoters and 5'UTRs of *NIN* and *NLP* genes from 37 angiosperm species (see Methods): (**A**) in a discriminative search for a motif that is present in 3 kb upstream regions of the *NIN* genes from nodulating FaFaCuRo species, but absent in 3 kb upstream regions of the *NIN* genes from species outside of the FaFaCuRo clade and absent in the 3 kb upstream regions of *NLP* genes; (**B**) in an independent, non-discriminative search in the 3 kb upstream regions of the *NIN* genes from nodulating species revealing that the most conserved nucleotides span a larger region than (**A**); (**C**) the resulted most conserved 29 nucleotides derived from upstream regions of *NIN* genes of nodulating FaFaCuRo species; (**D**) the resulted most conserved 29 nucleotides (*PACE*) derived from the upstream region of one representative *NIN* gene per species of nodulating FaFaCuRo species. (**E**) Motif analyses by FIMO using the upstream regions of the *NIN* and *NLP* genes from an expanded list of 163 species (see Methods). Left: pruned tree from the whole *NLP* tree (demarcated in the black rectangle in **Figure 1 – figure supplement 2**) corresponding to the *NIN* orthologs. Right: three versions of consensus sequence (left to right, (**A, B and D**), respectively) were used to retrieve motifs from the 5 kb upstream region of *NIN* genes *via* FIMO search, the output of which is displayed underneath the consensus sequences. Sequence names of nodulating species are coloured in blue. Blank lines represent the absence of significant motifs.

Figure 1 – figure supplement 2 | *PACE* is present exclusively in the FaFaCuRo clade. Motif analyses by FIMO using the using the regions upstream of the translational start site (ATG) thus representing the promoters and 5'UTRs of the *NIN* and *NLP* genes from an expanded list of 163 species (see Methods). Left: Maximum likelihood tree of *NLP* family (model: GTR+F+R10) of 163 species (**Figure 1 – Source Data 2**). Tree was rooted on the Charophytes algae *Klebsormidium nitens*. Black box demarcates the area that is displayed in **Figure 1 – figure supplement 1E**. Blank lines represent the absence of significant motifs. Sequence names of nodulating species are coloured in blue. The different NLP clades are indicated by branch colours and named according to the *Arabidopsis thaliana* nomenclature. Right: three versions of consensus sequence (left to right, **Figure 1 – figure supplement 1A, 1B and 1D**, respectively) were used to retrieve motifs from the 5 kb upstream region of *NIN* genes via FIMO search, the output of which is displayed underneath the consensuses sequences.

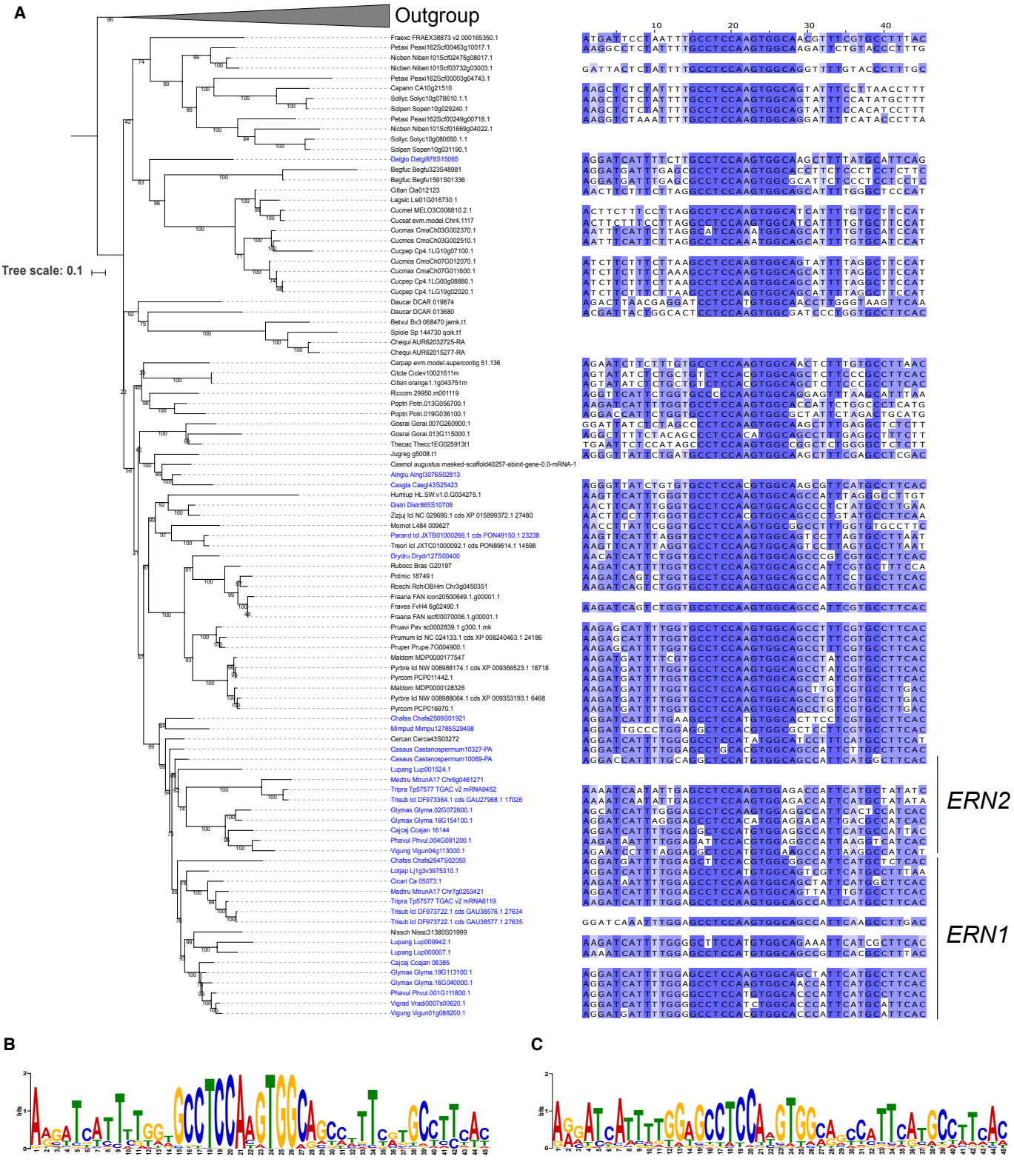

Figure 1 – figure supplement 3 | The presence of a motif encompassing the previously identified Cyclops binding site within the regions upstream of the translational start site (ATG) thus representing the promoters and 5'UTRs of *ERN1* genes extends beyond the FaFaCuRo clade. (**A**) Maximum likelihood of *ERN1/ERN2* (model: JTT+F+R5) from 87 species (**Supplementary file 1**) based on protein sequences. Tree was rooted using sequences from the *ERN1/ERN2* paralog *ERN3* (outgroup clade collapse and indicated by grey triangle marked "Outgroup"). Species belonging to the monophyletic FaFaCuRo clade (Stevens, 2017) are indicated by thicker black branches. *ERN1* and *ERN2* subclades are indicated. Sequence names of nodulating species are coloured in blue. These conserved motifs identified by MEME analyses in the 3 kb upstream regions were aligned and displayed next to species names. While the presence of a conserved Cyclops binding site containing motif in species outside of the FaFaCuRo clade is consistent with the role of *RAM1* in arbuscular mycorrhizal symbiosis, a function of *ERN1* in arbuscular mycorrhizal symbiosis has not been described and suggests a yet unidentified function of *ERN1* outside of the FaFaCuRo clade. (**B**) Consensus sequence of the Position Weight Matrix identified by MEME analyses of all the species. (**C**) Consensus sequence of the Position Weight Matrix identified by MEME analyses when analysing only the nodulating species.

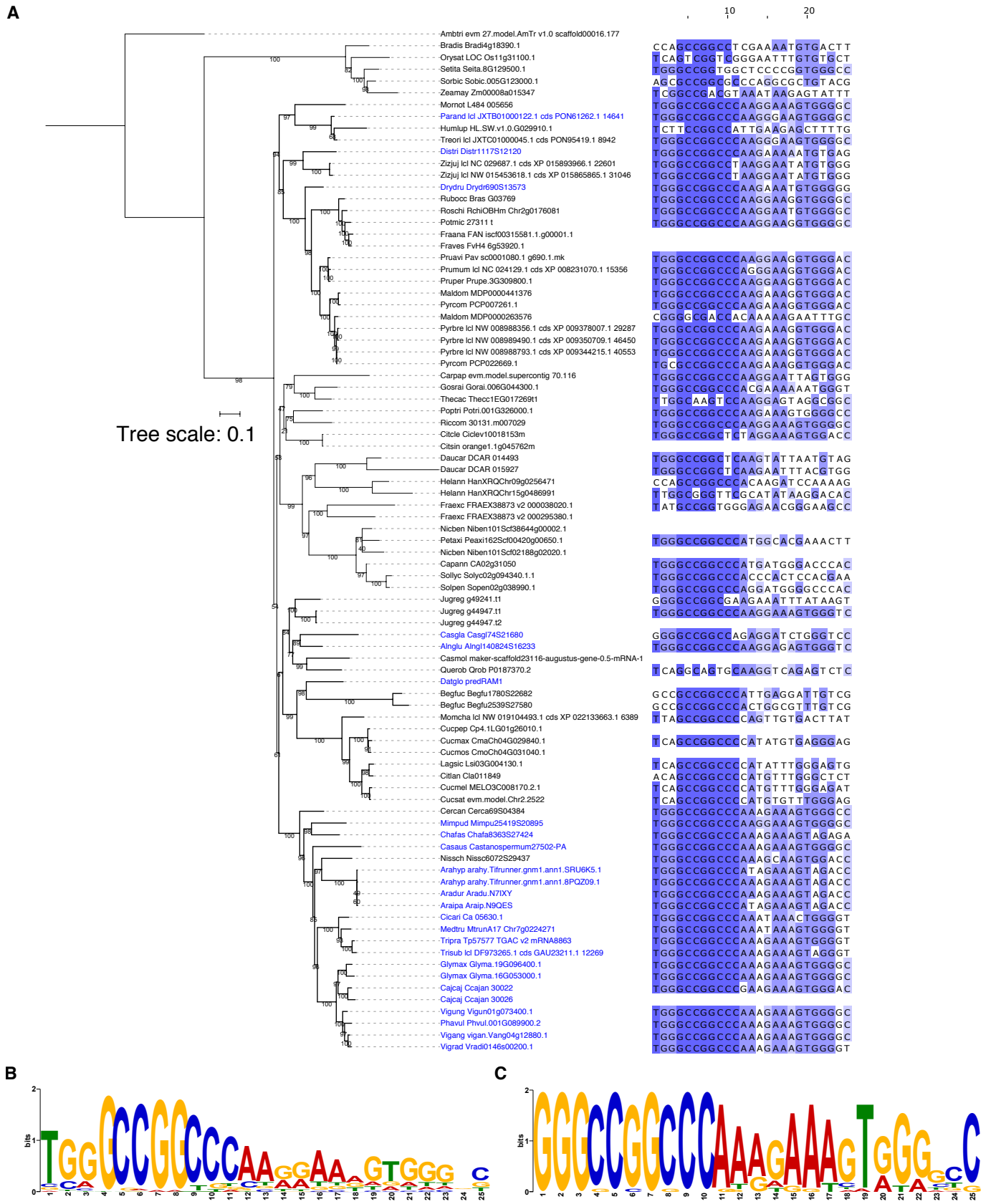

Figure 1 – figure supplement 4 | The presence of a motif encompassing the previously identified Cyclops binding site within the regions upstream of the translational start site (ATG) thus representing the promoters and 5'UTRs of *RAM1* genes extends beyond the FaFaCuRo clade. (**A**) Maximum likelihood of *RAM1* (model: JTT+F+R4) from 87 species (**Supplementary file 1**) engaging in arbuscular mycorrhizal symbiosis. Tree was rooted on the early-diverging angiosperm *Amborella trichopoda*. Species belonging to the monophyletic FaFaCuRo clade (Stevens, 2017) are indicated by thicker black branches. Sequence names of nodulating species are coloured in blue. These conserved motifs identified by MEME analyses in the 3 kb upstream regions are aligned and displayed next to species names. Blank lines represent the absence of identified motif due to genome contiguity issues. (**B**) Consensus sequence of the Position Weight Matrix identified by MEME analyses when analysing all the mycorrhizal species. (**C**) Consensus sequence of the Position Weight Matrix identified by MEME analyses when analysing only the nodulating species.

A

Abbre-viation	Species	Plant Order	RNS	FaFaCuRo member
Lj	*Lotus japonicus*	Fabales	Yes	Yes
Cg	*Casuarina glauca*	Fagales	Yes	Yes
Jr	*Juglans regia*	Fagales	No	Yes
Dd	*Dryas drummondii*	Rosales	Yes	Yes
Zj	*Ziziphus jujuba*	Rosales	No	Yes
Pp	*Prunus persica*	Rosales	No	Yes
Dg	*Datisca glomerata*	Cucurbitales	Yes	Yes
Sl	*Solanum lycopersicum* (tomato)	Solanales	No	No
Vv	*Vitis vinifera*	Vitales	No	No

B

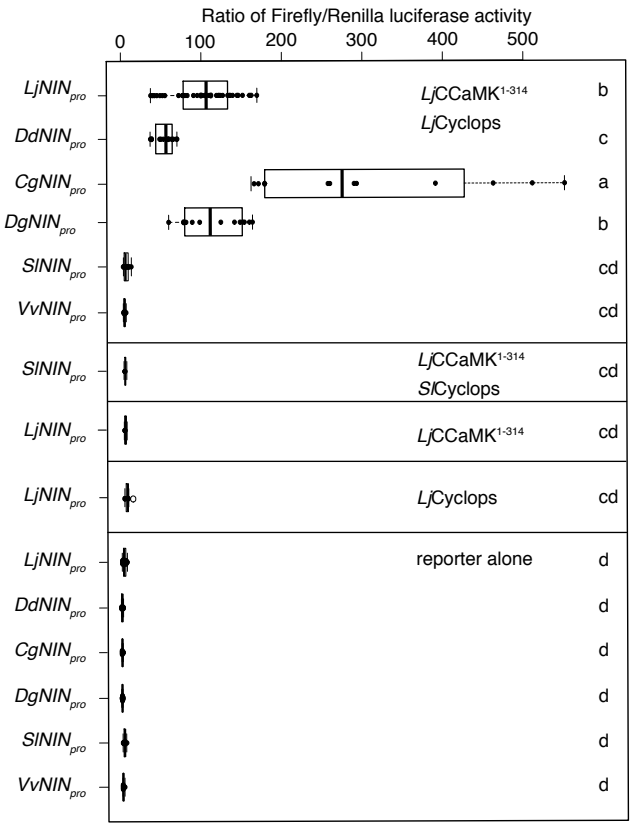

C

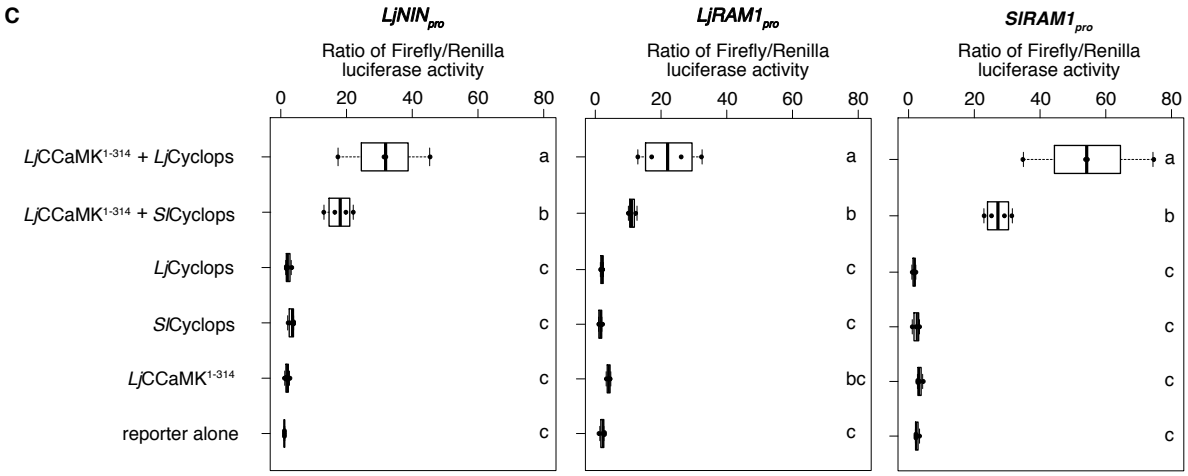

Figure 1 – figure supplement 5 | Transcriptional activation of *NIN promoter:Firefly luciferase* reporter gene by CCaMK$^{1-314}$/Cyclops is restricted to *NIN* promoters from species of the FaFaCuRo clade. *Nicotiana benthamiana* leaf cells were transformed with T-DNAs carrying a *Firefly luciferase* reporter gene driven by either of the indicated promoters in tandem with the *AtACT2$_{pro}$:Renilla luciferase* reporter fusion that provides a quantitative internal standard. (**A**) List of species within the FaFaCuRo clade (light red shade) and outside (light grey shade) and abbreviations. (**B**) Reporter gene activation by *L. japonicus* CCaMK$^{1-314}$/Cyclops via *NIN* promoters (*NIN$_{pro}$*) originating from listed species. (**C**) Comparison of the transactivation potential of Cyclops versions from *L. japonicus* and *S. lycopersicum*. Note that the expression of the *Firefly luciferase* reporter gene driven by *LjNIN$_{pro}$*, the *RAM1* promoters from *L. japonicus* and *S. lycopersicum* (*LjRAM1$_{pro}$* and *SlRAM1$_{pro}$*, respectively) was induced in the presence of CCaMK$^{1-314}$/Cyclops regardless of the origin of Cyclops. In contrast, the transactivation failed with the *SlNIN* promoter (panel (**A**)). The applied statistical method was ANOVA with *post hoc* Tukey: (**B**), $F_{14,214} = 71.07$, $p < 2x10^{-16}$; (**C**), plots from left to right: $F_{5,18} = 20.58$, $p = 7.14x10^{-7}$; $F_{5,18} = 25.38$, $p = 1.45x10^{-7}$ and $F_{5,18} = 40.49$, $p = 3.55x10^{-9}$, respectively. Different small letters indicate significant differences.

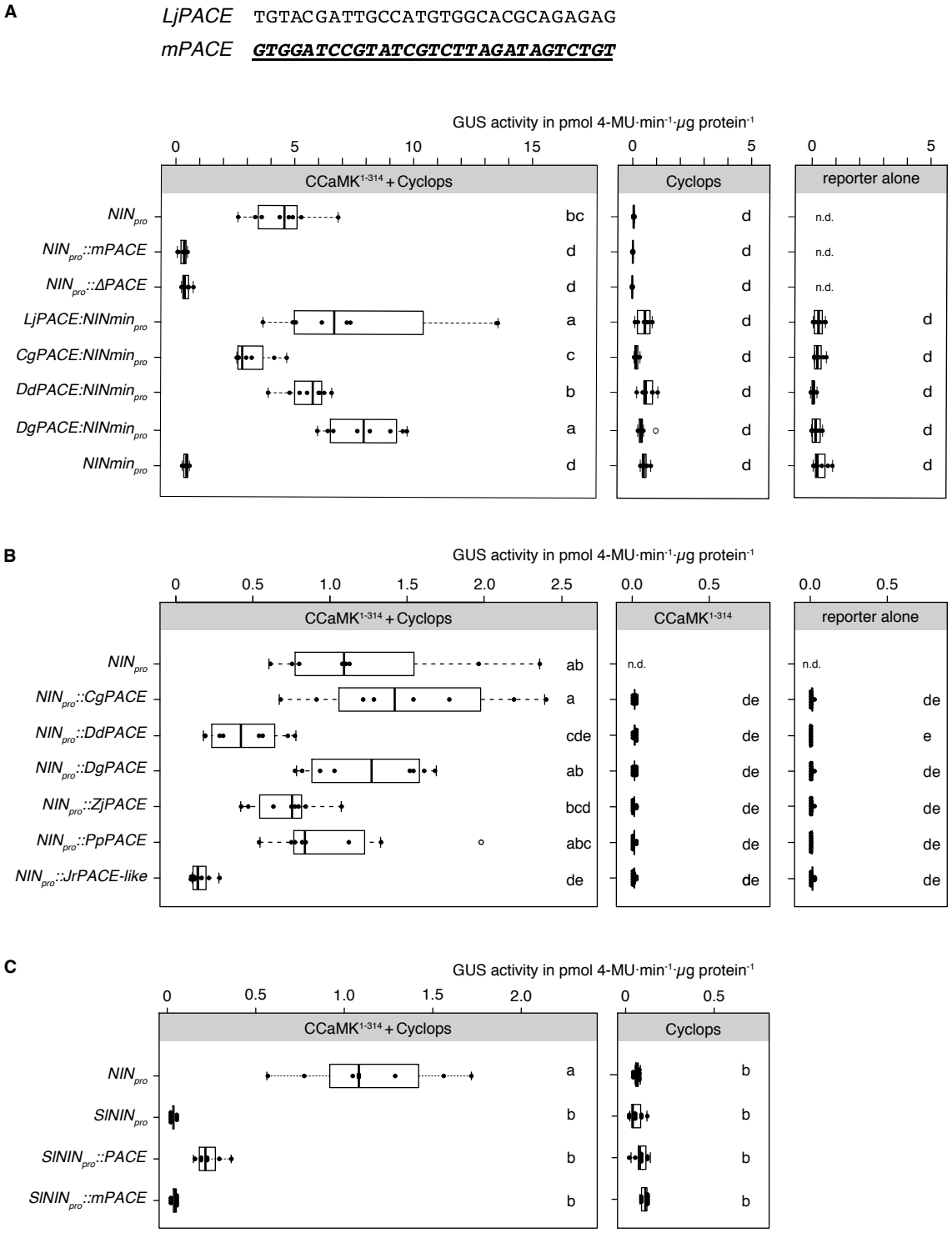

Figure 1 – figure supplement 6 | *PACE* sequence variants from species across the FaFaCuRo clade were able to functionally replace *L. japonicus PACE* in a *$LjNIN_{pro}$:GUS* reporter fusion. *N. benthamiana* leaf cells were transformed with T-DNAs carrying a *GUS* reporter gene driven by either of the indicated promoters: (**A**) the *L. japonicus NIN* promoter (*NIN_{pro}*), the *LjNIN* promoter with *PACE* mutated or deleted (*NIN_{pro}::mPACE* and *NIN_{pro}::ΔPACE*, respectively), or *PACE* sequence variants from the nodulating FaFaCuRo species fused to the *LjNIN* minimal promoter (*$NINmin_{pro}$*); (**B**) chimeric promoters where *LjPACE* in the *LjNIN* promoter was replaced with either one of the *PACE* variants from species tested in (**A**) or from non-nodulating FaFaCuRo species including the *Juglans regia PACE*-like motif (*JrPACE-like*); (**C**) the *S. lycopersicum NIN* promoter (*$SlNIN_{pro}$*), the *SlNIN* promoter with *LjPACE* (*$SlNIN_{pro}$::PACE*) or *mPACE* (*$SlNIN_{pro}$::mPACE*) inserted. For species abbreviations see **Figure 1 – figure supplement 5A**. Note in (**A**) that the deletion or mutation of *PACE* in *LjNIN* promoter resulted in a drastic reduction in reporter gene expression and in (**C**) insertion of *LjPACE* but not *mPACE* into the *S. lycopersicum* promoter confers transactivation by $CCaMK^{1-314}$/Cyclops. The applied statistical method was ANOVA with *post hoc* Tukey: (**A**) $F_{20,144} = 51.38$, $p < 2x10^{-16}$; (**B**), $F_{18,166} = 149.1$, $p < 2x10^{-16}$; (**C**) $F_{7,62} = 30.5$, $p = 7.02x10^{-7}$. Different small letters indicate significant difference. n.d., not determined.

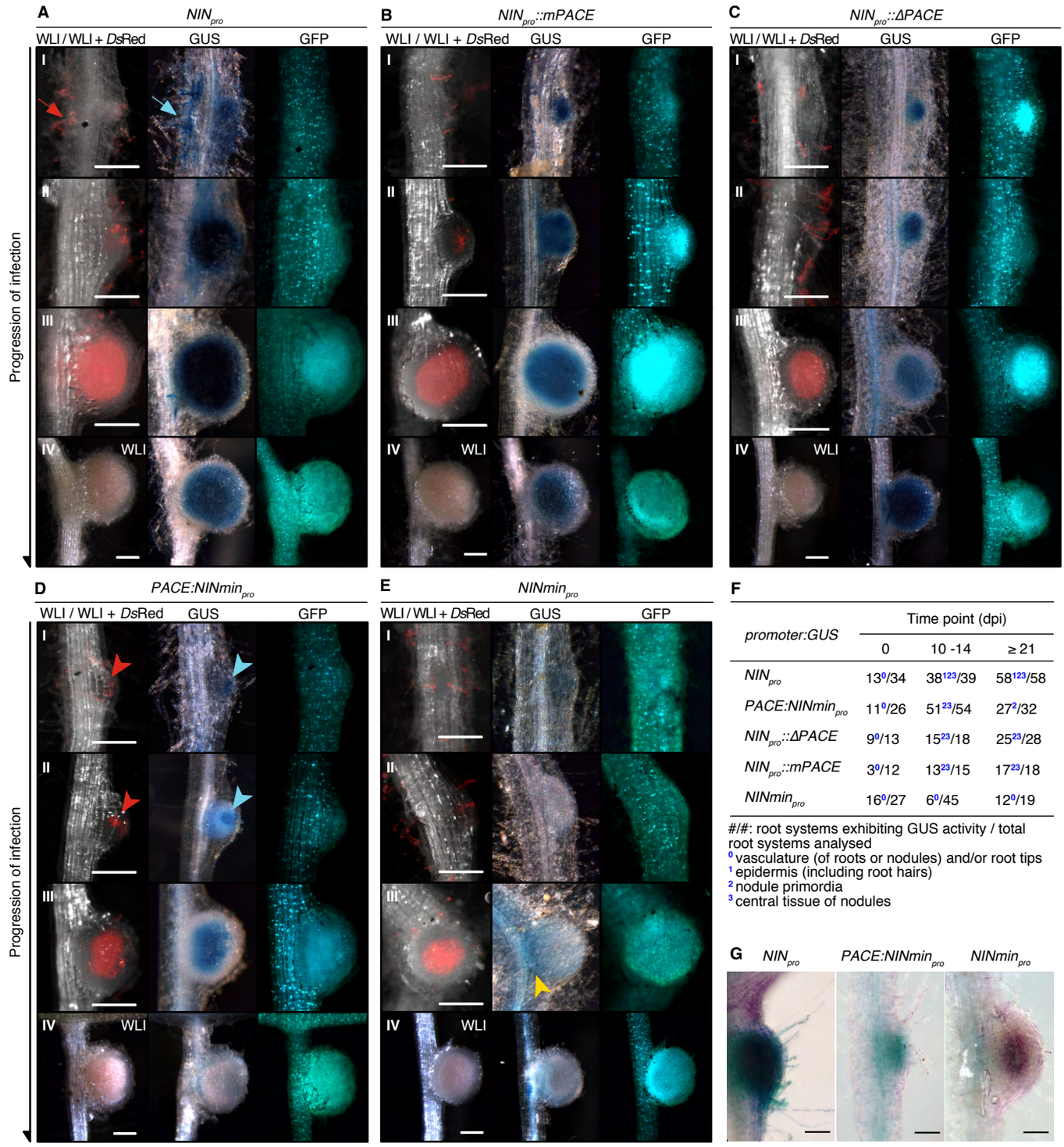

promoter:GUS	Time point (dpi)		
	0	10 -14	≥ 21
NIN_{pro}	13^{0}/34	38^{123}/39	58^{123}/58
$PACE:NINmin_{pro}$	11^{0}/26	51^{23}/54	27^{2}/32
NIN_{pro}::ΔPACE	9^{0}/13	15^{23}/18	25^{23}/28
NIN_{pro}::mPACE	3^{0}/12	13^{23}/15	17^{23}/18
$NINmin_{pro}$	16^{0}/27	6^{0}/45	12^{0}/19

#/#: root systems exhibiting GUS activity / total root systems analysed
[0] vasculature (of roots or nodules) and/or root tips
[1] epidermis (including root hairs)
[2] nodule primordia
[3] central tissue of nodules

Figure 2 – figure supplement 1 I Spatio-temporal *GUS* expression driven by *PACE* and the *NIN* promoter in *L. japonicus* roots during the bacterial infection process. *L. japonicus* wild-type hairy roots were transformed with T-DNAs carrying a $Ubq10_{pro}$:*NLS-GFP* transformation marker together with a *GUS* reporter gene driven by either of the indicated promoters: (**A**) the 3 kb *LjNIN* promoter (NIN_{pro}); the *LjNIN* promoter with *PACE* (**B**) mutated ($LjNIN_{pro}$::*mPACE*) or (**C**) deleted (NIN_{pro}::*ΔPACE*); (**D**) *PACE* fused to the *LjNIN* minimal promoter ($PACE:NINmin_{pro}$) or (**E**) the *LjNIN* minimal promoter ($NINmin_{pro}$). The progression of bacterial infection was determined by the *Ds*Red signal 10 - 14 days post inoculation (dpi) with *M. loti Ds*Red. Nodules undergoing different stages of infection (panels I to IV) were stained with X-Gluc to reveal the *GUS* expression pattern. Note the overlapping bacterial invasion zone and $PACE:NINmin_{pro}$:*GUS* expression in early infection stages (red and blue arrowheads in (**D**)) as well as the differences between $PACE:NINmin_{pro}$:*GUS* and the much broader NIN_{pro}:*GUS* expression at that stage (red and blue arrows in (**A**)). Red arrow and arrowheads: *M. loti Ds*Red. Blue arrow and arrowheads: GUS activity in root hairs bearing ITs and nodule primordia, respectively. The $NINmin_{pro}$:*GUS* fusion gave only rarely detectable signal, and if so in the vasculature (yellow arrowhead in (**E**)). Only pictures taken under white light illumination (WLI) are displayed for nodules in panel VI to reveal the pink colour of leghemoglobin, characteristic for mature and fully infected nodules. Note that $PACE:NINmin_{pro}$:*GUS* expression was absent at this stage, whereas the NIN_{pro}:*GUS* resulted in strong blue staining in the nodule regardless of the presence of *PACE* (compare panel IV in (**D**) and (**A - C**)). (**F**) Quantification of transgenic root systems exhibiting *GUS* expression in different cell types and tissues exemplarily displayed in (**A - E**). (**G**) *PACE* drove *GUS* reporter gene expression in the central tissue of primordia and nodules, but was not sufficient for expression in root hairs. Transgenic roots carrying promoter:GUS fusions same as in (**A, D and E**) were inoculated with *M. loti lacZ* and dual-stained with X-Gluc and Magenta-Gal. Purple: *M. loti lacZ*. Blue: GUS activity. Note the co-existence of blue and purple staining in root hairs on roots transformed by NIN_{pro}:*GUS*, but not that transformed by $PACE:NINmin_{pro}$:*GUS*. Bars, 250 µm.

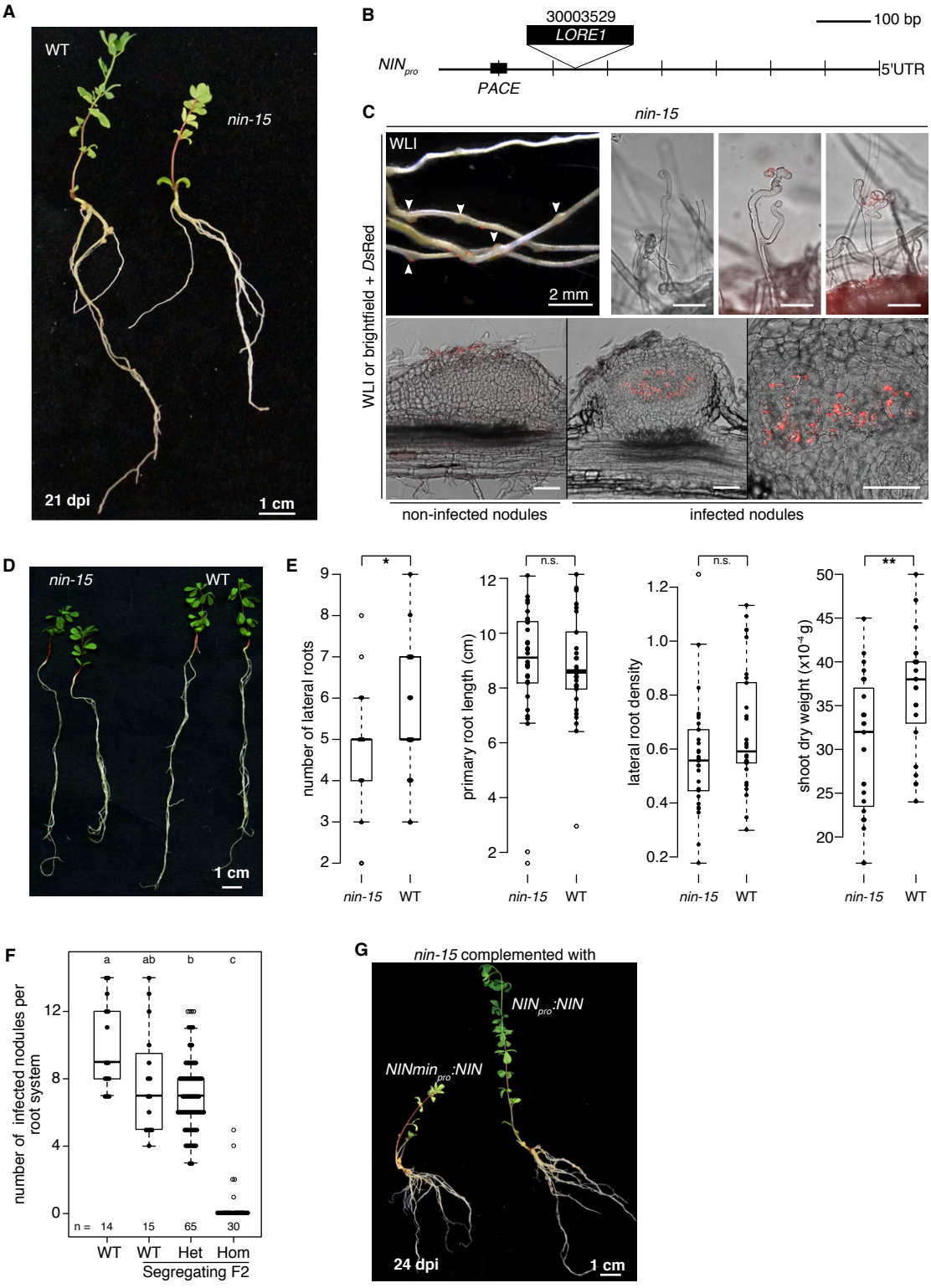

Figure 3 – figure supplement 1 I *L. japonicus nin-15* mutant phenotype. (**A**) A representative picture of *L. japonicus* wild-type (WT, left) and *nin-15* (right) plants 21 dpi with *M. loti Ds*Red. (**B**) Position of the *Lotus Retrotransposon 1* (*LORE1*) insertion within the *NIN* promoter in the *nin-15* mutant. (**C**) Representative pictures of *nin-15* root hairs and nodule sections 21 dpi with *M. loti Ds*Red. Forty-nine plants with a total number of 436 nodules were analysed: only four plants bore one or two IT(s) within root hairs and seven plants bore one or two infected nodule(s). Deformed or curled root hairs in the presence of *M. loti Ds*Red were abundant but infection threads were rarely found. Arrowheads: uninfected nodules. Unlabelled bars, 100 µm. (**D - E**) Phenotype of *nin-15* in the presence of a symbiosis-independent nitrogen source (15 mM KNO_3) for 28 days. (**D**) Pictures documenting the healthy status of *L. japonicus* WT and *nin-15* plants (compare (**D**) and (**A**)) and (**E**) quantitative assessment of parameters displayed in boxplots. Thirty plants per genotype were analysed. Each dot represents one plant. Lateral root density: number of lateral roots/primary root length (cm). The applied statistical method was pairwise *t*-test: $*p < 0.05$; $**p < 0.01$; n.s.: not significant. (**F**) Segregation analysis of *nin-15*. The applied statistical method was ANOVA with *post hoc* Tukey: $F_{3,120} = 84.1$, $p = 2x10^{-16}$. Different small letters indicate significant difference. (**G**) Representative pictures of *nin-15* plants with hairy roots transformed with the *NIN* gene driven by the *L. japonicus NIN* minimal promoter ($NINmin_{pro}$) or the 3 kb *NIN* promoter (NIN_{pro}) 24 dpi with *M. loti Ds*Red. WLI: white light illumination.

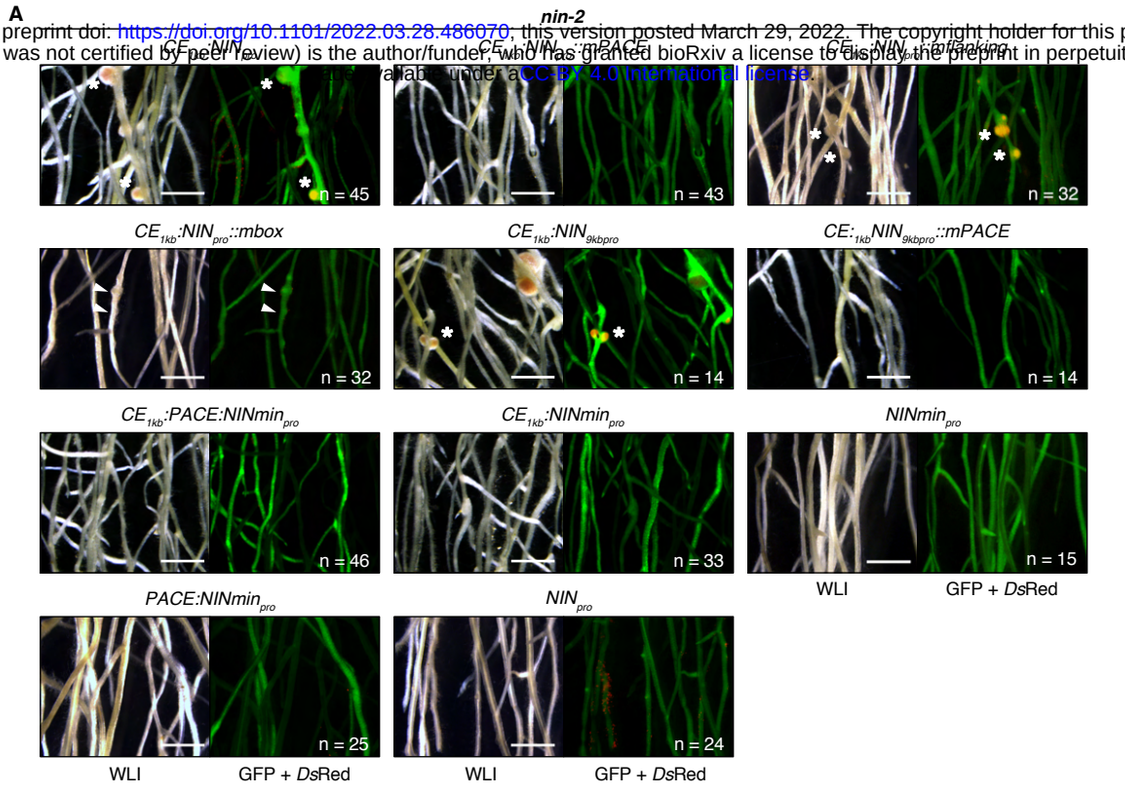

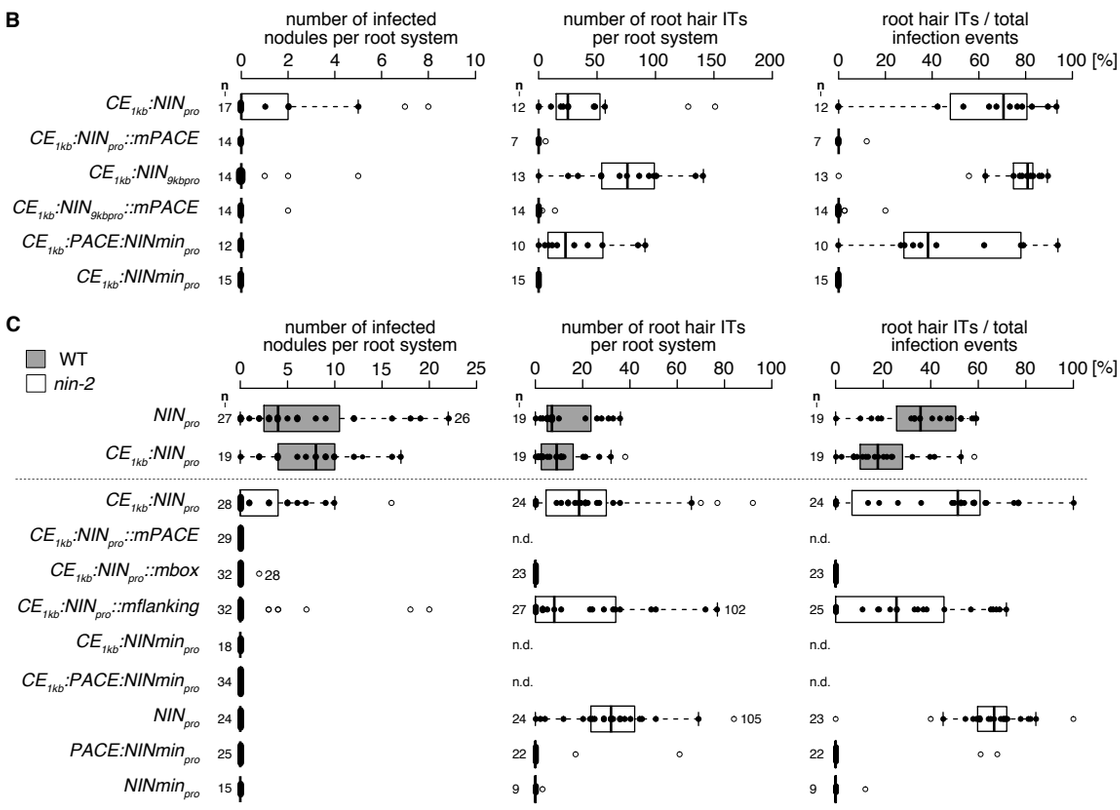

Figure 3 – figure supplement 2 | The *CYC-box* and flanking sequences of *PACE* are required for the complete restoration of the bacterial infection process in the *L. japonicus nin-2* mutant. *nin-2* roots were transformed with T-DNAs carrying a *Ubq10*$_{pro}$*:NLS-GFP* transformation marker in tandem with the *LjNIN* gene driven by either of the following promoter versions: the cytokinin element-containing region of 1 kb (*CE*$_{1kb}$) fused to the 3 kb or 9 kb *LjNIN* promoter (*CE*$_{1kb}$*:NIN*$_{pro}$ or *CE*$_{1kb}$*:NIN*$_{9kbpro}$, respectively); *CE*$_{1kb}$*:NIN*$_{pro}$ or *CE*$_{1kb}$*:NIN*$_{9kbpro}$ with *PACE* mutated (*CE*$_{1kb}$*:NIN*$_{pro}$*::mPACE* or *CE*$_{1kb}$*:NIN*$_{9kbpro}$*::mPACE*, respectively); *CE*$_{1kb}$*:NIN*$_{pro}$ carrying a mutated Cyclops binding site (*CYC-box*) (*CE*$_{1kb}$*:NIN*$_{pro}$*::mbox*); *CE*$_{1kb}$*:NIN*$_{pro}$ carrying mutated sequences flanking the *CYC-box* in *PACE* (*CE*$_{1kb}$*:NIN*$_{pro}$*::mflanking*); *CE*$_{1kb}$ fused to the *LjNIN* minimal promoter (*CE*$_{1kb}$*:NINmin*$_{pro}$); *CE*$_{1kb}$ fused to *PACE* and to *NINmin*$_{pro}$ (*CE*$_{1kb}$*:PACE:NINmin*$_{pro}$); *NIN*$_{pro}$, *PACE:NINmin*$_{pro}$ or *NINmin*$_{pro}$. (**A**) Representative overview pictures of transgenic root systems. Roots were analysed 21 dpi with *M. loti Ds*Red. White asterisks and arrowheads: infected and non-infected nodules, respectively. Bars, 2 mm. (**B - C**) Boxplots displaying the number of root hair ITs or infected nodules and the percentage of root hair ITs among total infection events (sum of bacterial entrapments and ITs). Each dot represents one transgenic *nin-2* root system or root piece. *L. japonicus* WT roots transformed with *NIN*$_{pro}$*:NIN* or *CE*$_{1kb}$*:NIN*$_{pro}$*:NIN* were included as controls. Note the loss of restoration of nodules and IT formation associated with the mutation of *PACE* or only the *CYC-box* in *PACE*; and the reduction of same when sequences flanking the *CYC-box* in *PACE* were mutated. n: number of transgenic root systems or root pieces analysed. Numbers above the boxplots: the value of individual data points outside of the plotting area. n.d.: not determined. WLI: white light illumination.

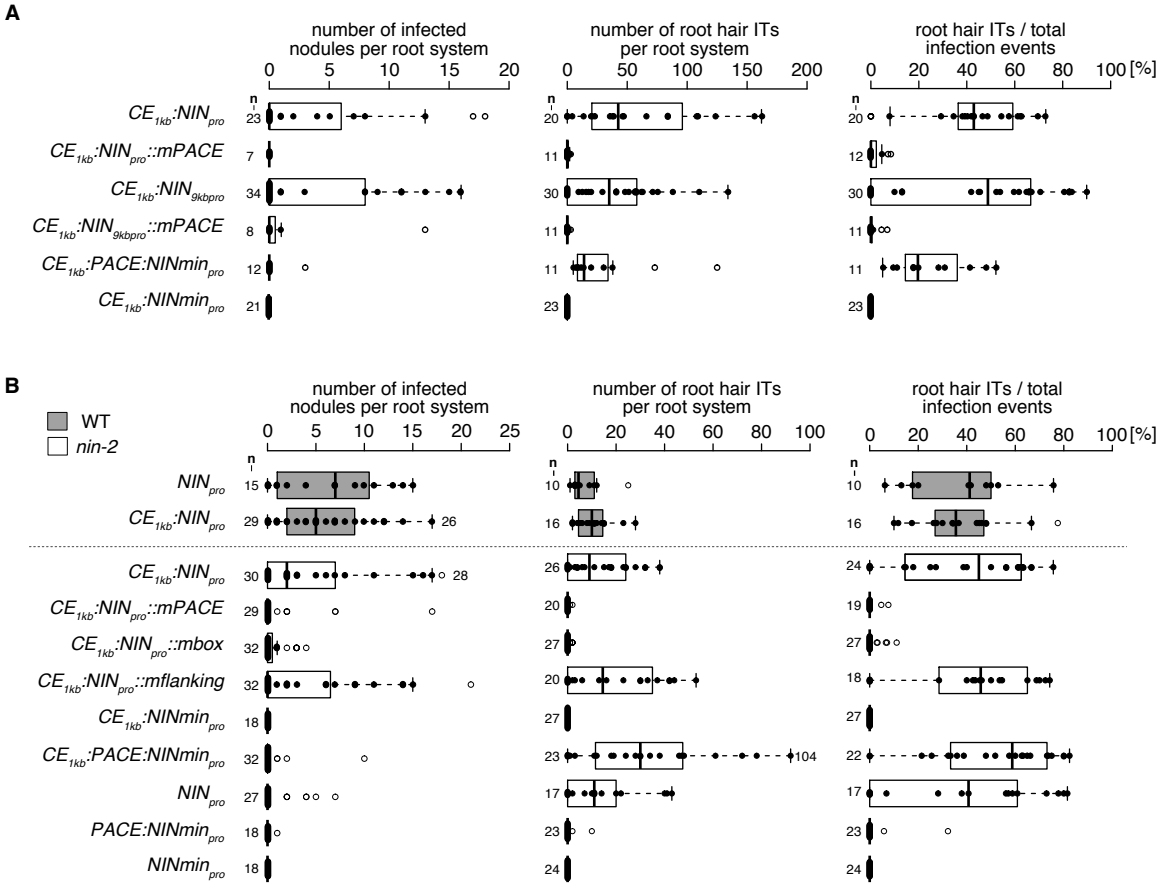

Figure 3 – figure supplement 3 | The *CYC-box* and flanking sequences of *PACE* are required for the complete restoration of the bacterial infection process in the *L. japonicus nin-2* mutant. Roots were from a subset of plants from the same experiment depicted in **Figure 3 – figure supplement 2** but analysed 35 dpi with *M. loti Ds*Red. (**A - B**) Boxplots displaying the number of root hair ITs or infected nodules and the percentage of root hair ITs among total infection events (sum of bacterial entrapments and ITs). Each dot represents one transgenic *nin-2* root system or root piece. *L. japonicus* WT roots transformed with NIN_{pro}:*NIN* or CE_{1kb}:NIN_{pro}:*NIN* were included as controls. Note that the results follow the same trend as those obtained 21 dpi with *M. loti Ds*Red (**Figure 3 – figure supplement 2**). n: number of transgenic root systems or root pieces analysed. Numbers above the boxplots: the value of individual data points outside of the plotting area.

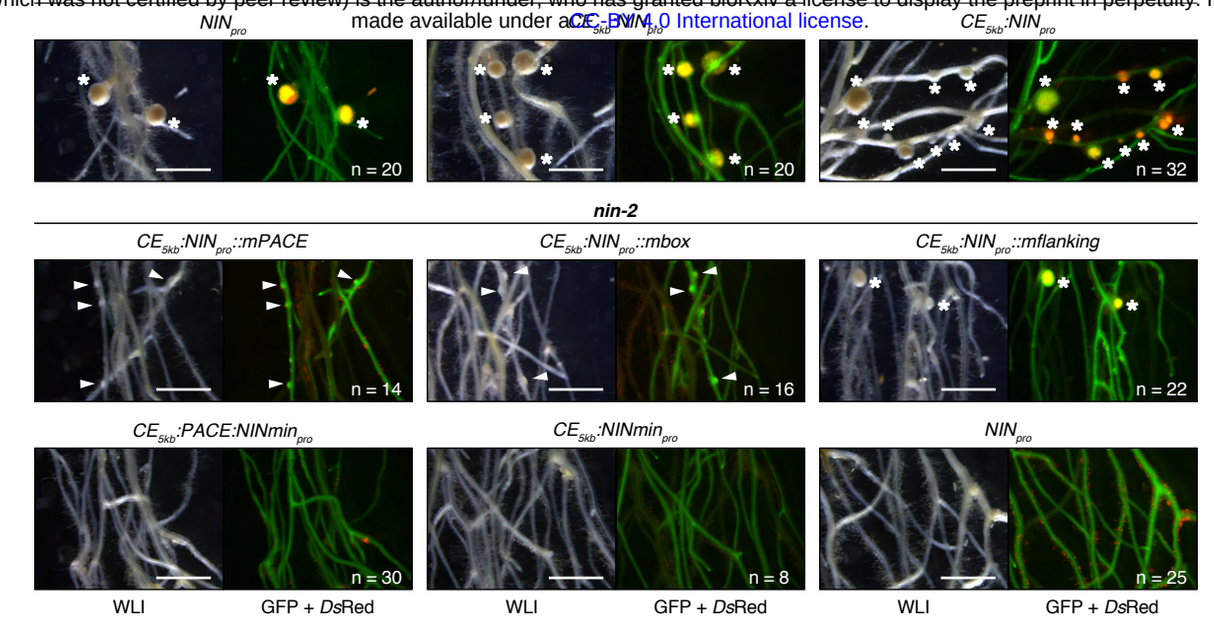

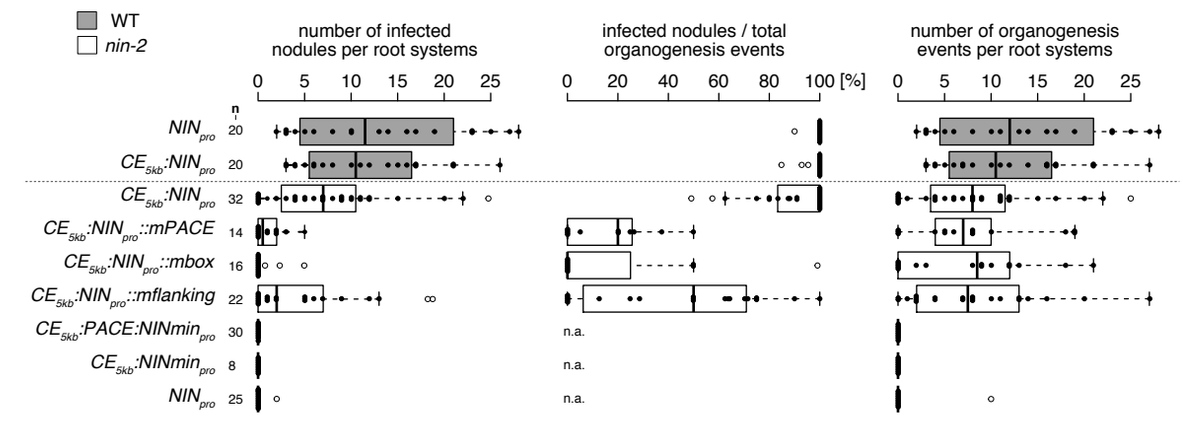

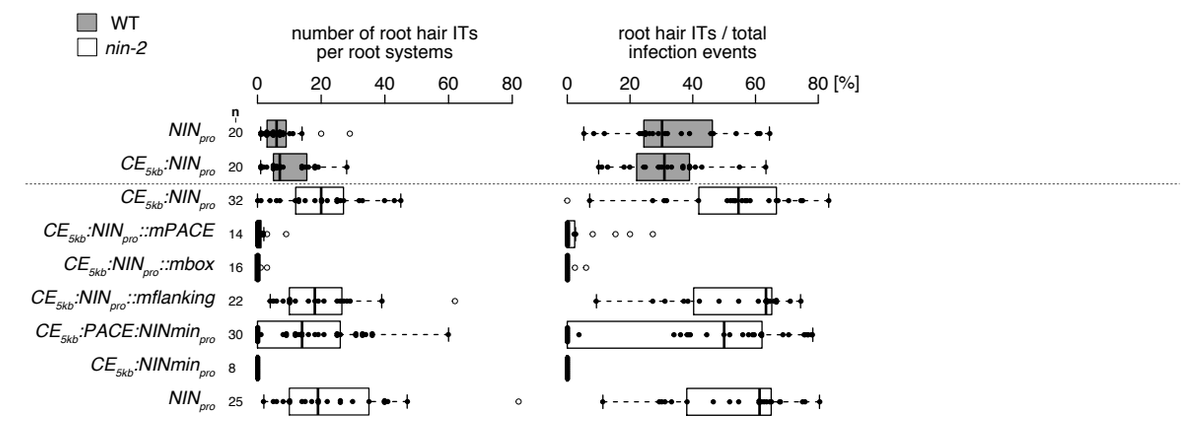

Figure 3 – figure supplement 4 | The *CYC-box* and flanking sequences of *PACE* are required for the complete restoration of the bacterial infection process but are dispensable for the nodule organogenesis process in the *L. japonicus nin-2* mutant. *nin-2* roots were transformed with T-DNAs carrying a *Ubq10*$_{pro}$*:NLS-GFP* transformation marker in tandem with the *LjNIN* gene driven by either of the following promoter versions: the cytokinin element-containing region of 5 kb (*CE*$_{5kb}$) fused to the 3 kb *LjNIN* promoter (*CE*$_{5kb}$*:NIN*$_{pro}$); *CE*$_{5kb}$*:NIN*$_{pro}$ with *PACE* mutated (*CE*$_{5kb}$*:NIN*$_{pro}$*::mPACE*); *CE*$_{5kb}$*:NIN*$_{pro}$ carrying a mutated Cyclops binding site (*CYC-box*) (*CE*$_{5kb}$*:NIN*$_{pro}$*::mbox*); *CE*$_{5kb}$*:NIN*$_{pro}$ carrying mutated sequences flanking the *CYC-box* in *PACE* (*CE*$_{5kb}$*:NIN*$_{pro}$*::mflanking*); *CE*$_{5kb}$ fused to the *LjNIN* minimal promoter (*CE*$_{5kb}$*:NINmin*$_{pro}$); *CE*$_{5kb}$ fused to *PACE* and to *NINmin*$_{pro}$ (*CE*$_{5kb}$*:PACE:NINmin*$_{pro}$) or *NIN*$_{pro}$. (**A**) Representative overview pictures of transgenic root systems. Roots were analysed 21 dpi with *M. loti Ds*Red. White asterisks and arrowheads: infected and non-infected nodules, respectively. Bars, 2 mm. (**B**) Boxplots displaying the number of infected nodules, the percentage of infected nodules among total organogenesis events (sum of infected and non-infected nodules) and the number of organogenesis events. (**C**) Boxplots displaying the number of root hair ITs and the percentage of root hair ITs among total infection events (sum of bacterial entrapments and ITs). Each dot represents one transgenic *nin-2* root system or root piece. *L. japonicus* WT roots transformed with *NIN*$_{pro}$*:NIN* or *CE*$_{5kb}$*:NIN*$_{pro}$*:NIN* were included as controls. Note that the mutation of *PACE* or only the *CYC-box* in *PACE* led to an almost complete loss of IT formation and infected nodules per root system while nodule organogenesis was not significantly reduced; and that mutation of sequences flanking the *CYC-box* in *PACE* led to a reduction of the number of infected nodules per root systems. n: number of transgenic root systems or root pieces analysed. Numbers above the boxplots: the value of individual data points outside of the plotting area. n.a.: not applicable. WLI: white light illumination.

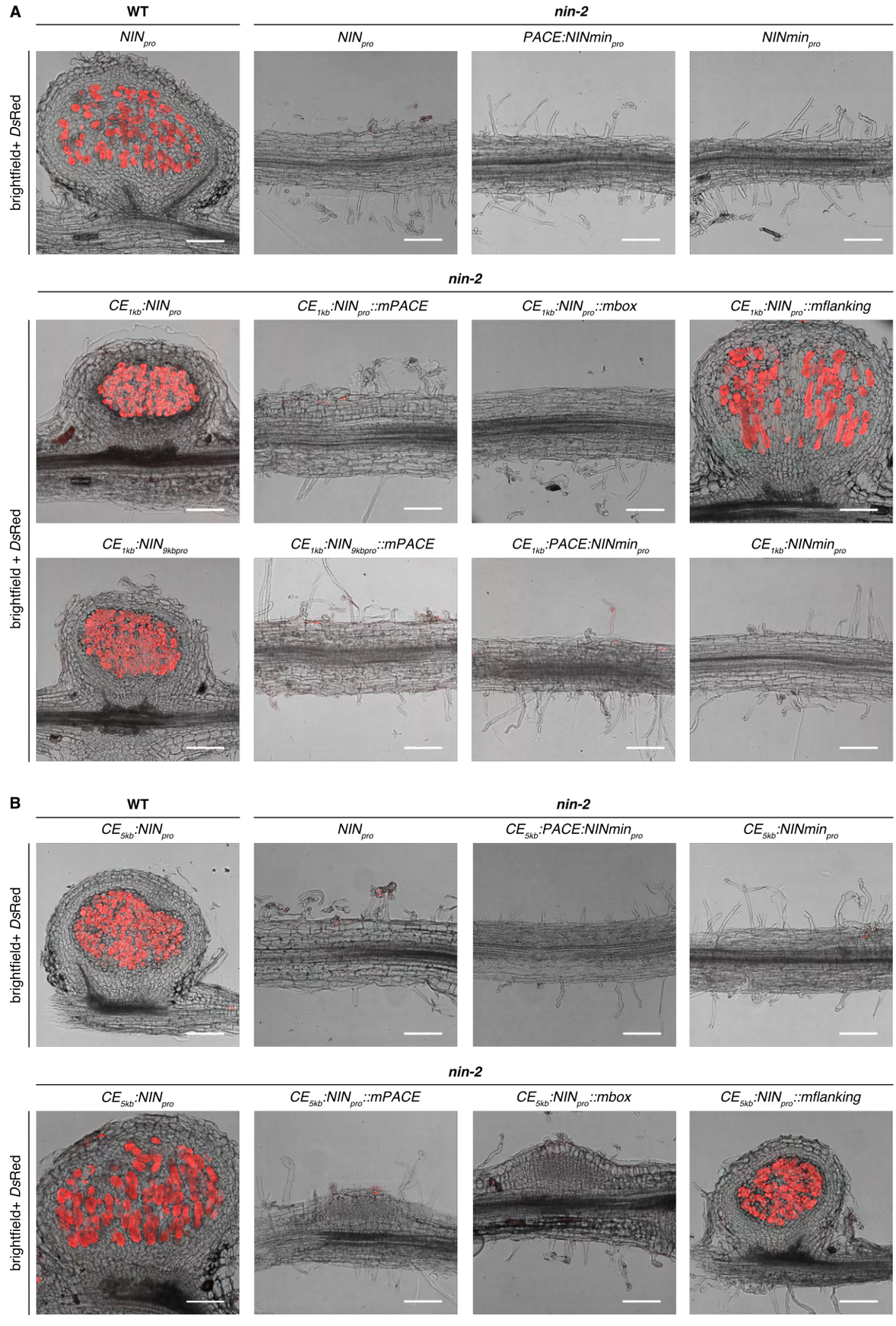

Figure 3 – figure supplement 5 | The *CYC-box* and flanking sequences of *PACE* are required for the complete restoration of the bacterial infection process but are dispensable for the nodule organogenesis process in the *L. japonicus nin-2* mutant. Pictures of nodule sections or roots from *L. japonicus nin-2* roots 21 dpi with *M. loti Ds*Red from the same experiments depicted in **Figure 3 – figure supplement 2** (**A**) and **Figure 3 – figure supplement 4** (**B**). Nodule sections from *L. japonicus* WT roots transformed with NIN_{pro}:*NIN* and $CE_{5kb}NIN_{pro}$:*NIN* were included for comparison. Note that when the cytokinin element-containing region of 1 kb was fused to NIN_{pro} nodule organogenesis was abolished by mutation of *PACE* or only the *CYC-box* in *PACE* and that these mutations did not abolish organogenesis when the cytokinin element-containing region of 5 kb was fused to NIN_{pro}. Bars, 100 µm.

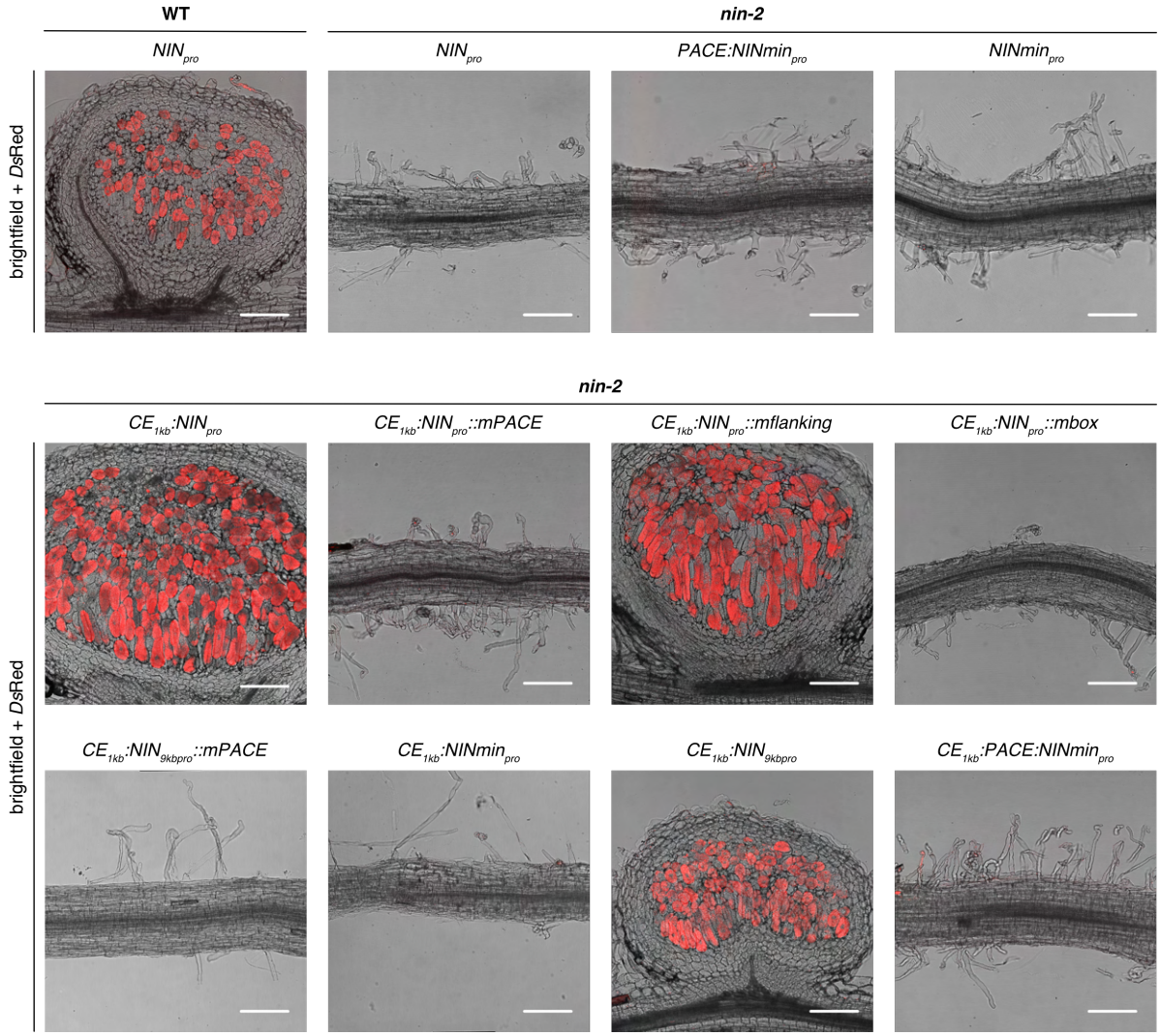

Figure 3 – figure supplement 6 | The *CYC-box* and flanking sequences of *PACE* are required for the complete restoration of the bacterial infection process in the *L. japonicus nin-2* mutant. Pictures of nodule sections or roots from *L. japonicus nin-2* roots 35 dpi with *M. loti Ds*Red from the same experiments depicted in **Figure 3 – figure supplement 3**. Upper left corner: a nodule section from a *L. japonicus* WT root transformed with NIN_{pro}*:NIN* was included for comparison. Bars, 100 µm.

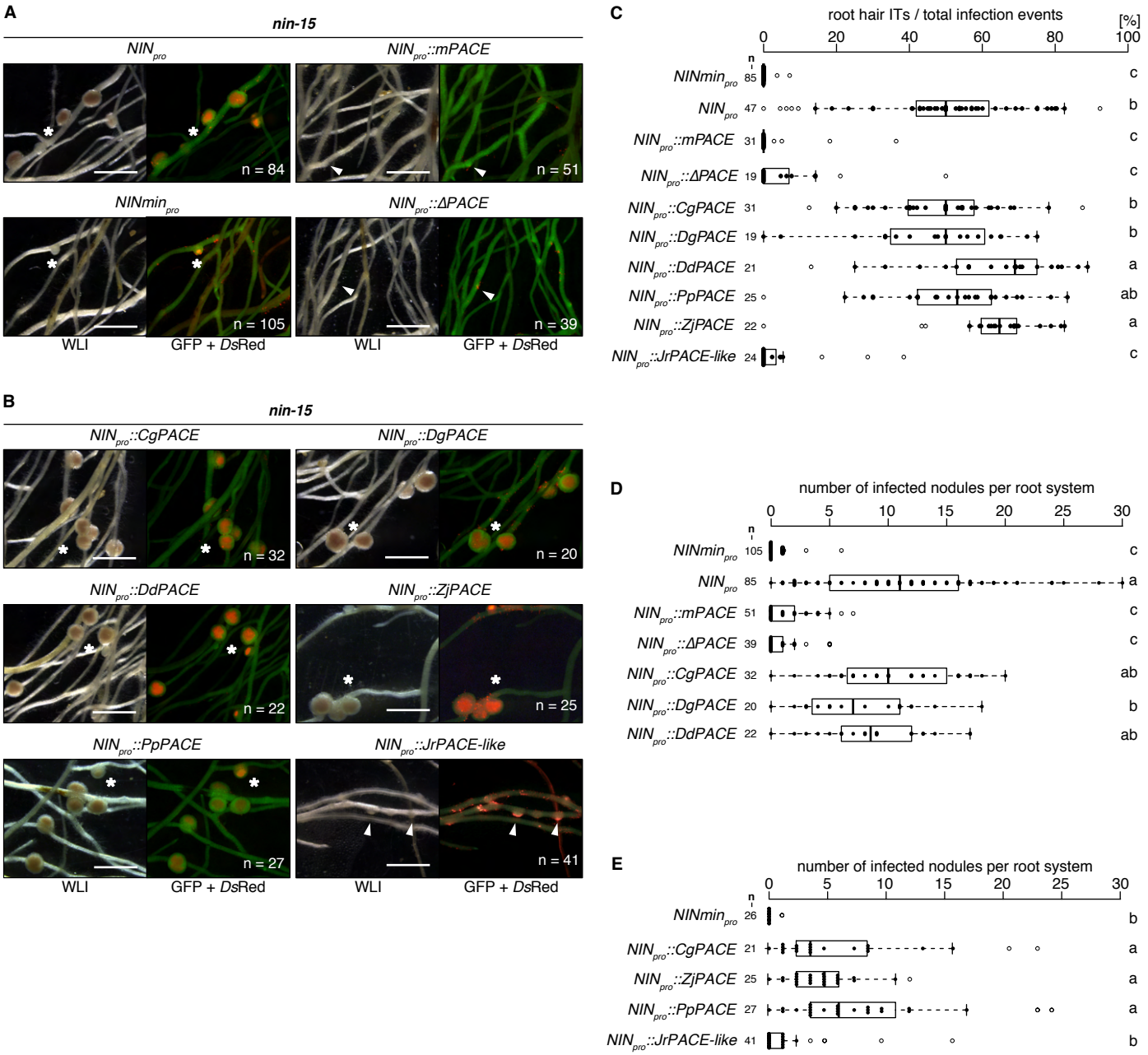

Figure 3 – figure supplement 7 | *PACEs* from FaFaCuRo species are functionally equivalent in restoring bacterial infection in the *L. japonicus nin-15* mutant. *L. japonicus nin-15* roots were transformed with T-DNAs carrying a *Ubq10*$_{pro}$*:NLS-GFP* transformation marker in tandem with the *LjNIN* gene driven by either of the following promoters: (**A**) the 3 kb *LjNIN* promoter (*NIN*$_{pro}$), the *LjNIN* minimal promoter (*NINmin*$_{pro}$), the 3 kb *LjNIN* promoter with *PACE* deleted (*NIN*$_{pro}$*::ΔPACE*) or mutated (*NIN*$_{pro}$*::mPACE*); (**B**) the 3 kb *LjNIN* promoter with *LjPACE* replaced with either of the *PACE* sequence variants from nodulating or non-nodulating FaFaCuRo species and analysed 21 dpi with *M. loti Ds*Red. (**A - B**) Representative overview pictures of *nin-15* transgenic roots systems. Sections of representative nodules are displayed in **Figure 3**. Note the drastic reduction of restoration of infection in nodules and root hairs associated with the mutation or deletion of *PACE* as well as the replacement of *PACE* with *JrPACE-like* in the context of the *LjNIN* promoter. White asterisks and arrowheads: infected and non-infected nodules, respectively. (**C - E**) Boxplots displaying **c,** the percentage of root hair ITs among total infection events (sum of bacterial entrapments and ITs) and (**D - E**) the number of infected nodules from two independent experiments. Each dot in (**D - E**) represents one *nin-15* transgenic root system. (**C**) displays merged data from all experiments as the percentage represents a normalised value calculated for each root piece (see **Figure 3 – Source Data 1**). n: number of transgenic root systems or root pieces analysed. For species abbreviations see **Figure 1 – figure supplement 5A**. The applied statistical method was ANOVA with *post hoc* Tukey: (**C**) $F_{9,313} = 106.7$, $p < 2x10^{-16}$; (**D**) $F_{6,346} = 82.89$, $p < 2x10^{-16}$; (**E**) $F_{4,135} = 20.18$, $p = 4.76x10^{-13}$. Different small letters indicate significant differences. Bars, 2 mm. WLI: white light illumination.

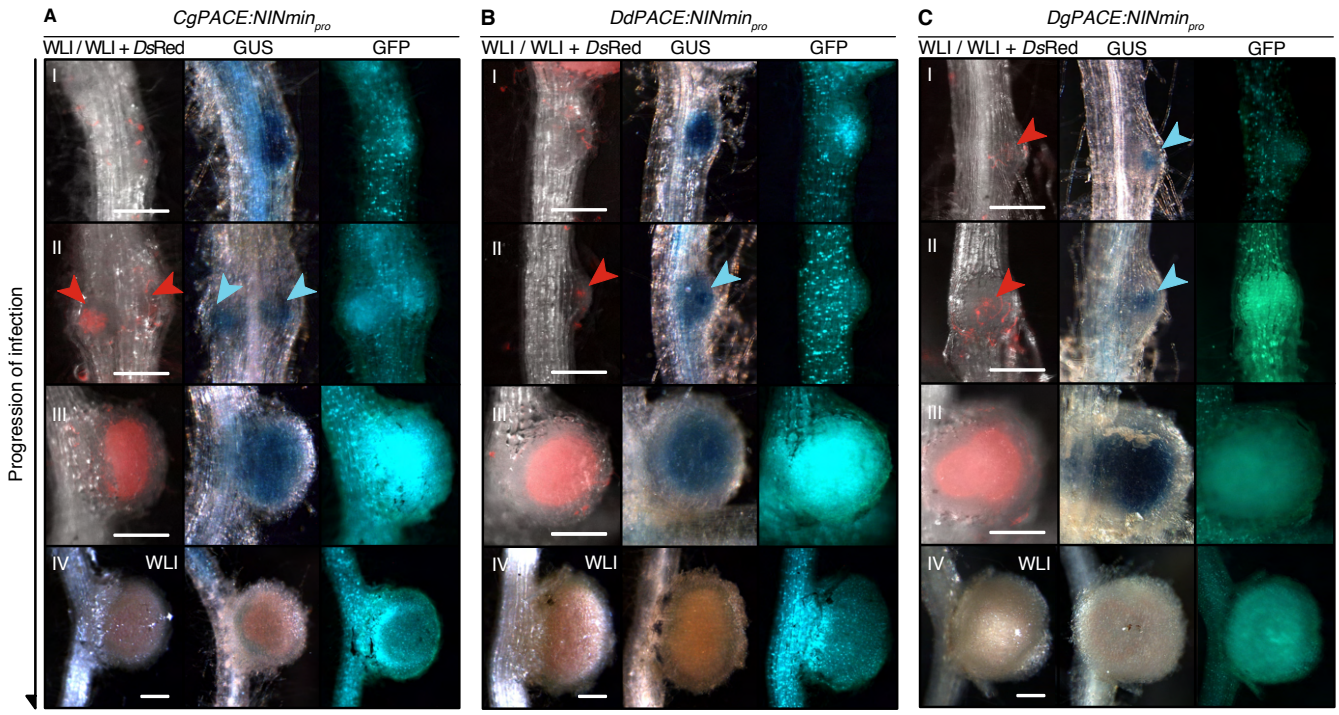

D

promoter:GUS	Time point (dpi)		
	0	10 -14	≥ 21
CgPACE:NINmin$_{pro}$	7[0]/7	14[23]/19	15[2]/20
DdPACE:NINmin$_{pro}$	8[0]/8	15[23]/18	17[2]/22
DgPACE:NINmin$_{pro}$	n.d.	35[23]/46	28[2]/38

#/#: root systems exhibiting GUS activity / total root systems analysed
[0] vasculature (of roots or nodules) and/or root tips
[1] epidermis (including root hairs)
[2] nodule primordia
[3] central tissue of nodules

Figure 3 – figure supplement 8 | Spatio-temporal *GUS* expression driven by *PACE* variants in *L. japonicus* roots during the bacterial infection process. *L. japonicus* WT roots were transformed with T-DNAs carrying a *Ubq10*$_{pro}$*:NLS-GFP* transformation marker together with a *GUS* reporter gene driven by either of the *PACE* variants from nodulating FaFaCuRo species fused to the *LjNIN* minimal promoter (*NINmin*$_{pro}$). For species abbreviations and experimental details see **Figure 1 – figure supplement 5A and Figure 2 – figure supplement 1**, respectively. Note the overlapping bacterial invasion zone and *PACE:NINmin*$_{pro}$*:GUS* expression in early infection stages (red and blue arrowheads in (**A - C**)). Red arrowheads: *M. loti Ds*Red. Blue arrowheads: GUS activity in nodule primordia. Only pictures taken under white light illumination (WLI) are displayed for nodules in panel VI to reveal the pink colour of leghemoglobin, characteristic for mature and fully infected nodules. Note that like *LjPACE*, the *PACE* variants-driven *GUS* expressions were absent at this stage (panel IV in (**A - C**) and panel IV in **Figure 2 – figure supplement 1D**). (**D**) Quantification of transgenic root systems exhibiting *GUS* expression in different cell types and tissues exemplarily displayed in (**A - C**). n.d.: not determined. Bars, 250 µm.

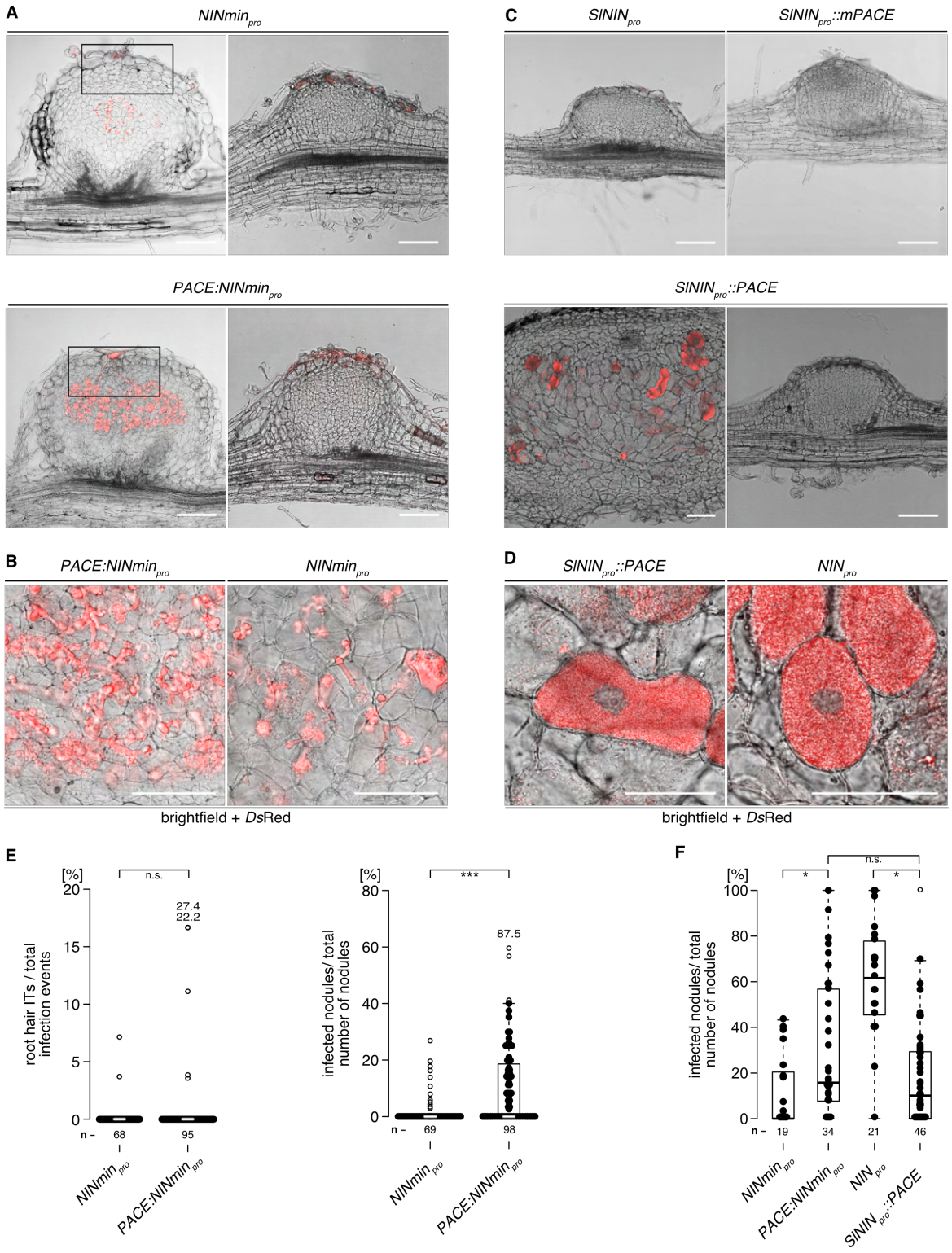

Figure 4 – figure supplement 1 | *PACE* alone or in the context of the *S. lycopersicum NIN* promoter (a species outside of the FaFaCuRo clade) enables IT formation in the cortex. (**A - D**) Representative pictures of sections of nodules formed on *L. japonicus nin-15* roots transformed with T-DNAs carrying a *Ubq10*$_{pro}$*:NLS-GFP* transformation marker together with the *LjNIN* gene driven by either of the following promoters: (**A - B**) the *L. japonicus NIN* minimal promoter (*NINmin*$_{pro}$) or *PACE* fused to *NINmin*$_{pro}$ (*PACE:NINmin*$_{pro}$); (**C - D**) the 3 kb *S. lycopersicum NIN* promoter (*SlNIN*$_{pro}$), the 3 kb *SlNIN* promoter with mutated *PACE* (*SlNIN*$_{pro}$*::mPACE*) or with *L. japonicus PACE* inserted (*SlNIN*$_{pro}$*::PACE*), 21 dpi with *M. loti Ds*Red (from the same experiments depicted in **Figure 4**). Black rectangles in (**A**) demarcate the enlarged area displayed in **Figure 4A and 4B** to focus on the initial infection structures. Note the absence of cells filled with symbiosomes in nodules transformed with the *LjNIN* gene driven by *PACE:NINmin*$_{pro}$ or *NINmin*$_{pro}$. By contrast, infected cells were often filled with symbiosomes in the *SlNIN*$_{pro}$*::PACE:NIN*-transformed nodules, like those resulted by *NIN*$_{pro}$*:NIN* (see (**C**) and compare the two sections in (**D**)). (**E - F**) Boxplots displaying the percentage of root hair ITs among total infection events (sum of bacterial entrapments and ITs) or the percentage of infected nodules among total number of nodules (**E**) 21 dpi and (**F**) 35 dpi with *M. loti Ds*Red, respectively. Each dot represents one *nin-15* transgenic root system or root piece. (**E**) displays results from an independent repetition from the experiment depicted in **Figure 4**. n: number of transgenic root systems or root pieces analysed. Numbers above the boxplots: the value of individual data points outside of the plotting area. The applied statistical method was Fisher's exact test: *$p < 0.05$; ***$p < 0.001$; n.s.: not significant. Bars, (**A and C**) 100 µm; (**B and D**) 50 µm.

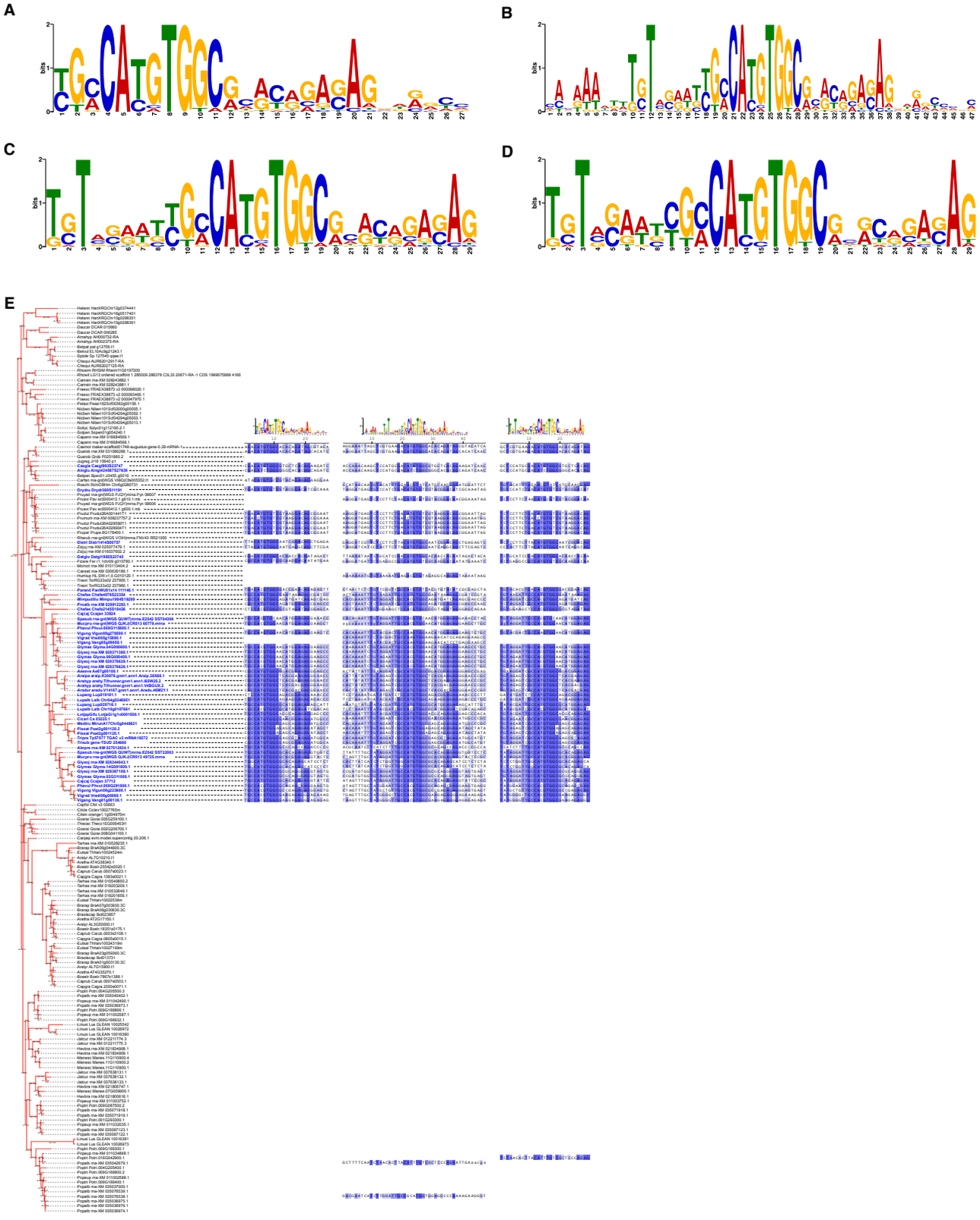

Figure 1 – figure supplement 1 | Discovery of *PACE* by MEME analyses. (**A - D**) Consensus sequence of the Position Weight Matrix identified by MEME analyses using the regions upstream of the translational start site (ATG) thus representing the promoters and 5'UTRs of *NIN* and *NLP* genes from 37 angiosperm species (see Methods): (**A**) in a discriminative search for a motif that is present in 3 kb upstream regions of the *NIN* genes from nodulating FaFaCuRo species, but absent in 3 kb upstream regions of the *NIN* genes from species outside of the FaFaCuRo clade and absent in the 3 kb upstream regions of *NLP* genes; (**B**) in an independent, non-discriminative search in the 3 kb upstream regions of the *NIN* genes from nodulating species revealing that the most conserved nucleotides span a larger region than (**A**); (**C**) the resulted most conserved 29 nucleotides derived from upstream regions of *NIN* genes of nodulating FaFaCuRo species; (**D**) the resulted most conserved 29 nucleotides (*PACE*) derived from the upstream region of one representative *NIN* gene per species of nodulating FaFaCuRo species. (**E**) Motif analyses by FIMO using the upstream regions of the *NIN* and *NLP* genes from an expanded list of 163 species (see Methods). Left: pruned tree from the whole *NLP* tree (demarcated in the black rectangle in **Figure 1 – figure supplement 2**) corresponding to the *NIN* orthologs. Right: three versions of consensus sequence (left to right, (**A, B and D**), respectively) were used to retrieve motifs from the 5 kb upstream region of *NIN* genes *via* FIMO search, the output of which is displayed underneath the consensus sequences. Sequence names of nodulating species are coloured in blue. Blank lines represent the absence of significant motifs.

Figure 1 – figure supplement 2 I *PACE* is present exclusively in the FaFaCuRo clade. Motif analyses by FIMO using the using the regions upstream of the translational start site (ATG) thus representing the promoters and 5'UTRs of the *NIN* and *NLP* genes from an expanded list of 163 species (see Methods). Left: Maximum likelihood tree of *NLP* family (model: GTR+F+R10) of 163 species (**Figure 1 – Source Data 2**). Tree was rooted on the Charophytes algae *Klebsormidium nitens*. Black box demarcates the area that is displayed in **Figure 1 – figure supplement 1E**. Blank lines represent the absence of significant motifs. Sequence names of nodulating species are coloured in blue. The different NLP clades are indicated by branch colours and named according to the *Arabidopsis thaliana* nomenclature. Right: three versions of consensus sequence (left to right, **Figure 1 – figure supplement 1A, 1B and 1D**, respectively) were used to retrieve motifs from the 5 kb upstream region of *NIN* genes via FIMO search, the output of which is displayed underneath the consensuses sequences.

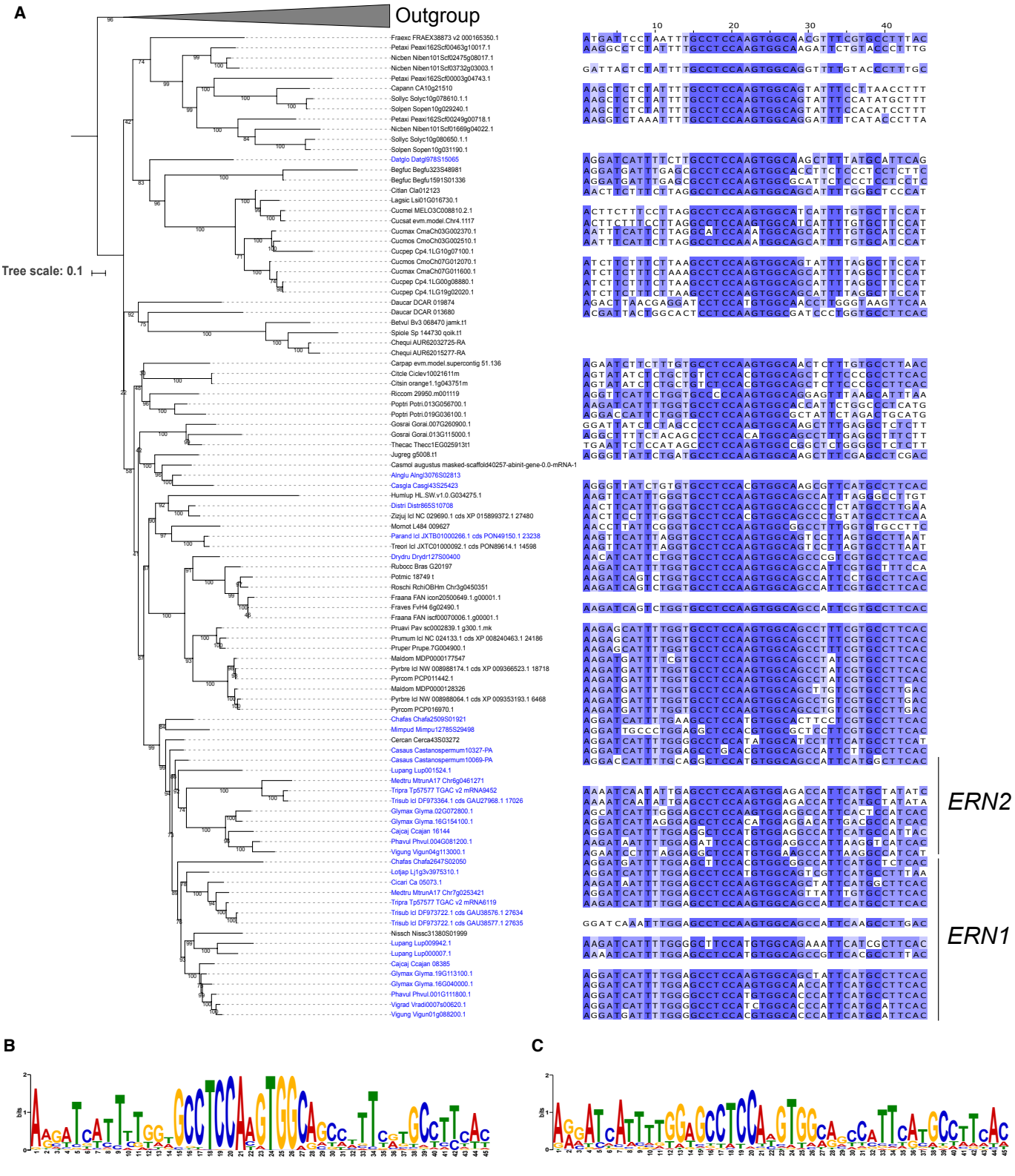

Figure 1 – figure supplement 3 | The presence of a motif encompassing the previously identified Cyclops binding site within the regions upstream of the translational start site (ATG) thus representing the promoters and 5'UTRs of *ERN1* genes extends beyond the FaFaCuRo clade. (**A**) Maximum likelihood of *ERN1/ERN2* (model: JTT+F+R5) from 87 species (**Supplementary file 1**) based on protein sequences. Tree was rooted using sequences from the *ERN1/ERN2* paralog *ERN3* (outgroup clade collapse and indicated by grey triangle marked "Outgroup"). Species belonging to the monophyletic FaFaCuRo clade (Stevens, 2017) are indicated by thicker black branches. *ERN1* and *ERN2* subclades are indicated. Sequence names of nodulating species are coloured in blue. These conserved motifs identified by MEME analyses in the 3 kb upstream regions were aligned and displayed next to species names. While the presence of a conserved Cyclops binding site containing motif in species outside of the FaFaCuRo clade is consistent with the role of *RAM1* in arbuscular mycorrhizal symbiosis, a function of *ERN1* in arbuscular mycorrhizal symbiosis has not been described and suggests a yet unidentified function of *ERN1* outside of the FaFaCuRo clade. (**B**) Consensus sequence of the Position Weight Matrix identified by MEME analyses of all the species. (**C**) Consensus sequence of the Position Weight Matrix identified by MEME analyses when analysing only the nodulating species.

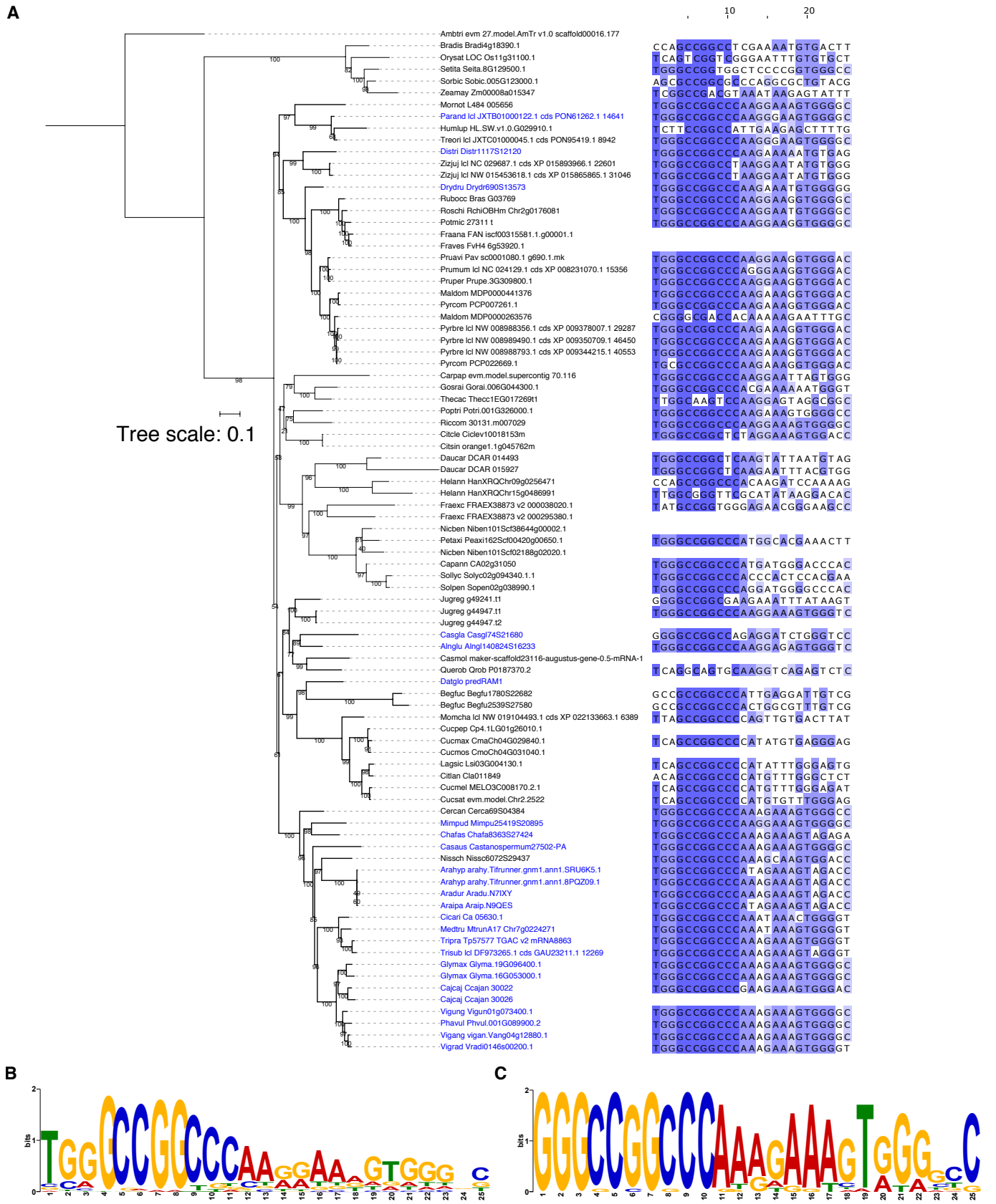

Figure 1 – figure supplement 4 | The presence of a motif encompassing the previously identified Cyclops binding site within the regions upstream of the translational start site (ATG) thus representing the promoters and 5'UTRs of *RAM1* genes extends beyond the FaFaCuRo clade. (**A**) Maximum likelihood of *RAM1* (model: JTT+F+R4) from 87 species (**Supplementary file 1**) engaging in arbuscular mycorrhizal symbiosis. Tree was rooted on the early-diverging angiosperm *Amborella trichopoda*. Species belonging to the monophyletic FaFaCuRo clade (Stevens, 2017) are indicated by thicker black branches. Sequence names of nodulating species are coloured in blue. These conserved motifs identified by MEME analyses in the 3 kb upstream regions are aligned and displayed next to species names. Blank lines represent the absence of identified motif due to genome contiguity issues. (**B**) Consensus sequence of the Position Weight Matrix identified by MEME analyses when analysing all the mycorrhizal species. (**C**) Consensus sequence of the Position Weight Matrix identified by MEME analyses when analysing only the nodulating species.

A

Abbre-viation	Species	Plant Order	RNS	FaFaCuRo member
Lj	*Lotus japonicus*	Fabales	Yes	Yes
Cg	*Casuarina glauca*	Fagales	Yes	Yes
Jr	*Juglans regia*	Fagales	No	Yes
Dd	*Dryas drummondii*	Rosales	Yes	Yes
Zj	*Ziziphus jujuba*	Rosales	No	Yes
Pp	*Prunus persica*	Rosales	No	Yes
Dg	*Datisca glomerata*	Cucurbitales	Yes	Yes
Sl	*Solanum lycopersicum* (tomato)	Solanales	No	No
Vv	*Vitis vinifera*	Vitales	No	No

B

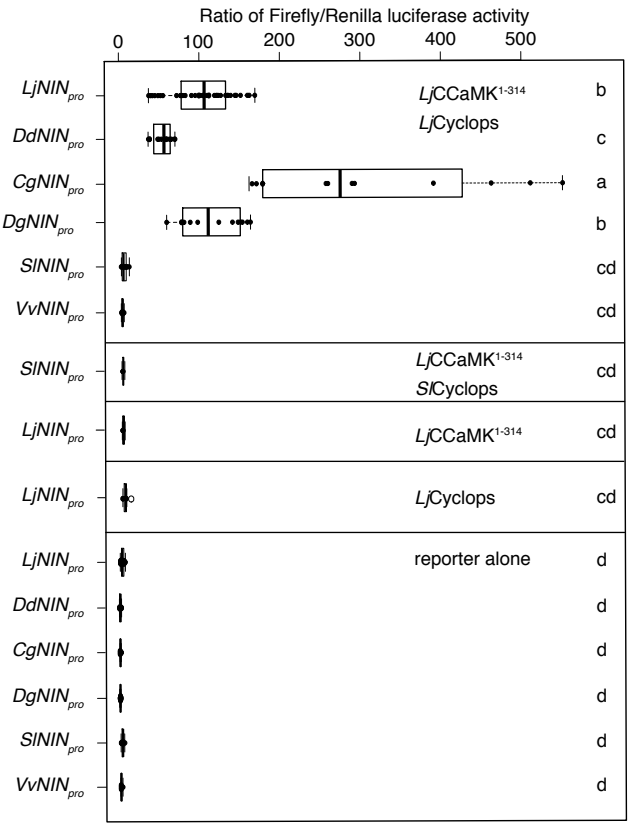

C

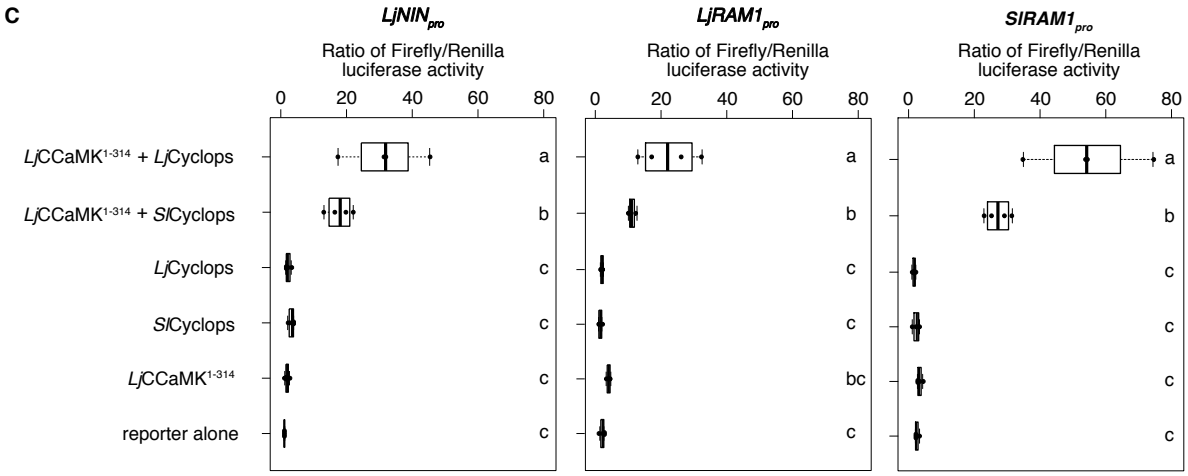

Figure 1 – figure supplement 5 | Transcriptional activation of *NIN promoter:Firefly luciferase* reporter gene by CCaMK$^{1-314}$/Cyclops is restricted to *NIN* promoters from species of the FaFaCuRo clade. *Nicotiana benthamiana* leaf cells were transformed with T-DNAs carrying a *Firefly luciferase* reporter gene driven by either of the indicated promoters in tandem with the *AtACT2$_{pro}$:Renilla luciferase* reporter fusion that provides a quantitative internal standard. (**A**) List of species within the FaFaCuRo clade (light red shade) and outside (light grey shade) and abbreviations. (**B**) Reporter gene activation by *L. japonicus* CCaMK$^{1-314}$/Cyclops via *NIN* promoters (*NIN$_{pro}$*) originating from listed species. (**C**) Comparison of the transactivation potential of Cyclops versions from *L. japonicus* and *S. lycopersicum*. Note that the expression of the *Firefly luciferase* reporter gene driven by *LjNIN$_{pro}$*, the *RAM1* promoters from *L. japonicus* and *S. lycopersicum* (*LjRAM1$_{pro}$* and *SlRAM1$_{pro}$*, respectively) was induced in the presence of CCaMK$^{1-314}$/Cyclops regardless of the origin of Cyclops. In contrast, the transactivation failed with the *SlNIN* promoter (panel (**A**)). The applied statistical method was ANOVA with *post hoc* Tukey: (**B**), $F_{14,214} = 71.07$, $p < 2x10^{-16}$; (**C**), plots from left to right: $F_{5,18} = 20.58$, $p = 7.14x10^{-7}$; $F_{5,18} = 25.38$, $p = 1.45x10^{-7}$ and $F_{5,18} = 40.49$, $p = 3.55x10^{-9}$, respectively. Different small letters indicate significant differences.

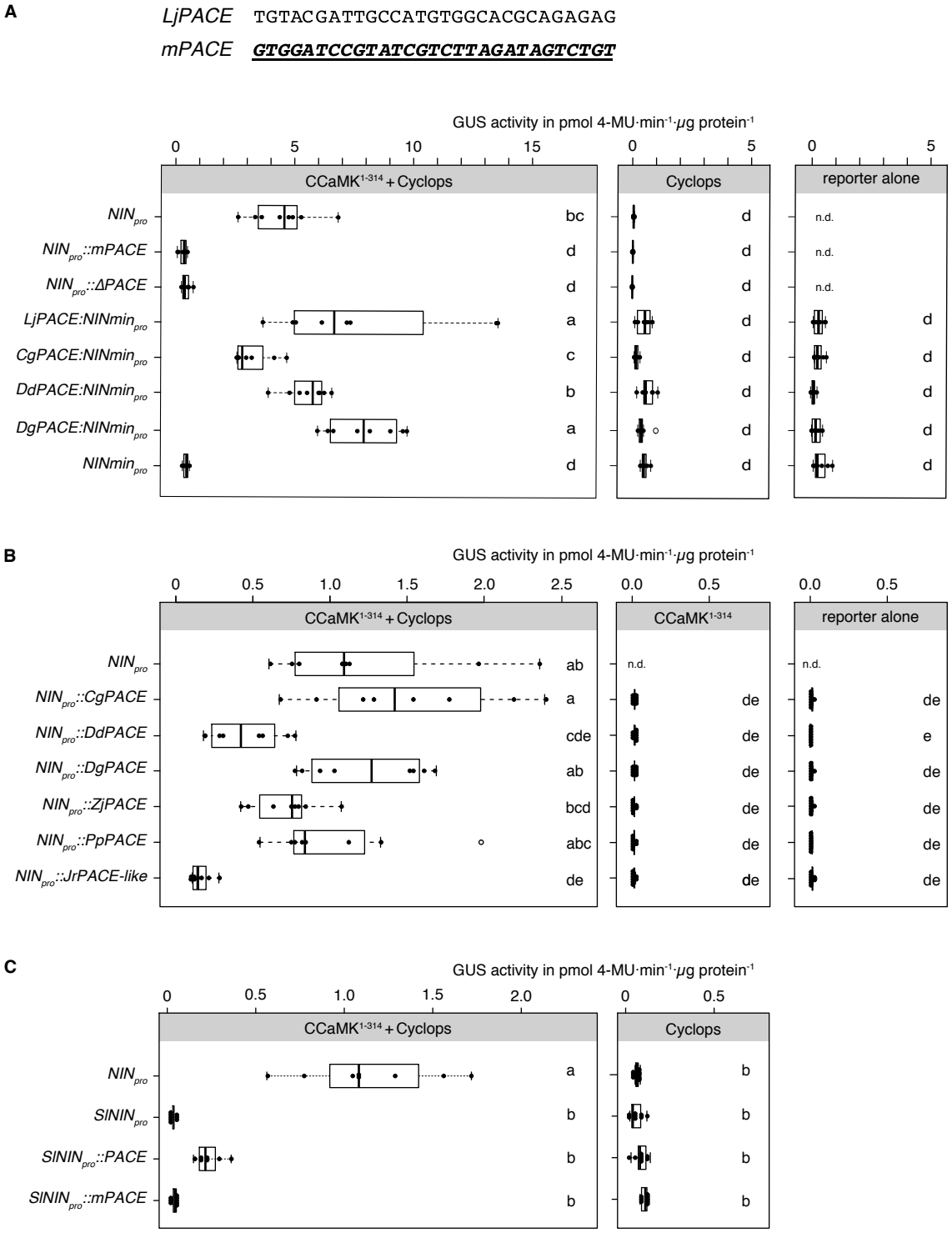

Figure 1 – figure supplement 6 | *PACE* sequence variants from species across the FaFaCuRo clade were able to functionally replace *L. japonicus PACE* in a *LjNIN$_{pro}$:GUS* reporter fusion. *N. benthamiana* leaf cells were transformed with T-DNAs carrying a *GUS* reporter gene driven by either of the indicated promoters: (**A**) the *L. japonicus NIN* promoter (*NIN$_{pro}$*), the *LjNIN* promoter with *PACE* mutated or deleted (*NIN$_{pro}$::mPACE* and *NIN$_{pro}$::ΔPACE*, respectively), or *PACE* sequence variants from the nodulating FaFaCuRo species fused to the *LjNIN* minimal promoter (*NINmin$_{pro}$*); (**B**) chimeric promoters where *LjPACE* in the *LjNIN* promoter was replaced with either one of the *PACE* variants from species tested in (**A**) or from non-nodulating FaFaCuRo species including the *Juglans regia PACE*-like motif (*JrPACE-like*); (**C**) the *S. lycopersicum NIN* promoter (*SlNIN$_{pro}$*), the *SlNIN* promoter with *LjPACE* (*SlNIN$_{pro}$::PACE*) or *mPACE* (*SlNIN$_{pro}$::mPACE*) inserted. For species abbreviations see **Figure 1 – figure supplement 5A**. Note in (**A**) that the deletion or mutation of *PACE* in *LjNIN* promoter resulted in a drastic reduction in reporter gene expression and in (**C**) insertion of *LjPACE* but not *mPACE* into the *S. lycopersicum* promoter confers transactivation by CCaMK$^{1-314}$/Cyclops. The applied statistical method was ANOVA with *post hoc* Tukey: (**A**) $F_{20,144} = 51.38$, $p < 2x10^{-16}$; (**B**), $F_{18,166} = 149.1$, $p < 2x10^{-16}$; (**C**) $F_{7,62} = 30.5$, $p = 7.02x10^{-7}$. Different small letters indicate significant difference. n.d., not determined.

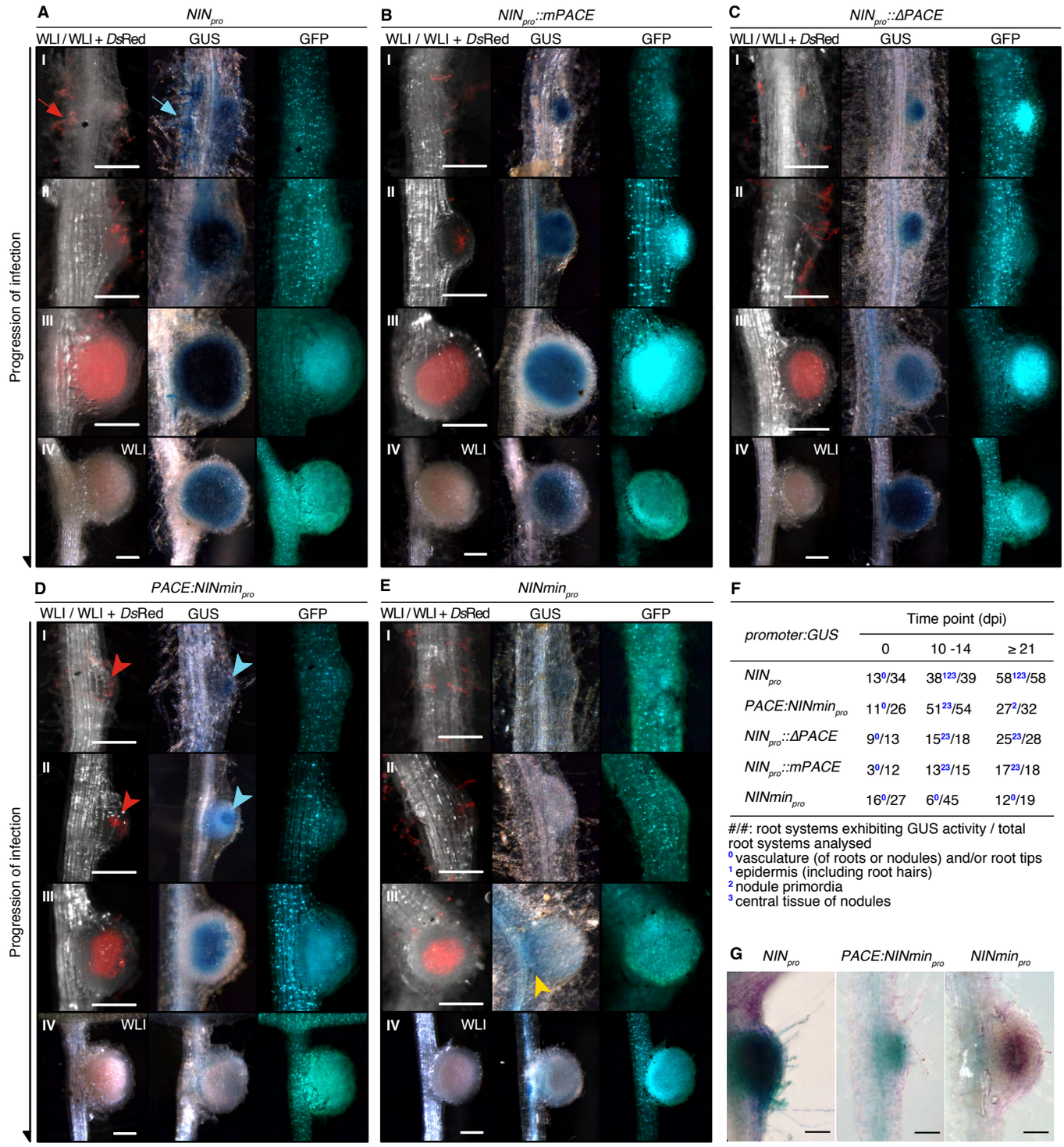

promoter:GUS	Time point (dpi)		
	0	10 -14	≥ 21
NIN_{pro}	$13^{0}/34$	$38^{123}/39$	$58^{123}/58$
$PACE:NINmin_{pro}$	$11^{0}/26$	$51^{23}/54$	$27^{2}/32$
NIN_{pro}::ΔPACE	$9^{0}/13$	$15^{23}/18$	$25^{23}/28$
NIN_{pro}::mPACE	$3^{0}/12$	$13^{23}/15$	$17^{23}/18$
$NINmin_{pro}$	$16^{0}/27$	$6^{0}/45$	$12^{0}/19$

#/#: root systems exhibiting GUS activity / total root systems analysed
[0] vasculature (of roots or nodules) and/or root tips
[1] epidermis (including root hairs)
[2] nodule primordia
[3] central tissue of nodules

Figure 2 – figure supplement 1 I Spatio-temporal *GUS* expression driven by *PACE* and the *NIN* promoter in *L. japonicus* roots during the bacterial infection process. *L. japonicus* wild-type hairy roots were transformed with T-DNAs carrying a $Ubq10_{pro}$:*NLS-GFP* transformation marker together with a *GUS* reporter gene driven by either of the indicated promoters: (**A**) the 3 kb *LjNIN* promoter (NIN_{pro}); the *LjNIN* promoter with *PACE* (**B**) mutated ($LjNIN_{pro}$::*mPACE*) or (**C**) deleted (NIN_{pro}::*ΔPACE*); (**D**) *PACE* fused to the *LjNIN* minimal promoter ($PACE:NINmin_{pro}$) or (**E**) the *LjNIN* minimal promoter ($NINmin_{pro}$). The progression of bacterial infection was determined by the *Ds*Red signal 10 - 14 days post inoculation (dpi) with *M. loti Ds*Red. Nodules undergoing different stages of infection (panels I to IV) were stained with X-Gluc to reveal the *GUS* expression pattern. Note the overlapping bacterial invasion zone and $PACE:NINmin_{pro}$:*GUS* expression in early infection stages (red and blue arrowheads in (**D**)) as well as the differences between $PACE:NINmin_{pro}$:*GUS* and the much broader NIN_{pro}:*GUS* expression at that stage (red and blue arrows in (**A**)). Red arrow and arrowheads: *M. loti Ds*Red. Blue arrow and arrowheads: GUS activity in root hairs bearing ITs and nodule primordia, respectively. The $NINmin_{pro}$:*GUS* fusion gave only rarely detectable signal, and if so in the vasculature (yellow arrowhead in (**E**)). Only pictures taken under white light illumination (WLI) are displayed for nodules in panel VI to reveal the pink colour of leghemoglobin, characteristic for mature and fully infected nodules. Note that $PACE:NINmin_{pro}$:*GUS* expression was absent at this stage, whereas the NIN_{pro}:*GUS* resulted in strong blue staining in the nodule regardless of the presence of *PACE* (compare panel IV in (**D**) and (**A - C**)). (**F**) Quantification of transgenic root systems exhibiting *GUS* expression in different cell types and tissues exemplarily displayed in (**A - E**). (**G**) *PACE* drove *GUS* reporter gene expression in the central tissue of primordia and nodules, but was not sufficient for expression in root hairs. Transgenic roots carrying promoter:GUS fusions same as in (**A, D and E**) were inoculated with *M. loti lacZ* and dual-stained with X-Gluc and Magenta-Gal. Purple: *M. loti lacZ*. Blue: GUS activity. Note the co-existence of blue and purple staining in root hairs on roots transformed by NIN_{pro}:*GUS*, but not that transformed by $PACE:NINmin_{pro}$:*GUS*. Bars, 250 µm.

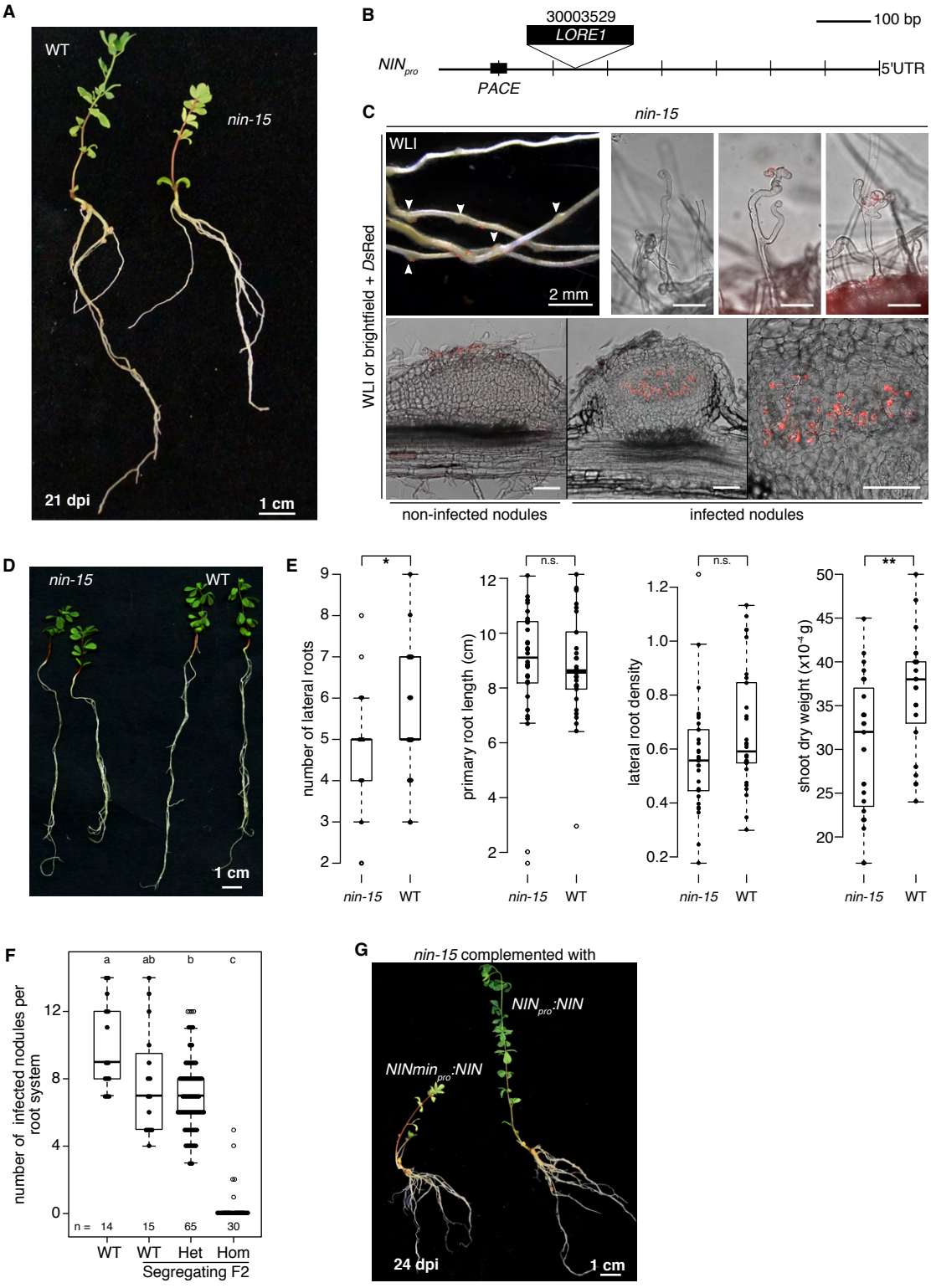

Figure 3 – figure supplement 1 I *L. japonicus nin-15* mutant phenotype. (**A**) A representative picture of *L. japonicus* wild-type (WT, left) and *nin-15* (right) plants 21 dpi with *M. loti Ds*Red. (**B**) Position of the *Lotus Retrotransposon 1* (*LORE1*) insertion within the *NIN* promoter in the *nin-15* mutant. (**C**) Representative pictures of *nin-15* root hairs and nodule sections 21 dpi with *M. loti Ds*Red. Forty-nine plants with a total number of 436 nodules were analysed: only four plants bore one or two IT(s) within root hairs and seven plants bore one or two infected nodule(s). Deformed or curled root hairs in the presence of *M. loti Ds*Red were abundant but infection threads were rarely found. Arrowheads: uninfected nodules. Unlabelled bars, 100 µm. (**D - E**) Phenotype of *nin-15* in the presence of a symbiosis-independent nitrogen source (15 mM KNO_3) for 28 days. (**D**) Pictures documenting the healthy status of *L. japonicus* WT and *nin-15* plants (compare (**D**) and (**A**)) and (**E**) quantitative assessment of parameters displayed in boxplots. Thirty plants per genotype were analysed. Each dot represents one plant. Lateral root density: number of lateral roots/primary root length (cm). The applied statistical method was pairwise *t*-test: $*p < 0.05$; $**p < 0.01$; n.s.: not significant. (**F**) Segregation analysis of *nin-15*. The applied statistical method was ANOVA with *post hoc* Tukey: $F_{3,120} = 84.1$, $p = 2x10^{-16}$. Different small letters indicate significant difference. (**G**) Representative pictures of *nin-15* plants with hairy roots transformed with the *NIN* gene driven by the *L. japonicus NIN* minimal promoter ($NINmin_{pro}$) or the 3 kb *NIN* promoter (NIN_{pro}) 24 dpi with *M. loti Ds*Red. WLI: white light illumination.

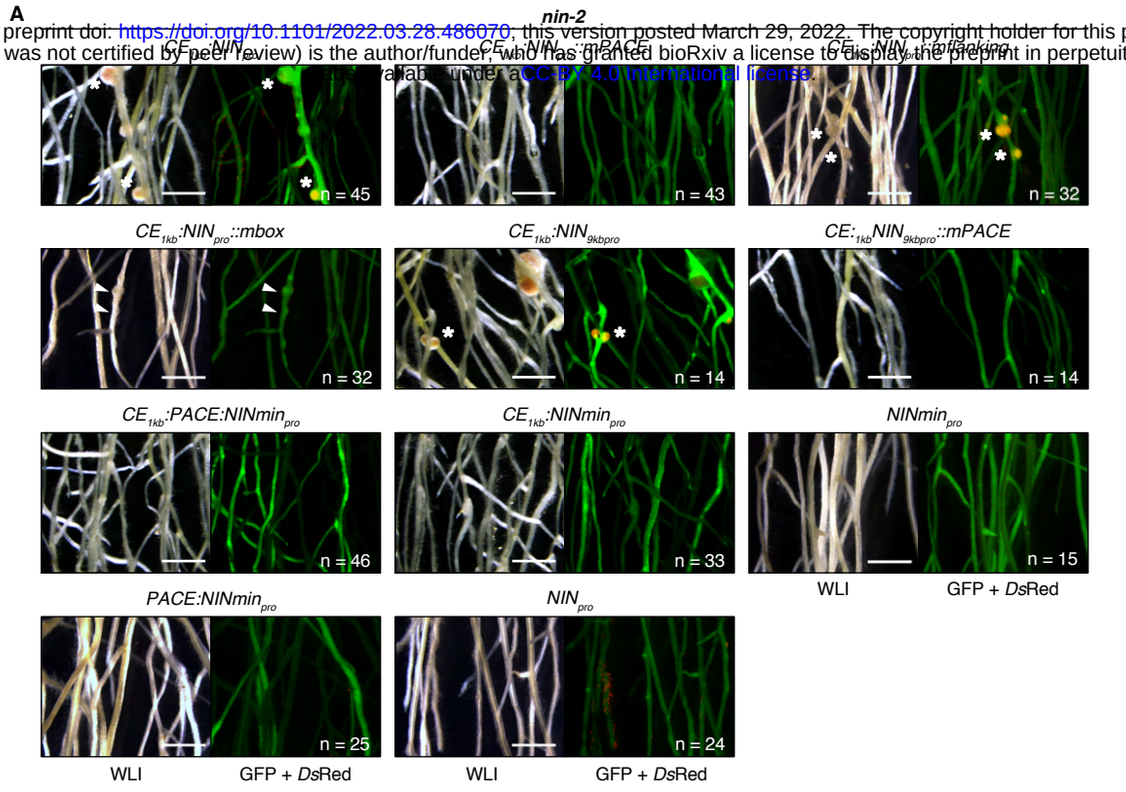

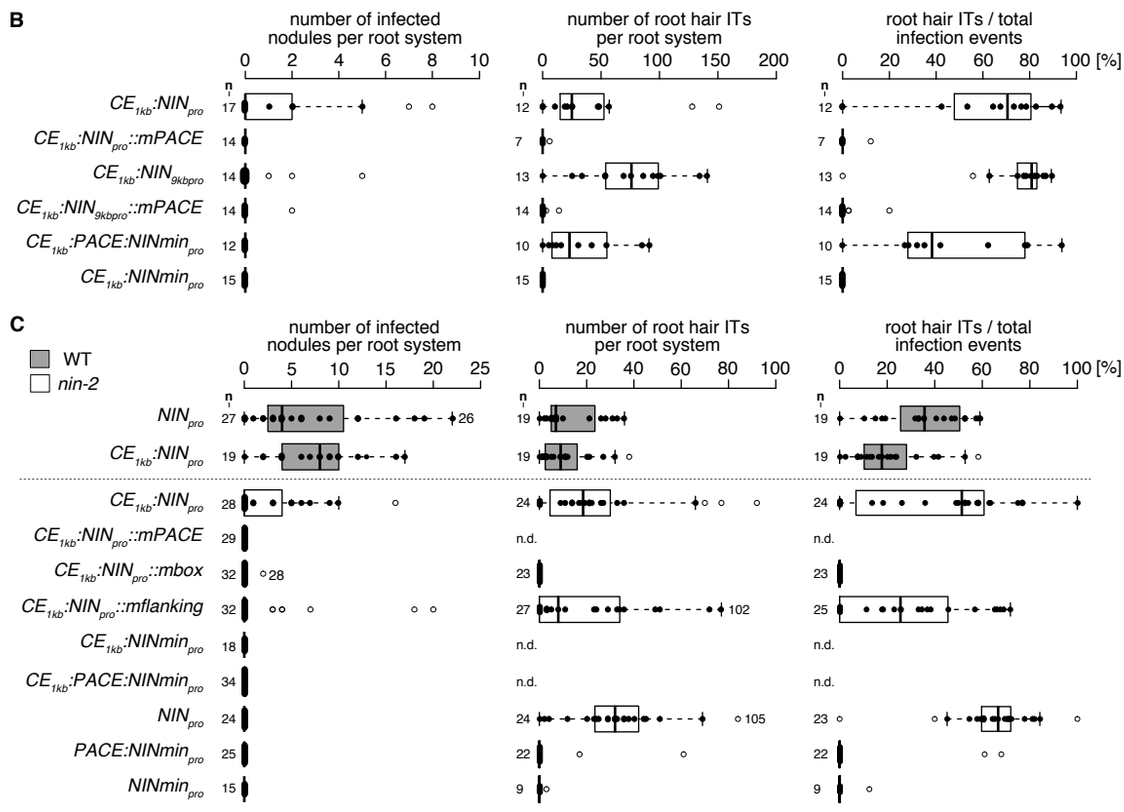

Figure 3 – figure supplement 2 | The *CYC-box* and flanking sequences of *PACE* are required for the complete restoration of the bacterial infection process in the *L. japonicus nin-2* mutant. *nin-2* roots were transformed with T-DNAs carrying a *Ubq10*$_{pro}$*:NLS-GFP* transformation marker in tandem with the *LjNIN* gene driven by either of the following promoter versions: the cytokinin element-containing region of 1 kb (*CE*$_{1kb}$) fused to the 3 kb or 9 kb *LjNIN* promoter (*CE*$_{1kb}$*:NIN*$_{pro}$ or *CE*$_{1kb}$*:NIN*$_{9kbpro}$, respectively); *CE*$_{1kb}$*:NIN*$_{pro}$ or *CE*$_{1kb}$*:NIN*$_{9kbpro}$ with *PACE* mutated (*CE*$_{1kb}$*:NIN*$_{pro}$*::mPACE* or *CE*$_{1kb}$*:NIN*$_{9kbpro}$*::mPACE*, respectively); *CE*$_{1kb}$*:NIN*$_{pro}$ carrying a mutated Cyclops binding site (*CYC-box*) (*CE*$_{1kb}$*:NIN*$_{pro}$*::mbox*); *CE*$_{1kb}$*:NIN*$_{pro}$ carrying mutated sequences flanking the *CYC-box* in *PACE* (*CE*$_{1kb}$*:NIN*$_{pro}$*::mflanking*); *CE*$_{1kb}$ fused to the *LjNIN* minimal promoter (*CE*$_{1kb}$*:NINmin*$_{pro}$); *CE*$_{1kb}$ fused to *PACE* and to *NINmin*$_{pro}$ (*CE*$_{1kb}$*:PACE:NINmin*$_{pro}$); *NIN*$_{pro}$, *PACE:NINmin*$_{pro}$ or *NINmin*$_{pro}$. (**A**) Representative overview pictures of transgenic root systems. Roots were analysed 21 dpi with *M. loti Ds*Red. White asterisks and arrowheads: infected and non-infected nodules, respectively. Bars, 2 mm. (**B - C**) Boxplots displaying the number of root hair ITs or infected nodules and the percentage of root hair ITs among total infection events (sum of bacterial entrapments and ITs). Each dot represents one transgenic *nin-2* root system or root piece. *L. japonicus* WT roots transformed with *NIN*$_{pro}$*:NIN* or *CE*$_{1kb}$*:NIN*$_{pro}$*:NIN* were included as controls. Note the loss of restoration of nodules and IT formation associated with the mutation of *PACE* or only the *CYC-box* in *PACE*; and the reduction of same when sequences flanking the *CYC-box* in *PACE* were mutated. n: number of transgenic root systems or root pieces analysed. Numbers above the boxplots: the value of individual data points outside of the plotting area. n.d.: not determined. WLI: white light illumination.

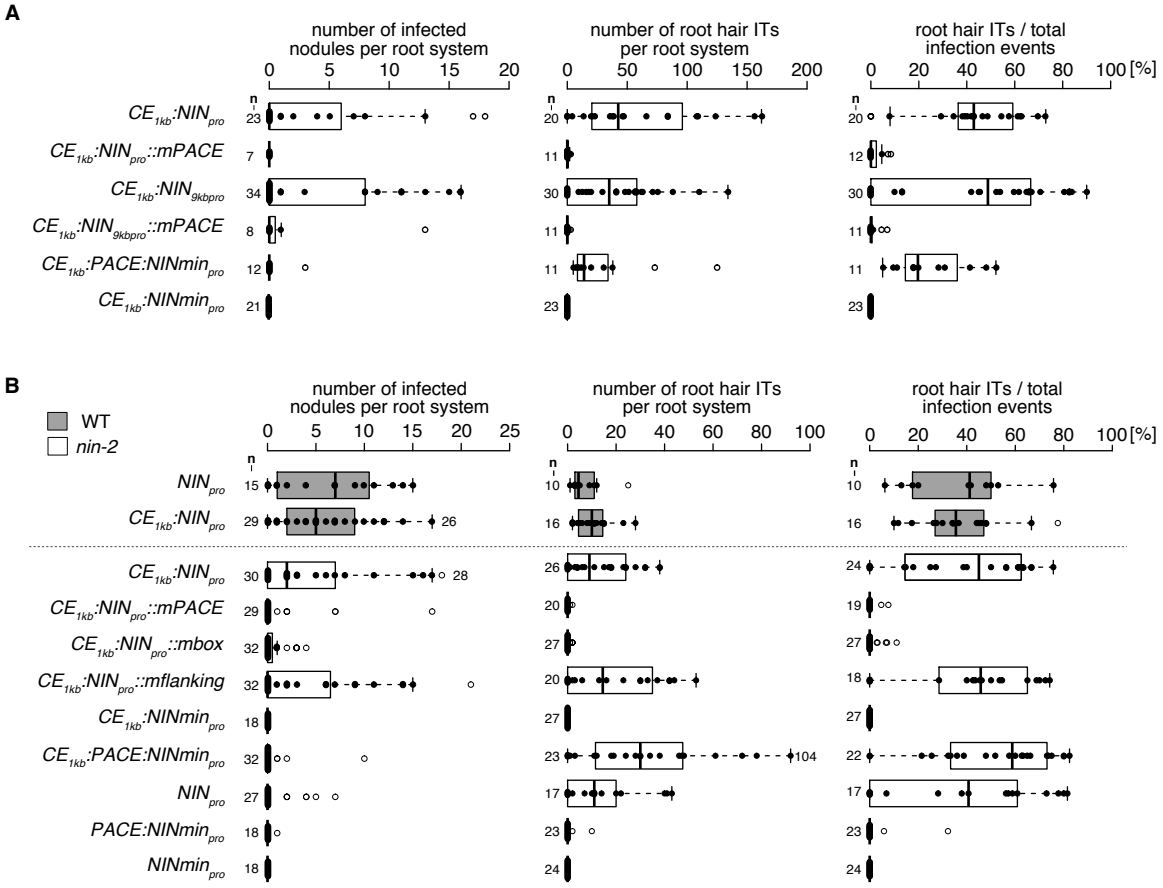

Figure 3 – figure supplement 3 | The *CYC-box* and flanking sequences of *PACE* are required for the complete restoration of the bacterial infection process in the *L. japonicus nin-2* mutant. Roots were from a subset of plants from the same experiment depicted in **Figure 3 – figure supplement 2** but analysed 35 dpi with *M. loti Ds*Red. (**A - B**) Boxplots displaying the number of root hair ITs or infected nodules and the percentage of root hair ITs among total infection events (sum of bacterial entrapments and ITs). Each dot represents one transgenic *nin-2* root system or root piece. *L. japonicus* WT roots transformed with NIN_{pro}:*NIN* or CE_{1kb}:NIN_{pro}:*NIN* were included as controls. Note that the results follow the same trend as those obtained 21 dpi with *M. loti Ds*Red (**Figure 3 – figure supplement 2**). n: number of transgenic root systems or root pieces analysed. Numbers above the boxplots: the value of individual data points outside of the plotting area.

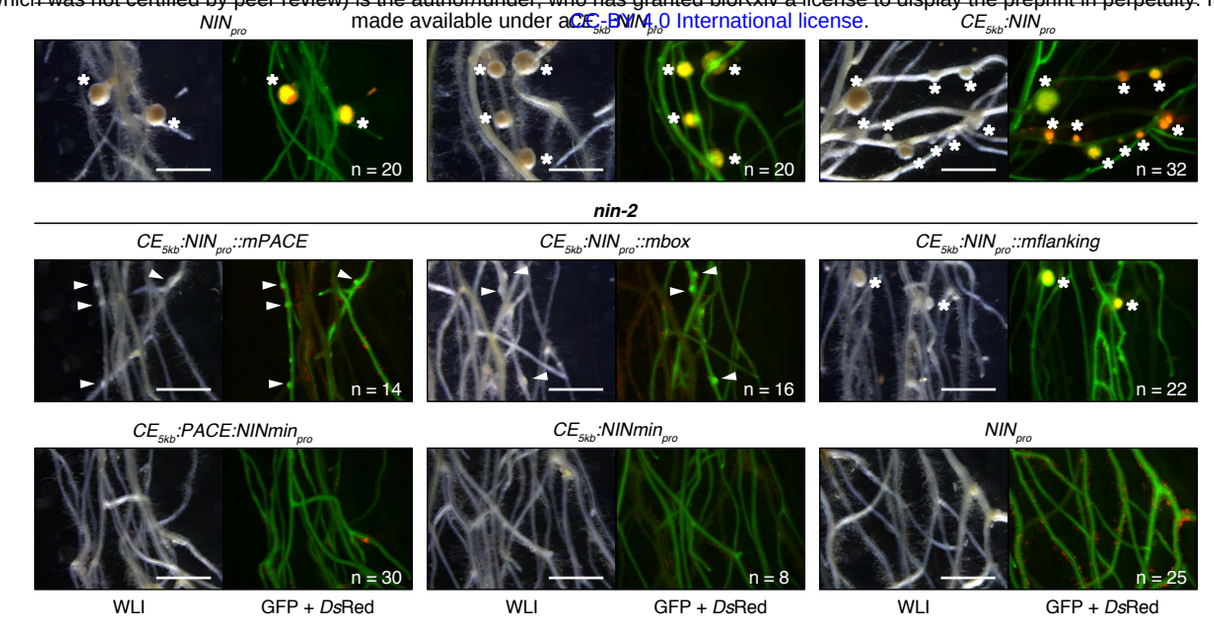

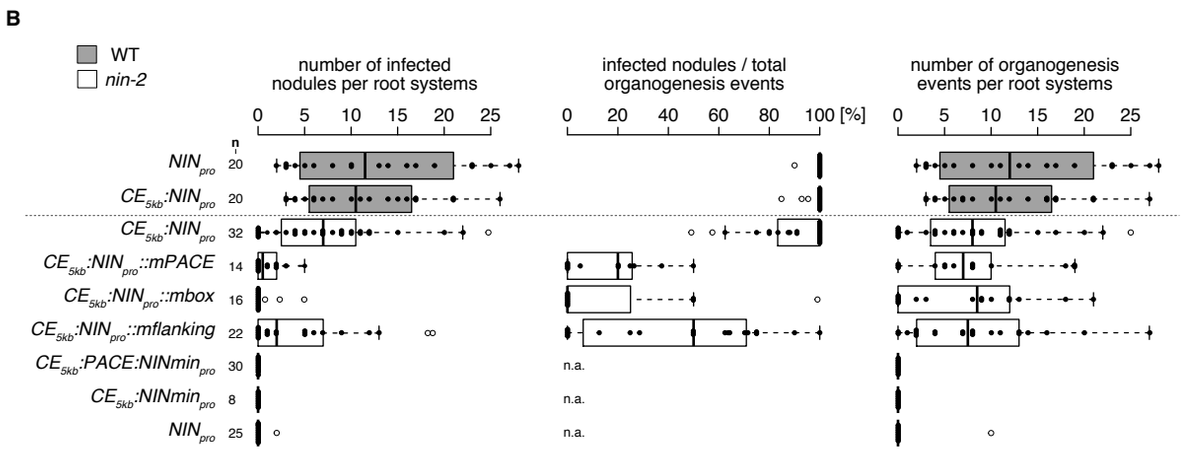

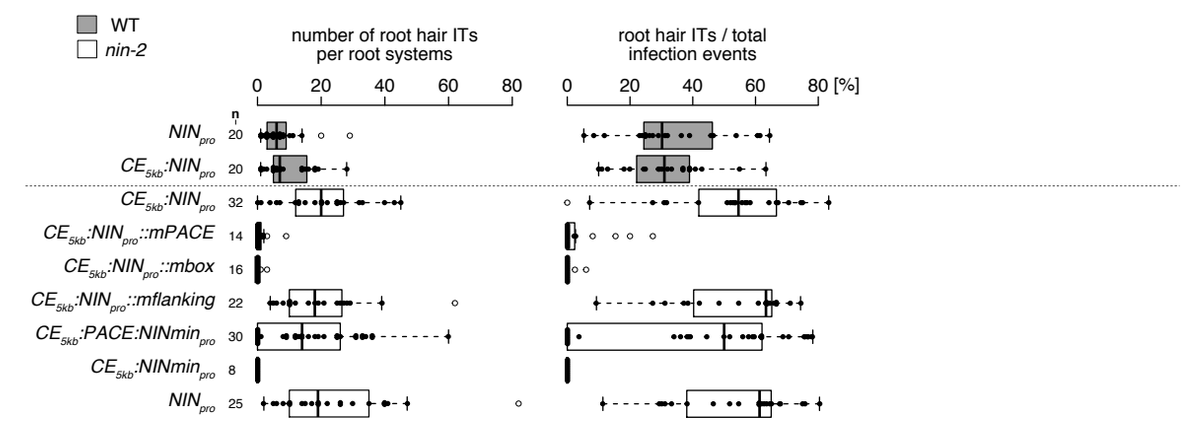

Figure 3 – figure supplement 4 | The *CYC-box* and flanking sequences of *PACE* are required for the complete restoration of the bacterial infection process but are dispensable for the nodule organogenesis process in the *L. japonicus nin-2* mutant. *nin-2* roots were transformed with T-DNAs carrying a *Ubq10*$_{pro}$*:NLS-GFP* transformation marker in tandem with the *LjNIN* gene driven by either of the following promoter versions: the cytokinin element-containing region of 5 kb (*CE*$_{5kb}$) fused to the 3 kb *LjNIN* promoter (*CE*$_{5kb}$*:NIN*$_{pro}$); *CE*$_{5kb}$*:NIN*$_{pro}$ with *PACE* mutated (*CE*$_{5kb}$*:NIN*$_{pro}$*::mPACE*); *CE*$_{5kb}$*:NIN*$_{pro}$ carrying a mutated Cyclops binding site (*CYC-box*) (*CE*$_{5kb}$*:NIN*$_{pro}$*::mbox*); *CE*$_{5kb}$*:NIN*$_{pro}$ carrying mutated sequences flanking the *CYC-box* in *PACE* (*CE*$_{5kb}$*:NIN*$_{pro}$*::mflanking*); *CE*$_{5kb}$ fused to the *LjNIN* minimal promoter (*CE*$_{5kb}$*:NINmin*$_{pro}$); *CE*$_{5kb}$ fused to *PACE* and to *NINmin*$_{pro}$ (*CE*$_{5kb}$*:PACE:NINmin*$_{pro}$) or *NIN*$_{pro}$. (**A**) Representative overview pictures of transgenic root systems. Roots were analysed 21 dpi with *M. loti Ds*Red. White asterisks and arrowheads: infected and non-infected nodules, respectively. Bars, 2 mm. (**B**) Boxplots displaying the number of infected nodules, the percentage of infected nodules among total organogenesis events (sum of infected and non-infected nodules) and the number of organogenesis events. (**C**) Boxplots displaying the number of root hair ITs and the percentage of root hair ITs among total infection events (sum of bacterial entrapments and ITs). Each dot represents one transgenic *nin-2* root system or root piece. *L. japonicus* WT roots transformed with *NIN*$_{pro}$*:NIN* or *CE*$_{5kb}$*:NIN*$_{pro}$*:NIN* were included as controls. Note that the mutation of *PACE* or only the *CYC-box* in *PACE* led to an almost complete loss of IT formation and infected nodules per root system while nodule organogenesis was not significantly reduced; and that mutation of sequences flanking the *CYC-box* in *PACE* led to a reduction of the number of infected nodules per root systems. n: number of transgenic root systems or root pieces analysed. Numbers above the boxplots: the value of individual data points outside of the plotting area. n.a.: not applicable. WLI: white light illumination.

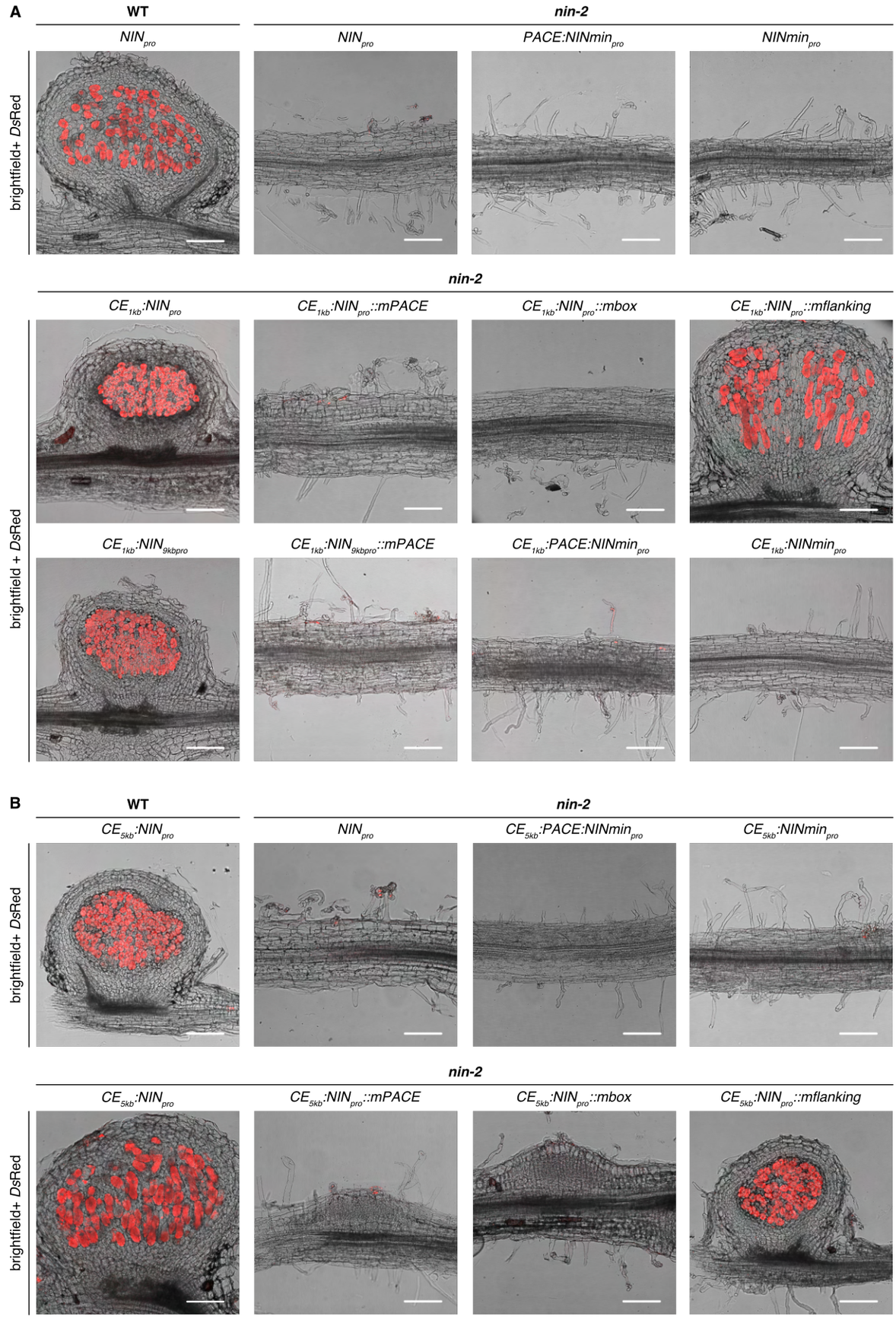

Figure 3 – figure supplement 5 | The *CYC-box* and flanking sequences of *PACE* are required for the complete restoration of the bacterial infection process but are dispensable for the nodule organogenesis process in the *L. japonicus nin-2* mutant. Pictures of nodule sections or roots from *L. japonicus nin-2* roots 21 dpi with *M. loti Ds*Red from the same experiments depicted in **Figure 3 – figure supplement 2** (**A**) and **Figure 3 – figure supplement 4** (**B**). Nodule sections from *L. japonicus* WT roots transformed with NIN_{pro}:*NIN* and $CE_{5kb}NIN_{pro}$:*NIN* were included for comparison. Note that when the cytokinin element-containing region of 1 kb was fused to NIN_{pro} nodule organogenesis was abolished by mutation of *PACE* or only the *CYC-box* in *PACE* and that these mutations did not abolish organogenesis when the cytokinin element-containing region of 5 kb was fused to NIN_{pro}. Bars, 100 µm.

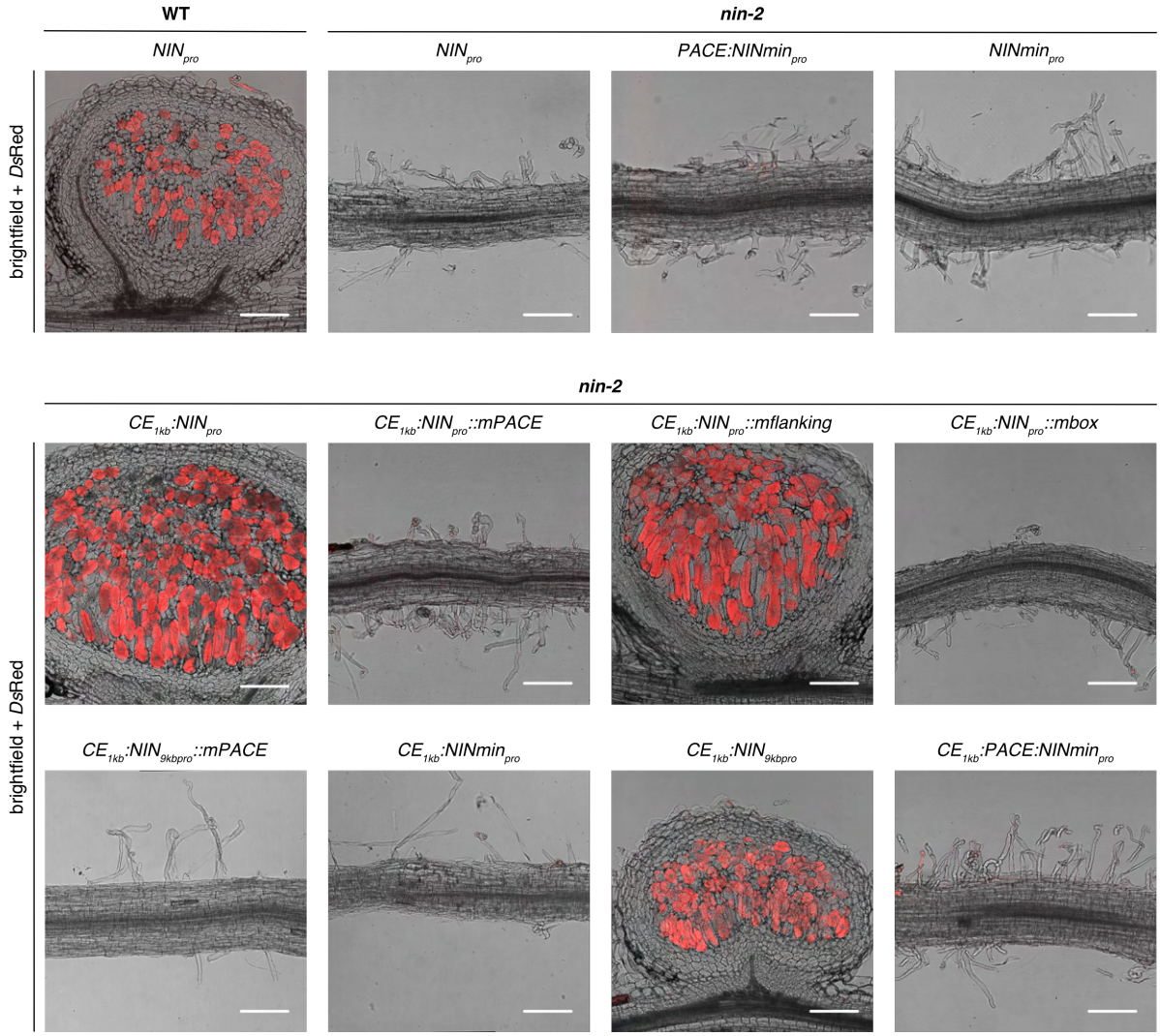

Figure 3 – figure supplement 6 | The *CYC-box* and flanking sequences of *PACE* are required for the complete restoration of the bacterial infection process in the *L. japonicus nin-2* mutant. Pictures of nodule sections or roots from *L. japonicus nin-2* roots 35 dpi with *M. loti Ds*Red from the same experiments depicted in **Figure 3 – figure supplement 3**. Upper left corner: a nodule section from a *L. japonicus* WT root transformed with NIN_{pro}*:NIN* was included for comparison. Bars, 100 µm.

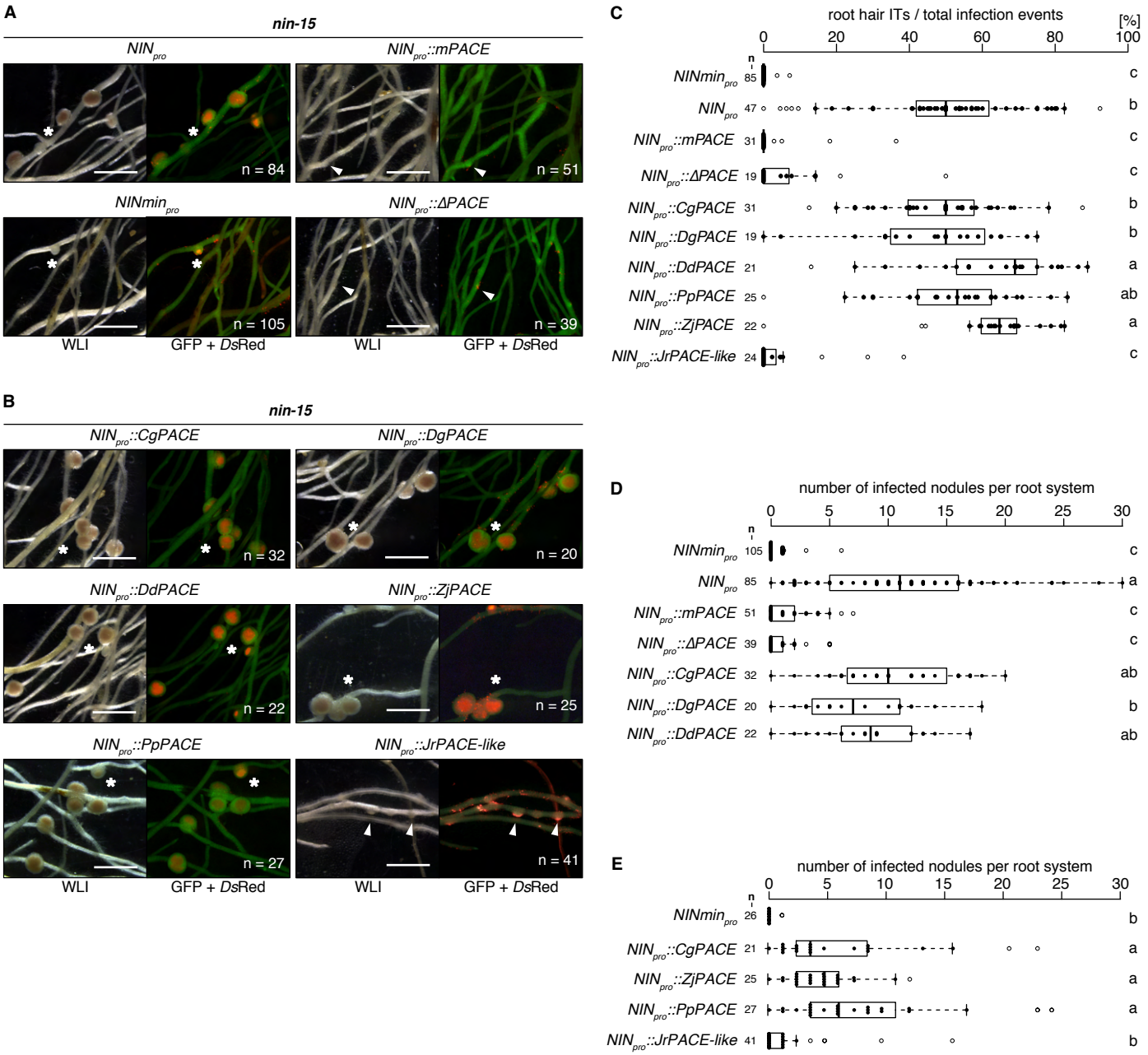

Figure 3 – figure supplement 7 | *PACEs* from FaFaCuRo species are functionally equivalent in restoring bacterial infection in the *L. japonicus nin-15* mutant. *L. japonicus nin-15* roots were transformed with T-DNAs carrying a *Ubq10*$_{pro}$*:NLS-GFP* transformation marker in tandem with the *LjNIN* gene driven by either of the following promoters: (**A**) the 3 kb *LjNIN* promoter (*NIN*$_{pro}$), the *LjNIN* minimal promoter (*NINmin*$_{pro}$), the 3 kb *LjNIN* promoter with *PACE* deleted (*NIN*$_{pro}$*::ΔPACE*) or mutated (*NIN*$_{pro}$*::mPACE*); (**B**) the 3 kb *LjNIN* promoter with *LjPACE* replaced with either of the *PACE* sequence variants from nodulating or non-nodulating FaFaCuRo species and analysed 21 dpi with *M. loti Ds*Red. (**A - B**) Representative overview pictures of *nin-15* transgenic roots systems. Sections of representative nodules are displayed in **Figure 3**. Note the drastic reduction of restoration of infection in nodules and root hairs associated with the mutation or deletion of *PACE* as well as the replacement of *PACE* with *JrPACE-like* in the context of the *LjNIN* promoter. White asterisks and arrowheads: infected and non-infected nodules, respectively. (**C - E**) Boxplots displaying **c,** the percentage of root hair ITs among total infection events (sum of bacterial entrapments and ITs) and (**D - E**) the number of infected nodules from two independent experiments. Each dot in (**D - E**) represents one *nin-15* transgenic root system. (**C**) displays merged data from all experiments as the percentage represents a normalised value calculated for each root piece (see **Figure 3 – Source Data 1**). n: number of transgenic root systems or root pieces analysed. For species abbreviations see **Figure 1 – figure supplement 5A**. The applied statistical method was ANOVA with *post hoc* Tukey: (**C**) $F_{9,313} = 106.7$, $p < 2x10^{-16}$; (**D**) $F_{6,346} = 82.89$, $p < 2x10^{-16}$; (**E**) $F_{4,135} = 20.18$, $p = 4.76x10^{-13}$. Different small letters indicate significant differences. Bars, 2 mm. WLI: white light illumination.

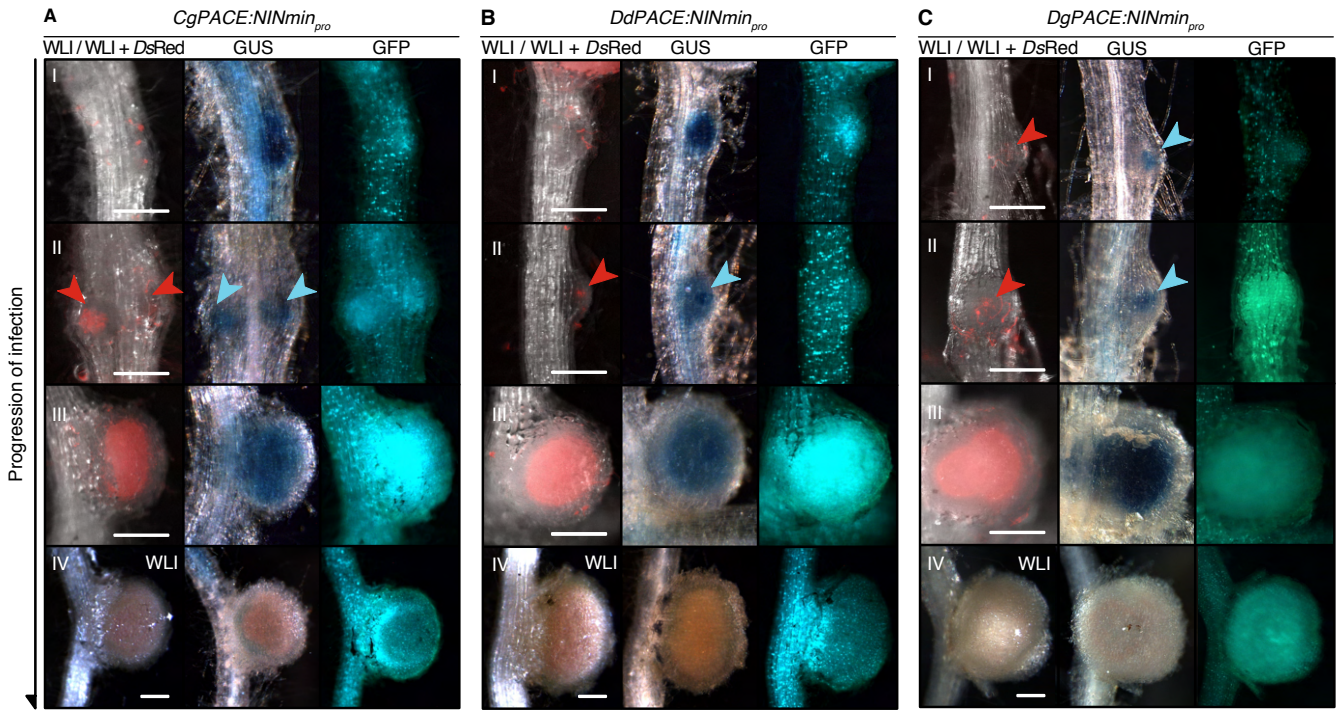

D

promoter:GUS	Time point (dpi)		
	0	10 -14	≥ 21
CgPACE:NINmin$_{pro}$	7[0]/7	14[23]/19	15[2]/20
DdPACE:NINmin$_{pro}$	8[0]/8	15[23]/18	17[2]/22
DgPACE:NINmin$_{pro}$	n.d.	35[23]/46	28[2]/38

#/#: root systems exhibiting GUS activity / total root systems analysed
[0] vasculature (of roots or nodules) and/or root tips
[1] epidermis (including root hairs)
[2] nodule primordia
[3] central tissue of nodules

Figure 3 – figure supplement 8 | Spatio-temporal *GUS* expression driven by *PACE* variants in *L. japonicus* roots during the bacterial infection process. *L. japonicus* WT roots were transformed with T-DNAs carrying a *Ubq10*$_{pro}$*:NLS-GFP* transformation marker together with a *GUS* reporter gene driven by either of the *PACE* variants from nodulating FaFaCuRo species fused to the *LjNIN* minimal promoter (*NINmin*$_{pro}$). For species abbreviations and experimental details see **Figure 1 – figure supplement 5A and Figure 2 – figure supplement 1**, respectively. Note the overlapping bacterial invasion zone and *PACE:NINmin*$_{pro}$*:GUS* expression in early infection stages (red and blue arrowheads in (**A - C**)). Red arrowheads: *M. loti Ds*Red. Blue arrowheads: GUS activity in nodule primordia. Only pictures taken under white light illumination (WLI) are displayed for nodules in panel VI to reveal the pink colour of leghemoglobin, characteristic for mature and fully infected nodules. Note that like *LjPACE*, the *PACE* variants-driven *GUS* expressions were absent at this stage (panel IV in (**A - C**) and panel IV in **Figure 2 – figure supplement 1D**). (**D**) Quantification of transgenic root systems exhibiting *GUS* expression in different cell types and tissues exemplarily displayed in (**A - C**). n.d.: not determined. Bars, 250 µm.

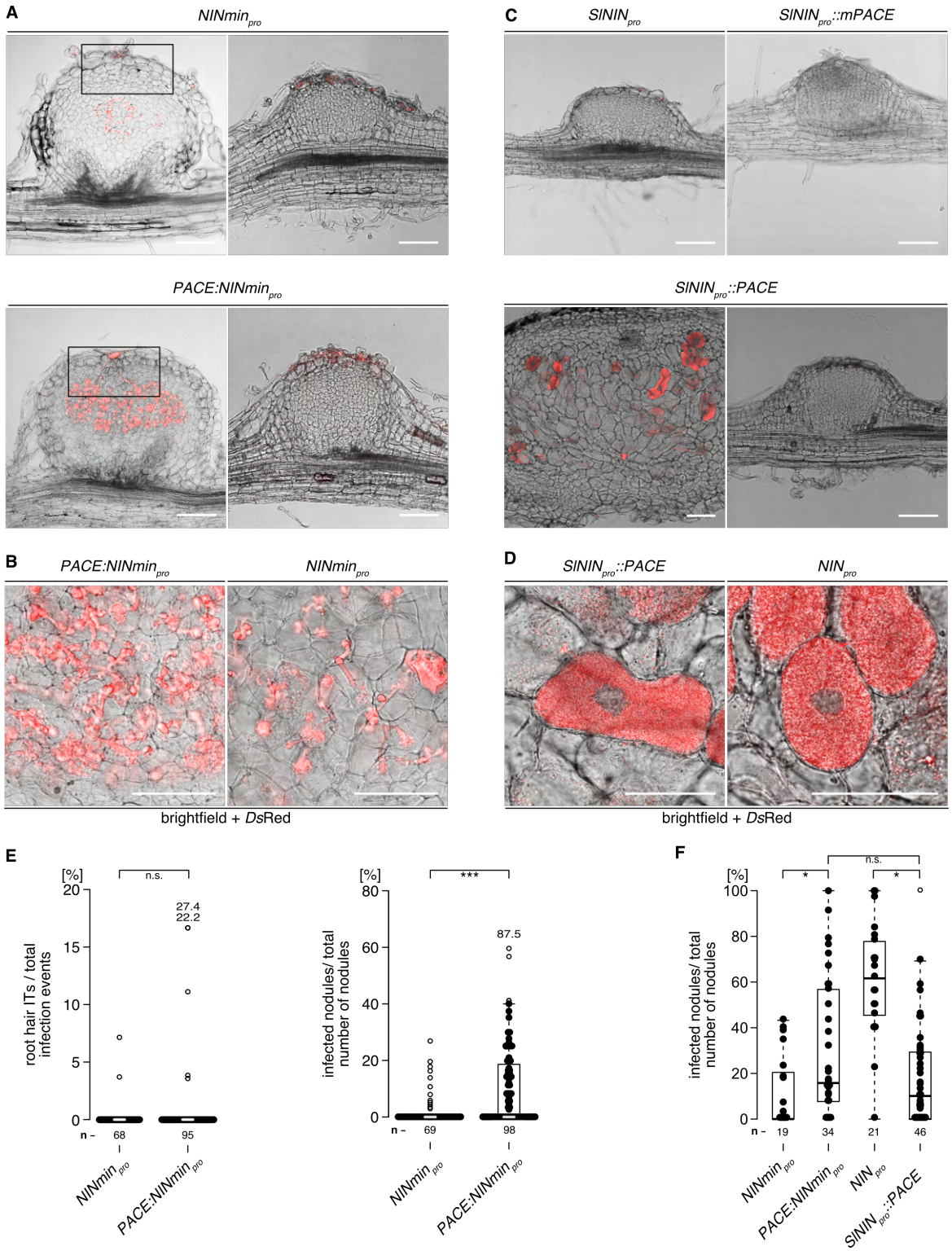

Figure 4 – figure supplement 1 | *PACE* alone or in the context of the *S. lycopersicum NIN* promoter (a species outside of the FaFaCuRo clade) enables IT formation in the cortex. (**A - D**) Representative pictures of sections of nodules formed on *L. japonicus nin-15* roots transformed with T-DNAs carrying a *Ubq10*$_{pro}$*:NLS-GFP* transformation marker together with the *LjNIN* gene driven by either of the following promoters: (**A - B**) the *L. japonicus NIN* minimal promoter (*NINmin*$_{pro}$) or *PACE* fused to *NINmin*$_{pro}$ (*PACE:NINmin*$_{pro}$); (**C - D**) the 3 kb *S. lycopersicum NIN* promoter (*SlNIN*$_{pro}$), the 3 kb *SlNIN* promoter with mutated *PACE* (*SlNIN*$_{pro}$*::mPACE*) or with *L. japonicus PACE* inserted (*SlNIN*$_{pro}$*::PACE*), 21 dpi with *M. loti Ds*Red (from the same experiments depicted in **Figure 4**). Black rectangles in (**A**) demarcate the enlarged area displayed in **Figure 4A and 4B** to focus on the initial infection structures. Note the absence of cells filled with symbiosomes in nodules transformed with the *LjNIN* gene driven by *PACE:NINmin*$_{pro}$ or *NINmin*$_{pro}$. By contrast, infected cells were often filled with symbiosomes in the *SlNIN*$_{pro}$*::PACE:NIN*-transformed nodules, like those resulted by *NIN*$_{pro}$*:NIN* (see (**C**) and compare the two sections in (**D**)). (**E - F**) Boxplots displaying the percentage of root hair ITs among total infection events (sum of bacterial entrapments and ITs) or the percentage of infected nodules among total number of nodules (**E**) 21 dpi and (**F**) 35 dpi with *M. loti Ds*Red, respectively. Each dot represents one *nin-15* transgenic root system or root piece. (**E**) displays results from an independent repetition from the experiment depicted in **Figure 4**. n: number of transgenic root systems or root pieces analysed. Numbers above the boxplots: the value of individual data points outside of the plotting area. The applied statistical method was Fisher's exact test: *$p < 0.05$; ***$p < 0.001$; n.s.: not significant. Bars, (**A and C**) 100 µm; (**B and D**) 50 µm.